

# Impact of precursor materials and synthesis procedures on structure and performance of TiO<sub>2</sub> supported Pd-catalysts in the gas phase acetoxylation of toluene



Dissertation

zur

Erlangung des akademischen Grades

doctor rerum naturalium (Dr. rer. nat.)

der Mathematisch-Naturwissenschaftlichen Fakultät

der Universität Rostock

vorgelegt von

Suresh Gatla M. Sc.

geboren am 10.04.1983 in Velpur, Indien

aus Rostock

Rostock, 26-08-2011

**Name:** Suresh Gatla

**Defense date:** 6<sup>th</sup> December 2011 at 16:00 hr

**Defense place:** Hörsaal 001, Institutes für Chemie, Universität Rostock

**Thesis Title:** Impact of precursor materials and synthesis procedures on structure and performance of TiO<sub>2</sub> supported Pd-catalysts in the gas phase acetoxylation of toluene

**Referees:**

1. Prof. Dr. Angelika Brückner  
Leibniz Institute für Katalyse  
Albert-Einstein-Str 29a  
18059, Rostock  
Germany
2. Habil. Dr. Andreas Martin  
Leibniz Institute für Katalyse  
Albert-Einstein-Str 29a  
18059, Rostock  
Germany
3. Prof. Dr. Wolfgang Grünert  
Ruhr-Universität Bochum  
Lehrstuhl für Technische Chemie,  
Postfach 102148  
44780 Bochum  
Germany

<b>Contents.....</b>	<b>ii</b>
<b>Declaration .....</b>	<b>vi</b>
<b>Glossary and abbreviations .....</b>	<b>vii</b>
<b>Abstract .....</b>	<b>viii</b>
<b>Zusammenfassung .....</b>	<b>x</b>
<b>Acknowledgements .....</b>	<b>xii</b>
<b>Structure of the thesis .....</b>	<b>xiii</b>
<b>Chapter 1 Motivation, objective of the thesis and state of the art .....</b>	<b>1</b>
1.1 Motivation .....	2
1.2 Objective of the thesis .....	3
1.3 State of the art.....	3
1.3.1 Importance of supported metal catalysts .....	3
1.3.2 Application of supported Pd-catalysts in heterogeneous catalysis.....	4
1.3.3 Synthesis of supported Pd-catalysts .....	5
1.3.4 Effect of thermal pretreatments on the Pd-catalysts.....	7
1.3.5 Influence of co-components for Pd-catalysts .....	8
1.3.6 Role of supports for Pd-particles .....	10
1.4 Liquid-phase reactions for acetoxylation of toluene .....	12
1.5 Gas-phase reactions for acetoxylation of toluene.....	14
<b>Chapter 2 Preparation and testing of the catalysts, principle and applications of the characterization methods.....</b>	<b>17</b>
2.1 Catalysts preparation and testing.....	18
2.1.1 General procedure .....	18
2.1.2 Preparation of 10 wt.-% Pd,16 wt.-% Sb/TiO <sub>2</sub> (anatase, rutile) using Sb <sub>2</sub> O <sub>3</sub> , without additives.....	20
2.1.3 Preparation of 10 wt.-% Pd,8 wt.-% M/TiO <sub>2</sub> anatase (M=Sb, Mn, Co, Au) with oxide and chloride precursors, without additives .....	21
2.1.4 Catalyst testing .....	21
2.2 Principle and applications of the characterization methods .....	23
2.2.1 Inductively coupled plasma-optical emission spectroscopy (ICP-OES).....	23
2.2.2 X-ray fluorescence (XRF) spectroscopy .....	24
2.2.3 Elemental analysis (CHNS).....	25
2.2.4 N <sub>2</sub> -physisorption (BET-surface area and pore size distribution) .....	26
2.2.5 CO-adsorption analyzed by Fourier transform infrared (FT-IR) spectroscopy.....	28
2.2.6 Thermo gravimetry-Differential thermal analysis (TG-DTA) .....	29
2.2.7 X-ray diffraction (XRD).....	30
2.2.8 X-ray absorption near edge structure (XANES).....	32
2.2.9 X-ray photoelectron spectroscopy (XPS).....	33
2.2.10 Transmission electron microscopy (TEM).....	34
<b>Chapter 3 Exploring the synthesis conditions for supported Pd-particles of optimum size and composition .....</b>	<b>37</b>
3.1 Influence of different metal precursors .....	38

3.1.1 Thermal analysis (TG-DTG).....	38
3.1.2 X-ray diffraction (XRD) .....	39
3.2 Effect of various ammonium additives .....	40
3.2.1 Thermal analyses (TG-DTA) .....	40
3.2.2 X-ray fluorescence (XRF).....	41
3.2.3 X-ray diffraction (XRD) .....	42
3.2.4 In situ - XRD investigations .....	43
3.2.5 Size and morphological studies with transmission electron microscopy (TEM)....	47
3.2.6 Surface and elemental compositional analysis by X-ray photo electron spectroscopy (XPS).....	49
3.3 Influence of pretreatment on catalytic performance .....	50
3.4 Conclusions.....	51
<b>Chapter 4 Tailoring synthesis and thermal pretreatment of a 10Pd,16Sb/TiO<sub>2</sub> catalyst towards maximum performance and stability .....</b>	<b>55</b>
4.1 Catalytic tests .....	56
4.2 Catalyst characterization .....	57
4.2.1 Elemental analysis and N <sub>2</sub> -adsorption .....	57
4.2.2 X-ray diffraction (XRD) .....	59
4.2.3 Transmission electron microscopy (TEM) .....	61
4.2.4 X-ray photoelectron spectroscopy (XPS) .....	64
4.3 Conclusions.....	66
<b>Chapter 5 Influence of co-components (M) on the state of Pd and on the performance of 10Pd,8M/TiO<sub>2</sub> (anatase) catalysts.....</b>	<b>69</b>
5.1 Catalytic tests .....	70
5.2 Catalyst characterization .....	71
5.2.1 Elemental analysis and surface Area .....	71
5.2.2 TG-DTA analysis for spent samples.....	72
5.2.3 X-ray diffraction (XRD) .....	73
5.3.4 X-ray absorption near edge structure (XANES) studies.....	76
5.3.5 X-ray photo electron spectroscopy (XPS) .....	77
5.3.6 FT-IR analysis of CO adsorption .....	78
5.3 Conclusions.....	80
<b>Chapter 6 Role of supports (anatase, rutile) on the improved performance of 10 wt.-% Pd, 16 wt.-% Sb catalyst.....</b>	<b>83</b>
6.1 Catalytic tests .....	84
6.2 Catalyst characterization .....	85
6.2.1 Elemental analysis.....	85
6.2.2 N <sub>2</sub> -physisorption .....	85
6.2.3 Thermogravimetry-differential thermal analysis (TG-DTA).....	86
6.2.4 X-ray diffraction (XRD) .....	87
6.2.5 Transmission electron microscopy (TEM) .....	88
6.2.6 X-ray photoelectron spectroscopy (XPS) .....	90
6.2.7 FT-IR of adsorbed CO .....	93
6.3 Conclusions.....	93



<b>Summary .....</b>	<b>95</b>
<b>References .....</b>	<b>97</b>
<b>List of scientific publications .....</b>	<b>101</b>
<b>List of contribution in conferences .....</b>	<b>102</b>
<b>Lebenslauf .....</b>	<b>104</b>

# Declaration

I declare that the work presented in this thesis is my own and done independently, and carried out entirely at the Leibniz Institute for Catalysis (LIKAT), Rostock, Germany under the supervision of Prof. Dr. Angelika Brückner (Head of Department "Catalytic in situ-Studies") and Dr. Jörg Radnik. The research work reported here has not been submitted, either wholly or in part, to any other academic institution for admission to a higher degree.

Rostock, 26<sup>th</sup> August 2011

Suresh Gatla

## Glossary and abbreviations

Å	Angstrom
BE	Binding Energy
BET ( $S_{\text{BET}}$ )	Brunauer-Emmett-Teller (BET Surface area)
° C	Celsius (unit of measurement for temperature)
DSC	Differential Scanning Calorimetry
DTA	Differential Thermal Analysis
EDX	Energy-Dispersive X-ray (spectroscopy)
eV	Electron volts (used as a unit for binding energy in XPS)
FCC	Face-centred cubic
FWHM	Full width at Half Maximum
FID	Flame Ionization Detector
FT-IR	Fourier Transformation Infrared Spectroscopy
GC	Gas Chromatography
GHSV	Gas Hourly Space Velocity
HAADF	High Angle Annular Dark-Field
HPLC	High Performance Liquid Chromatography
HRTEM	High Resolution Transmission Electron Microscopy
ICP - OES	Inductive Coupled Plasma Optical Electron Spectroscopy
K	Kelvin, ( $^{\circ}\text{C}$ ) = (K) – 273.15, (unit of measurement for temperature)
kV	Kilo Volts
MFC	Mass Flow Controller
nm	Nanometer
PZC	Point of Zero Charge
S-BA	Selectivity of Benzyl Acetate (%)
TEM	Transmission Electron Microscopy
TGA	Thermo Gravimetric Analysis
UV-Vis DRS	Ultraviolet–Visible Diffuse Reflectance Spectroscopic
X-Tol	Toluene conversion (%)
XRD	X-ray Diffraction
XRF	X-Ray Fluorescence (Spectroscopy)
XPS	X-ray Photoelectron Spectroscopy
Y-BA	Yields of Benzyl Acetate (%)

## Abstract

Benzyl acetate (BA) and its hydrolysis product benzyl alcohol are widely used chemicals in the perfumery, food, cosmetic industries, and commonly used solvents in the manufacturing of plastics and resins. Unfortunately, the current production of BA and benzyl alcohol is based on the environmentally problematic chlorine route [1]. Gas phase acetoxylation of toluene to BA, an eco-friendly route, over Pd-based catalysts using molecular oxygen can be an alternative for the BA production [2-14].

It has been shown previously that the yield of benzyl acetate obtained in the gas phase acetoxylation of toluene depends merely on the different types of catalysts used. Highest catalytic performance was obtained with a catalyst consisting of 10 wt.-% Pd and 8 wt.-% Sb supported on anatase, which reached a maximum BA selectivity of 86 % at a toluene conversion of 68.5 % [9]. The striking drawbacks of this catalyst were long conditioning time of about 12 h and fast deactivation. Good long-term stability at rather high toluene conversion (60 %) and BA selectivity (95 %) was also obtained with a 10 wt.-% Pd, 8 wt.-% Cu/TiO<sub>2</sub> catalyst, however with even longer conditioning times of 50 h [11]. It was claimed that bigger metallic Pd particles of 80-100 nm are necessary for a good performance of the catalyst.

Motivated by these findings, the aim of this study is to explore systematically the role of different starting materials, thermal treatment procedures, the co-components and supports on the catalytic performance of supported Pd-particles in the acetoxylation of toluene.

Initially, different Pd-catalysts containing 10 wt.-% Pd and 8 wt.-% Sb or Cu, on TiO<sub>2</sub> (anatase) were prepared by a two-step impregnation procedure involving the impregnation with Sb or Cu precursors (chlorides / nitrates / acetates) in the first step followed by impregnation with Pd-precursors (chlorides / nitrates / acetates) in the second step. Different additives such as (NH<sub>4</sub>)<sub>2</sub>SO<sub>4</sub>, NH<sub>4</sub>NO<sub>3</sub>, (NH<sub>4</sub>)<sub>2</sub>CO<sub>3</sub> and urea were added during the preparation to ensure the removal of Cl from the metal chloride precursors during thermal treatments. (NH<sub>4</sub>)<sub>2</sub>SO<sub>4</sub> was found to be the best agent to remove chloride anion. Further, In-situ XRD analysis up to 650 °C (in helium and 10 % H<sub>2</sub>/He) for Pd-Cu and Pd-Sb catalysts revealed the formation of unstable Pd-chloramine complexes which act as intermediate precursors for Pd-particles. Catalytic tests for gas phase acetoxylation of toluene were performed with Pd,Sb/TiO<sub>2</sub> catalysts after different thermal treatments. High temperature thermal treatment at 600 °C in helium shortened effectively the equilibration time by creating bigger Pd-particles. However, a total yield of benzyl acetate (BA) was lower than conventional catalysts. This is attributed to the partial loss of Sb (from SbCl<sub>3</sub>) upon high temperature thermal pretreatment. Moreover, the sulfide species which were formed from (NH<sub>4</sub>)<sub>2</sub>SO<sub>4</sub> poison the catalyst and lowered the BA yield [12].

Therefore, a new synthesis procedure was developed using Sb<sub>2</sub>O<sub>3</sub> instead of SbCl<sub>3</sub> as starting material, which made the addition of ammonium sulfate dispensable. Then, 10 wt.-% Pd, 16 wt.-% Sb/TiO<sub>2</sub> catalyst was prepared using Sb<sub>2</sub>O<sub>3</sub> and PdCl<sub>2</sub>, and explored the effect of

pretreatment temperature (600 °C) and atmosphere (air, and 10 % H<sub>2</sub>/He) on the size and nature of Pd-particles as well as on the catalyst performance. Thermal treatment at 600 °C was beneficial for shortening the activation period, whereas treatment atmosphere affected the long term stability. Surprisingly, sample treated in H<sub>2</sub>/He was found to be inactive due to the presence of stable Pd<sub>8</sub>Sb<sub>3</sub> alloy. Air and helium pretreatment samples showed Sb-containing Pd-particles at their maximum activity. TEM-EDX analysis showed that, intermixing of Pd and Sb is more prominent for helium pretreated sample with an atomic ratio of Pd to Sb ≈ 5. Moreover, XPS studies revealed the mixed Pd<sup>0</sup>/PdO surface state for palladium. Incorporated Sb stabilized the oxidized Pd-species and led to more stable catalysts [13].

Thereafter, influence of standard reduction potential ( $E^0$ ) of the co-components on the Pd-valance, and consequently, on the performance of 10Pd,8M/TiO<sub>2</sub> catalysts was studied. For this purpose, co-components (M: Mn, Co, Sb, Au) with a wide range of standard reduction potentials ( $E^0$ : Mn<sup>2+</sup>/Mn = -1.18 eV, Co<sup>2+</sup>/Co = -0.28 eV, Sb<sup>3+</sup>/Sb = +0.2 eV and Au<sup>3+</sup>/Au = +1.52 eV) were selected. Catalyst containing Mn with low  $E^0$  was more active but less selective, whereas Au with high  $E^0$  was highly selective but showed low toluene conversion. The other two components (Sb and Co) with  $E^0$  nearly zero offered a best compromise between activity and selectivity. It was observed that the co-components with low  $E^0$  stabilized the Pd in its oxidized form, while those with high  $E^0$  supported the formation of metallic Pd [15].

Finally, the role of different phases of TiO<sub>2</sub> (anatase and rutile) as supports on the Pd-particle size, composition, and on the performance of 10 wt-% Pd, 16 wt-% Sb catalyst was explored in more detail. Pd, Sb supported especially on rutile showed extremely high (> 95 %) selectivity for the BA and displayed long term stability (> 30 h). Sb incorporated Pd-particles with the beneficial atomic ratio ≈ 5 were found in rutile samples. The surface of these particles contains of metallic and oxidized Pd. The anatase sample, which was deactivated (> 30 h), showed agglomerated particles with Pd/Sb atomic ratio ≈ 3, which are inactive. In addition, slightly reduced state for palladium (Pd<sup>δ-</sup>) was noticed by XPS which was formed due to the interaction of Pd-particles with deposited coke. This detrimental Pd<sup>δ-</sup> state was not formed in the rutile sample since coke was deposited on rutile support rather Pd-particles.

The variation of different synthesis parameters like co-component, precursor, thermal pretreatment and support allows tuning the long-term stability, activity and selectivity of the catalysts. In a systematic study the best catalytic performance were obtained for a 10 wt-% Pd, 16 wt-% Sb/TiO<sub>2</sub> pretreated in He. The results gained with rutile as supports show that an optimization of the support, probably by the variation of the anatase / rutile ratio seems to be very promising to increase the catalytic performance. Another promising way could be the combination of different co-components like Au and Mn.

## Zusammenfassung

Benzylacetat und sein Hydrolyseprodukt Benzylalkohol sind weitverbreitete Chemikalien in der Parfüm-, Lebensmittel- und Kosmetikindustrie, ebenfalls gebräuchliche Lösungsmittel in der Herstellung von Kunststoffen und Harzen. Leider beruht die gegenwärtige Produktion von BA und Benzylalkohol auf den umweltschädlichen Chlorprozess [1]. Die Gasphasenacetoxylierung von Toluol zu BA, ein umweltfreundlicher Prozess, über Pd-haltige Katalysatoren mit Sauerstoff als Oxidationsmittel kann eine Alternative zur BA Produktion sein [2-14].

Vorher wurde gezeigt, dass die Ausbeute an Benzylacetat, die in der Gasphasenacetoxylierung erzielt werden kann, wesentlich von den eingesetzten Katalysatoren abhängt. Die besten Ergebnisse konnte mit einem Katalysator erzielt werden, der 10 Gew. % Pd und 8 Gew. % Sb, geträgert auf Anatas, enthält. Mit diesem Katalysator wurde eine maximale BA Selektivität von 86% bei einem Toluolumsatz von 68,5 % erzielt [9]. Offensichtliche Nachteile dieses Katalysators waren die lange Konditionierungszeit von ungefähr 12 h und eine schnelle Deaktivierung. Eine gute Langzeitstabilität bei einem ziemlich hohen Toluolumsatz (60 %) und BA Selektivität (95 %) wurde mit einem 10 Gew. % Pd, 8 Gew. % Cu / TiO<sub>2</sub> Katalysator erreicht, allerdings mit noch längeren Konditionierungszeiten von 50 h [11]. Es wurde vermutet, dass größere Pd Partikel von 80 zu 100 nm für die Leistungsfähigkeit des Katalysators notwendig sind.

Angeregt durch diese Erkenntnisse war die Zielsetzung der gegenwärtigen Studie die Rolle unterschiedlicher Ausgangsmaterialien, thermischen Vorbehandlungsprozeduren, Ko-Komponenten und Trägermaterialien auf die Leistungsfähigkeit der Pd-Partikel in der Acetoxylierung von Toluol systematisch zu erkunden.

Anfangs wurden verschiedene Pd-Katalysatoren durch eine zweistufige Imprägnierung mit Sb oder Cu Prekursoren (Chloride / Nitrate / Acetate) im ersten Schritt und mit Pd-Prekursoren (Chloride / Nitrate / Acetate) im zweiten Schritt präpariert, die 10 Gew.-% und 8 Gew.-% Sb oder Cu auf Anatas enthalten. Verschiedene Additive wie (NH<sub>4</sub>)<sub>2</sub>SO<sub>4</sub>, NH<sub>4</sub>NO<sub>3</sub>, (NH<sub>4</sub>)<sub>2</sub>CO<sub>3</sub> and Harnstoff wurde während der Präparation hinzugefügt um Cl aus den Metallprekursoren während der thermischen Behandlung zu entfernen. (NH<sub>4</sub>)<sub>2</sub>SO<sub>4</sub> wurde als bestes Reagenz zur Entfernung des Chloridanions gefunden. Weiterhin wurden in situ XRD Analysen bis 650°C (in He und 10 % H<sub>2</sub>/He), die zeigten, dass instabile Pd-Chloramin-Komplexe als Zwischenprodukte für die Pd-Partikel gebildet werden. Katalytische Tests wurden für die Gasphasenacetoxylierung von Toluol wurde mit Pd,Sb/TiO<sub>2</sub> Katalysatoren nach verschiedenen thermischen Behandlungen durchgeführt. Thermische Behandlung bei 600°C in Helium verkürzt effektiv die Einstellung bis Erreichung des Gleichgewichts durch die Bildung großer Pd-Partikel. Allerdings war die Ausbeute an Benzylacetat (BA) niedriger als bei den bisherigen Katalysatoren. Dies ist auf einen teilweisen Verlust an Sb (aus SbCl<sub>3</sub>) durch die Vorbehandlung bei hohen Temperaturen. Zusätzlich wurden Sulfidspezies aus dem (NH<sub>4</sub>)<sub>2</sub>SO<sub>4</sub> gebildet, die den Katalysator vergifteten und die BA-Ausbeute erniedrigten [12].

Daher wurde eine neue Syntheseprozedur entwickelt, die Sb<sub>2</sub>O<sub>3</sub> an Stelle von SbCl<sub>3</sub> als Edukt benutzt, was die Zugabe von Ammoniumsulfat überflüssig macht. Danach wurde ein Katalysator mit 10 Gew.-% Pd und 16 Gew.-% Sb/TiO<sub>2</sub> hergestellt, und der Effekt der

Vorbehandlungstemperatur (600 °C) und Atmosphäre (Luft und 10 % H<sub>2</sub>/He) auf die Größe und Eigenschaften der Pd-Partikel als auch auf die katalytischen Eigenschaften untersucht. Thermische Behandlung bei 600 °C war günstig, um die Aktivierungsperiode zu verkürzen, wogegen die Atmosphäre die Langzeitstabilität beeinflusste. Überraschenderweise war die in H<sub>2</sub>/He behandelte Probe aufgrund der Anwesenheit der stabilen Pd<sub>8</sub>Sb<sub>3</sub> Legierung inaktiv. In Luft und Helium vorbehandelte Proben zeigten Sb-enthaltende Pd-Partikel bei ihrer maximalen Aktivität. TEM-EDX-Analyse zeigte, dass eine Durchmischung von Pd und Sb für die Helium-vorbehandelte Probe mit einem Atomverhältnis von Pd zu Sb von ungefähr 5 stärker ausgeprägt ist. Zusätzlich zeigten XPS Untersuchungen gemischte Pd<sup>0</sup>/PdO Zustände an der Oberfläche. Eingebautes Sb stabilisiert die oxidierten Pd-Spezies und führten zu stabileren Katalysatoren [13].

Danach wurde der Einfluss des Standardreduktionspotential ( $E^0$ ) der Ko-Komponenten auf die Pd-Valenz und auf die Leistungsfähigkeit der 10Pd,8M/TiO<sub>2</sub>-Katalysatoren untersucht. Zu diesem Zweck wurden Ko-Komponenten (M: Mn, Co, Sb, Au) mit unterschiedlichen Standard-Reduktions-Potential ( $E^0$ : Mn<sup>2+</sup>/Mn = -1.18 eV, Co<sup>2+</sup>/Co = -0.28 eV, Sb<sup>3+</sup>/Sb = +0.2 eV and Au<sup>3+</sup>/Au = +1.52 eV) ausgewählt. Der Katalysator, der Mn enthielt, mit einem niedrigem  $E^0$  war sehr aktiv, aber wenig selektiv, wogegen Au mit hohem  $E^0$ -Wert zu einem sehr selektiven Katalysator führt, der aber nur einen geringen Toluol-Umsatz hat. Die anderen zwei Ko-Komponenten (Sb und Co) mit einem  $E^0$  um Null boten den besten Kompromiss zwischen Aktivität und Selektivität. Es wurde beobachtet, dass die Ko-Komponenten mit niedrigen  $E^0$ -Werten oxidiertes Pd stabilisieren, während die mit hohen  $E^0$ -Werten die Bildung von metallischem Pd unterstützen[15].

Schließlich wurde die Rolle der verschiedenen Phasen von TiO<sub>2</sub> (Anatas und Rutil) als Träger auf die Pd-Partikelgröße, Zusammensetzung und Leistungsfähigkeit des 10 Gew.% Pd, 16 Gew.% Sb Katalysator detailliert untersucht. Speziell auf Rutil geträgertes Pd, Sb zeigte extrem hohe Selektivitäten (> 95 %) für BA und eine hohe Langzeitstabilität (> 30 h). Pd-Partikel mit eingebautem Sb und dem günstigen Atomverhältnis  $\approx 5$  wurden in der Rutilprobe gefunden. Die Oberfläche dieser Partikel zeigte metallisches und oxidiertes Pd. Die deaktivierte Anatasprobe (< 30 h) zeigte agglomerierte Partikel mit einem Pd/Sb Atomverhältnis von ungefähr 3, welche inaktiv sind. Zusätzlich wurde ein schwach reduzierter Pd-Zustand (Pd<sup>δ-</sup>) gefunden, der sich durch die Wechselwirkung zwischen den Pd-Partikeln mit abgelagertem Kohlenstoff bildet. Dieser schädliche Pd<sup>δ-</sup>-Zustand bildet sich nicht in der Rutilprobe, weil dort Kohlenstoff eher auf dem Rutilträger als auf den Pd-Partikeln abgelagert wird.

Die Änderung von verschiedenen Syntheseparametern wie Ko-Komponenten, Prekursoren, thermische Vorbehandlung und Träger erlaubt die Abstimmung von Langzeitstabilität, Aktivität und Selektivität der Katalysatoren. In einer systematischen Studie wurden die besten katalytischen Eigenschaften für ein 10 Gew.-% Pd, 16-Gew.-% Sb/TiO<sub>2</sub> in He-vorbehandeltem Katalysator erzielt. Die mit Rutil als Träger erhaltenen Ergebnisse zeigen, dass eine Optimierung des Trägers, vielleicht durch die Veränderung des Anatas / Rutil Verhältnis, scheint ein vielversprechender Weg, die katalytischen Eigenschaften zu verbessern. Ein anderer erfolgreicher Weg kann die Kombination verschiedener Ko-Komponenten wie Au und Mn sein.



# Acknowledgements

It has been my privilege to meet and work with a lot of nice and talented people over the course of my PhD at Leibniz Institute for Catalysis (LIKAT) in Rostock and as well as in Berlin (1<sup>st</sup> October 2007 to 1<sup>st</sup> May 2009), Germany. So I would like to thank each and every person. Special thanks to some of the important persons.

Primarily, I would like express gratitude to my supervisor, **Prof. Dr. Angelika Brückner**, for believing and providing an opportunity to work on this project. First, I am grateful for her constant encouragement, suggestions (which provided a concrete shape to my ideas) and assistance for implementing the ideas in effective way. I would rather say ‘without her help work would not be possible’.

I am truly thankful to **Dr. Jörg Radnik** for his constant engagement with my work, providing motivation and enthusiasm. I appreciate all his contributions of time, ideas for my success. I am thankful to him for guiding me and teaching the research skills.

Special thanks to **Dr. habil. Andreas Martin**, **Dr. V.N. Kalevaru** and **Prof. Bernhard Lücke** for their outstanding assistance and numerous scientific discussions. Their excellent knowledge, perception and personal experience have a great impact on my thesis.

My deep appreciation to **Neetika Madaan** for teaching me about the handling of reaction setup. I am thankful to her for explaining patiently each and every even a small doubt.

In addition my thanks go to analytical staff members of the LIKAT for their timely assistance, who have involved in the analytics of this work

Particularly, Dr Schnider and Fr Winlker and for XRD measurements (for more than 300 patterns), Dr. M.-M. Pohl for very important TEM investigations and Dr. U. Bentrup for FT-IR investigations.

I would also like to extend my thanks to all the persons who helped me directly or indirectly.

**26-08-2011**

**Suresh Gatla**



# Structure of the thesis

The present thesis is separated into six chapters on the basis of motivation and objective, literature survey, catalyst preparation, characterization methods and catalytic results and discussion.

**Chapter 1** contains the motivation, objective of the current study and general introduction about the importance of supported catalysts in the gas phase reactions, including supported Pd-catalysts. State of the art about the effect of preparation conditions, influence of thermal pretreatments, co-components as well as supports on the state of Pd in various reactions is given. Finally, a thorough literature survey on acetoxylation of toluene is presented.

**Chapter 2** describes the preparation procedure about the supported Pd-catalysts used in the present investigations. The basic principle and applications of different characterization methods is given. The experimental conditions related to the catalysts testing are described.

**Chapter 3** deals with the results and discussion about the effect of various preparation parameters such as metal precursors (chlorides versus nitrates and acetates), different additives (ammonium sulfate, nitrate, carbonate and urea) and thermal treatments (300 °C, 400 °C and 600 °C) in different atmospheres, which are adopted for 10 wt.-% Pd, 8 wt.-% Sb/TiO<sub>2</sub> and 10 wt.-% Pd, 8 wt.-% Cu/TiO<sub>2</sub> catalysts with an aim to get Pd-particles which are close to the equilibrium catalyst particles.

**Chapter 4** describes the impact of high temperature thermal treatment at 600 °C in different atmospheres (air, helium and H<sub>2</sub>) on Pd-particle size, composition and on the acetoxylation activity of 10 wt.-% Pd, 16 wt.-% Sb/TiO<sub>2</sub> catalyst. More importantly, catalysts at their maximum activity are exclusively studied with XRD, XPS and HAADF-STEM to explore the structure-activity relationship.

**Chapter 5** explores the influence of co-components on the nature of the Pd. Elements with a wide scope of standard reduction potentials ( $E^0$ : Mn<sup>2+</sup>/Mn = -1.18 eV, Co<sup>2+</sup>/Co = - 0.28 eV, Sb<sup>3+</sup>/Sb = 0.15 eV and Au<sup>3+</sup>/Au = 1.52 eV) are chosen as co-components for PdM/TiO<sub>2</sub> catalyst and tested for the gas phase acetoxylation of toluene.

**Chapter 6** Role of different polymorphs of TiO<sub>2</sub> (anatase and rutile) as supports on the 10 wt.-% Pd, 16 wt.-% Sb/TiO<sub>2</sub> catalyst activity and selectivity is studied.



## Chapter 1

### **Motivation, objective of the thesis and state of the art**

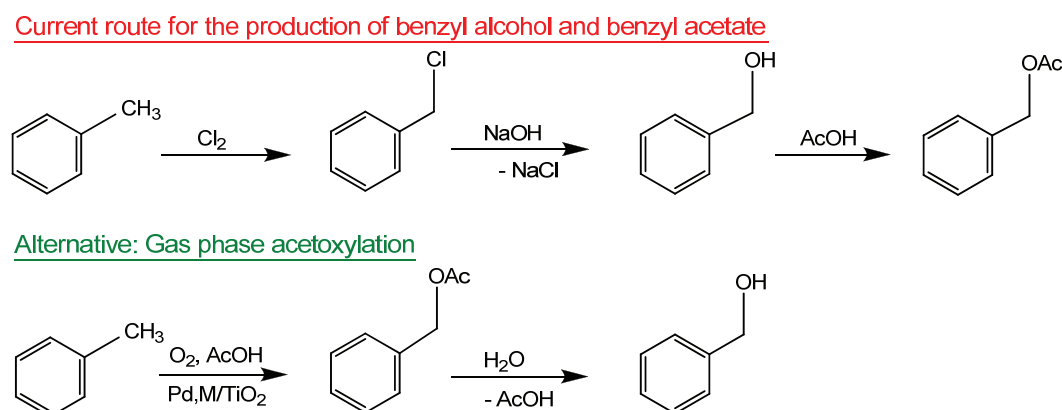
---

At first, this chapter introduces the motivation, which includes the importance of the gas acetoxylation reaction of toluene and the use of different Pd-based catalysts for this reaction. An objective section followed the motivation. Finally, the state of art, which covers the influence of different preparation methods, metal precursors, thermal pretreatments, co-components and supports on the state of Pd as well as on the performance of Pd-based catalysts in various gas phase reactions. An exclusive survey on the literature is presented, which covers the origin and progress of the acetoxylation of toluene including liquid phase reactions.

---

## 1.1 Motivation

Palladium particles supported on oxidic carriers are effective catalysts for a wide variety of heterogeneous catalytic reactions, including the acetoxylation of hydrocarbons. Thus, acetoxylation of ethylene over supported Pd/SiO<sub>2</sub> is the most important technical process to produce vinyl acetate monomer [16]. In the case of toluene, acetoxylation with molecular oxygen [2-5, 8-11, 17, 18] could be an attractive alternative route for the production of benzyl acetate and its hydrolysis product benzyl alcohol (widely used chemicals in the food, perfumery, and chemical industries), which is still based on the environmentally problematic chlorine chemistry [1] (Scheme 1.1).



**Scheme 1.1** Current industrial route for the production of benzyl acetate through harmful benzyl chloride intermediate and proposed alternative eco-friendly gas phase reaction using molecular oxygen.

A complete survey on the literature of Pd-catalysts for acetoxylation of toluene reveals that most of the initial work reported is confined to liquid-phase and batch reactors [19], whereas vapor-phase processes were previously not successful in terms of obtaining higher yields of BA with acceptable time on stream stability of the catalysts. However, recently developed Pd,Sb/TiO<sub>2</sub> (anatase) catalysts have shown the best performance. Especially a 10Pd,8Sb/TiO<sub>2</sub> catalyst displayed 86 % selectivity of benzyl acetate (BA) at 68.5 % toluene conversion in the direct gas phase acetoxylation of toluene [10]. Remarkably, the activity of this catalyst increased dramatically within the initial 10-12 h on stream and this went along with a marked increase of the metal particle size. Unfortunately, this catalyst deactivated rather quickly after reaching the maximum toluene conversion at ca. 12 h. It has been shown that this deactivation can be effectively suppressed by doping with bismuth or copper. However, this led to a drop of the total activity and to a marked increase of the conditioning time [10, 11]. For improving the industrial relevance of such catalysts, the conditioning time

must be shortened and the catalyst stability must be increased while maintaining high activity and selectivity.

## 1.2 Objective of the thesis

Inspired by these previous findings, the present study is focused mainly to explore the influence of different preparation parameters on phase composition and Pd-particle size, such as temperature and atmosphere of thermal pretreatment, metal precursors (chlorides versus nitrates and acetates), co-components (Cu, Sb, Mn, Co, Au), additives ( $(\text{NH}_4)_2\text{SO}_4$ ,  $\text{NH}_4\text{NO}_3$ ,  $(\text{NH}_4)_2\text{CO}_3$  and urea) as well as supports ( $\text{TiO}_2$  anatase and rutile). Based on these results, optimized synthesis parameters shall be identified for the preferential formation of metallic nanostructured Pd-particles with a size as close as possible to that observed in equilibrated catalysts (80-100 nm). From an academic point of view such investigations are desirable to get new insights into the structure-activity relationship of the catalysts. Economically, proper synthesis of Pd-particles of desired size and structure might improve the total performance of the catalyst in terms of shorter conditioning time, stable performance and high selectivity for desired product.

## 1.3 State of the art

This section contains a general importance supported metal catalysts and applications of the Pd-catalysts in heterogeneous catalysis, and the effect of different thermal treatments, co-components as well supports especially on the Pd-catalysts in the realm of heterogeneous gas phase reactions including acetoxylation of toluene.

### 1.3.1 Importance of supported metal catalysts

In general, supported metal catalysts contain metal particles anchored on an oxide support [20]. These metal particles contain active centers, usually at the surface, at which the catalytic reaction takes place. In addition, apart from the metal particles, metal oxides and intermetallics can also act as active centers. The desired state for the supported particles can be attained by pursuing the appropriate thermal treatments in different atmospheres or sometimes it can be achieved in situ under reaction conditions. In any case, a chemical interaction takes place between the reactant molecules after their proper adsorption on these active centers lead to the product formation and followed by desorption. A simple description of the metal particles deposited on a support and molecular interactions can be seen in Fig. 1.1 (a similar mechanism is also being likely possible on the supported Pd-catalysts as well).

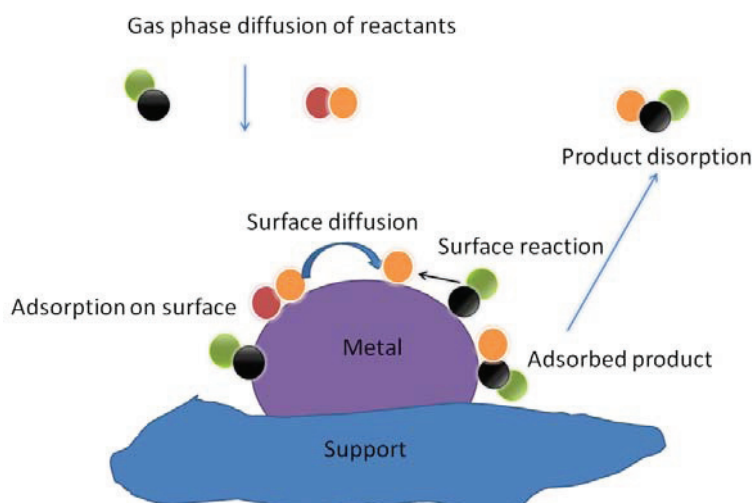


**Fig. 1.1** Active metal particle on a support and various physical and chemical processes on the surface of the particles. Figure is redrawn from ‘the basis and applications of heterogeneous catalysis’ by Michael Bowker.

A general consensus about the catalytic process is that the chemical bonds are broken and new bonds are formed [21]. It is well known that, when a heterogeneous catalytic reaction occurs, several physical and chemical processes will take place for the supported particles as well. Usually, an ideal catalyst should retain its identity after a catalytic cycle in the reaction. However, this is not the case in many solid supported catalysts. Different modifications can take place for the catalyst particles under the reaction conditions due to the interactions of reactant or intermediate molecules with the catalyst surface. These modifications certainly include particle growth, oxidation or reduction (change in the valence state), loss or gain in the crystallinity, as well as morphological modifications. Sometimes such changes are also useful to increase the number of active sites in the catalyst, which in turn improve the catalyst overall performance. By comprehensive characterization of the solid catalyst with different analytical techniques like XRD, TEM, XPS, XANES, FT-IR analysis of adsorbed probe molecules such as CO and pyridine, it is possible to gain information on the nature of the active sites. Such information is useful to tailor the catalyst, with desired active sites, which works more efficiently in the catalytic reactions.

### 1.3.2 Application of supported Pd-catalysts in heterogeneous catalysis

Generally, Pd-particles deposited on various oxide supports are used in a wide variety of catalytic processes like hydrogenation [22-25], dehydrogenation, hydrodehalogenation [26-29], petroleum cracking [30], water gas shift [31, 32], steam reforming [33, 34] and finally in total oxidation reactions. Apart from these, Pd-catalysts are also widely used in the direct and

controlled partial oxidation of various hydrocarbons to get desired oxygenates. The nature of Pd certainly influences the activity of the catalysts in all the above reactions.

There are multiple ways in which the state of the Pd-phase can be affected. Generally, the method of preparation, precursor materials and additives, thermal pretreatment, co-components and supports sensitively govern the nature of the active Pd-components.

### 1.3.3 Synthesis of supported Pd-catalysts

Depending on the requirement, preparation of the supported Pd-catalysts also has been using the different available methods like (i) electrostatic adsorption (ii) impregnation, (iii) sol-gel (iv) precipitation, co-precipitation and deposition-precipitation, (vi) hydrothermal synthesis and finally (vii) chemical vapor deposition (CVD). Preparation of the supported metal catalysts with desired active sites is often a challenging task because even minor alterations of the preparation conditions can have a significant effect on the catalyst properties, which often influences the delicate balance of the demands like high activity, high selectivity and long lifetime of the catalysts in the catalytic reaction.

Method of preparation, use of different metal precursors (chloride, nitrate, acetates, complexes and ligands) and additives (precipitating or reducing), supports (high or low surface area) and thermal treatments can alter the chemical features and performance of the final catalyst because they can influence considerably the nature and size of the metal particles and their interactions with the support, which determine the catalytic behavior [35] of the supported catalyst. In this section, we are going to describe the preparation of Pd-based catalyst mainly by precipitation, deposition and impregnation because they cover the most of the above mentioned parameters.

#### 1.3.3.1 Precipitation and co-precipitation

The formation of a precipitate from a homogeneous solution may occur as a result of physical transformations such as temperature or solvent evaporation, but mostly by chemical processes such as addition of acid or base, presence of impurities as well as use of complex forming agents [36]. These chemical processes also influence the morphology, texture and structure of the final precipitates. In contrast to precipitation method in which preparation takes place for a single component system, co-precipitation rarely allows macroscopic homogeneity. However, this route is preferred whenever a better intermixing of catalyst components (main and co-components) is required. For example, N. Iwasa et al. observed that Pd/Zn/CeO<sub>2</sub> catalyst prepared by co-precipitation method is more active in steam reforming of methanol, due to high dispersion of active components in the CeO<sub>2</sub> support, with the highest rate of hydrogen

production of  $966 \text{ cm}^3 \text{ g}^{-1} \text{ h}^{-1}$ . This catalyst was prepared by the addition of  $\text{Na}_2\text{CO}_3$  solution to a mixed solution of palladium chloride, zinc nitrate and cerium nitrate. In another study, addition of  $\text{Na}_2\text{CO}_3$  solution to the mixture of Pd, Fe-nitrate precursors ( $\text{Pd}(\text{NO}_3)_2$ ,  $\text{Fe}(\text{NO}_3)_3 \cdot 9\text{H}_2\text{O}$ ) gave an active Pd-Fe-O catalyst for oxidative dehydrogenation of butane [37].

### 1.3.3.2 Deposition-precipitation

Deposition-precipitation is similar to the precipitation method except that the precipitate after its immediate formation deposits on the support, which is present in the reaction vessel. For example, N.S. Babu et al. have prepared in this way 1 wt.-% Pd/TiO<sub>2</sub> by using the 1M  $\text{Na}_2\text{CO}_3$  as precipitating agent for two different precursors namely  $\text{Pd}(\text{NO}_3)_2$  and  $\text{PdCl}_2$ , and used for hydrodechlorination of chlorobenzene [38]. Authors observed that the catalyst prepared by deposition-precipitation using the chloride precursor exhibited higher dispersion and different electronic properties compared to the other catalysts and exhibited considerable hydrodechlorination activity and long term stability. The generation of active electron deficient Pd-species ( $\text{Pd}^{\text{n}+}$ ) on the catalyst surface appears to be the main reason for this behavior. In another study, a Pd/TiO<sub>2</sub> catalyst contains well-dispersed Pd-nanoparticles with very small size (less than 3 nm) which were formed by reducing the  $\text{PdCl}_2$  with the sodium borohydride ( $\text{NaBH}_4$ ) exhibited very high turnover frequencies of HCHO oxidation and showed high activity (100 % HCHO conversion) [39]. Authors claimed that SMSI (Strong-Metal Support Interaction), negatively charged metallic Pd-nanoparticles, and the oxygen adsorbed by Pd-particles might be responsible for high catalytic activity. Finally, the size and dispersion of the metal particles formed by precipitation depend on the size of the pores and the extent of the interaction with the support. The deposition-precipitation method generally provides well-dispersed active component even though the metal content is high and there is a possibility for the occurrence of SMSI.

### 1.3.3.3 Impregnation and drying

Generally, an impregnation process is related the introduction of the dissolved aqueous metal precursors onto the supports [36], after which the solvent will be eliminated by drying. If the volume of the solution either equal or less than the pore volume of the support, then the method is referred to as incipient wetness. E. Marceau et al. proposed four important parameters related to the method of the impregnation [40], are as follows:



- 1) During impregnation, the dissolved precursor migrates into the pores of the support, on which it may adsorb.
- 2) The support can be used as a powder support but most often in industry it appears in the form of extrudates or pellets of specific size and shape, implying a transport of matter in the solid at a macroscopic scale and a distribution that may not be homogeneous.
- 3) The impregnation solution contains several chemical species: the metal precursors of the active phase, its counter ions, coimpregnants; precursors are also selected according to their physicochemical properties and cost.
- 4) Choice of the parameters such as concentration and temperature is crucial. Depending on these, different physicochemical phenomena may lead to different types of deposited phases and ultimately to more or less active catalysis.

For the Pd-based catalysts preparation,  $\text{H}_2\text{PdCl}_4$ ,  $\text{Pd}(\text{NO}_3)_2 \cdot 2\text{H}_2\text{O}$ ,  $\text{Na}_2\text{PdCl}_4$ ,  $\text{K}_2\text{PdCl}_4$ ,  $\text{Pd}(\text{NH}_3)_4\text{Cl}_2$ ,  $\text{Pd}(\text{Oac})_2$ ,  $\text{Pd}(\text{acac})_2$  and  $\text{Pd}(\text{NH}_3)_4\text{NO}_3$  are commonly used precursors [40-45]. In the impregnation method, after the drying procedure, thermal pretreatment influences ultimately the final state of the catalyst in terms of chemical nature, dispersion and size of metal particles. The effect of such pretreatment on the nature of Pd-catalysts is described in the next section.

#### 1.3.4 Effect of thermal pretreatments on the Pd-catalysts

Thermal pretreatment either externally or in the catalytic reactor prior to the exposure to reactants (in-situ activation) for the catalyst after its preparation is very important to convert the metal precursors into the active metal oxide, metal particles and/or intermetallics. This can be achieved by using the appropriate temperature, heating rate and atmosphere during the thermal treatments such as oxidizing (air), inert ( $\text{N}_2$ , He, Ar) or reducing atmosphere (diluted  $\text{H}_2$ ). Selection of suitable temperature for the thermal treatment is often based on the thermal stability of the precursors used in the synthesis. The effect of pretreatment on the dispersion of Pd-catalysts supported on silica has been studied for a  $[\text{Pd}(\text{NH}_3)_4](\text{NO}_3)_2$  complex precursor by W. Zou et al., in air, He and  $\text{H}_2$  atmospheres [43]. In reducing atmosphere, dispersion of Pd-particles was found to be very poor, while pretreatment in inert atmosphere (He or Ar) increased the dispersion by decomposing the surface complex.

On the other hand, in methane oxidation reactions, supported PdO has been formed by calcination at rather high temperature ( $> 600\text{ }^\circ\text{C}$ ) in air, whereas Pd-phase formed under reaction conditions [46-49]. These studies revealed that the metallic Pd or PdO phases alone

are less active for this reaction. However, their simultaneous presence made the catalyst highly active since adsorption of the methane molecules is readily possible on a metallic Pd-surface, whereas PdO is useful to abstract the hydrogen from adsorbed methane [46]. This indicates that the treatment atmosphere is important to get desired state of the metal particles. In addition, the reaction feed can also restructure the phases. On the other hand, thermal treatment influences also the size of the metal particles.

Hydrogenation of dimethyl ethynyl carbinol is one of the reactions in which Pd-particles with a size of 9, 15, 25 and 75 Å have been achieved by varying the temperature up to 400 °C [50]. Most importantly, the selectivity of the catalysts rises with increasing the particle size.

Sometimes, thermal treatments affect the migration of some reduced support constituents, or the presence of certain co-components leads to the formation of mixed metal particles or intermetallics. Migration of carbon into the Pd-bulk and surface was observed for a Pd/C catalyst upon reductive pretreatment at 300 °C [51]. However, the Pd-surface has been successfully protected from contamination by calcination at 300 °C in 4 % oxygen or by cooling in the oxidized atmospheres. Nevertheless, the presence of carbon atoms in the Pd-bulk or on the surface is also sometimes useful for example, in hydrogenation of benzene or in the oxidation or reduction of CO [52].

In the case of a bimetallic Pd,Pt/Al<sub>2</sub>O<sub>3</sub> catalyst, a change in the surface Pd/Pt atomic ratio (by XPS) was observed upon treatment in H<sub>2</sub> at 400 °C [53]. In this case, Pd was virtually inactive and acted as a site blocker, which decreased the size of Pt ensembles and hindered the formation of the bulky transition complex between the reactant and the chiral modifier in enantioselective hydrogenation of ethyl pyruvate and ketopanto-lactone.

In the present investigations (described in the Chapter 3 and 4), the thermal treatment has also been found to be very important (especially in helium), because such treatment reduced the conditioning time due to the preferential formation large Pd-particles. In addition, it was also essential for removing chloride from metal precursor in presence of additives [12].

### 1.3.5 Influence of co-components for Pd-catalysts

Frequently, the active Pd-particles are modified by adding a second metal to improve their stability and catalytic performance. Generally, reasons for the beneficial influence of co-components on the catalytic performance could be geometric or electronic in nature, known as ensemble or ligand effects. For Pd-based catalysts, e.g., Bi, Pb, Sb or Au have been used as co-components or promoters in several reactions [54-56]. Co-components can influence the nature and catalytic performance of supported Pd-catalysts in different ways. Thus, geometrical blocking of active sites which catalyze undesired side reactions

can enhance the selectivity of the target product. This has been achieved for example in the oxidation of 1-phenylethanol by modifying the Pd-catalyst with Bi [57]. Another beneficial effect is the improvement of the catalyst stability by suppressing the deposition of coke or by altering the nature of carbon deposits [11]. On the other hand, alloy formation between Pd and the co-component can create new surface sites, which may facilitate the adsorption of necessary intermediates, e.g., hydroperoxy intermediates in the oxidation of alcohols [58]. However, as we have shown recently, the formation of a crystalline Pd<sub>8</sub>Sb<sub>3</sub> alloy after thermal pretreatment in 10 % H<sub>2</sub>/He, leads to complete activity loss in the acetoxylation of toluene to benzyl acetate (BA) [13]. In some reactions, which require a high dispersion of the active Pd-site, the addition of a second metal can be helpful to enhance the dispersion. For instance, the addition of Ni to supported Pd-catalysts in CO oxidation is one such example [59]. Au as a noble metal stabilizes the metallic Pd in many reactions. One such reaction is the acetoxylation of ethylene to vinyl acetate monomer (VAM) [60-63], which is the most important gas phase acetoxylation reaction in industry. Addition of Au inhibited effectively the formation of detrimental PdC<sub>x</sub> due to Pd-Au alloy surface species and enhances the dispersion of Pd-species.

M. Chen et al. proposed for the same reaction that the spacing between active centers (Pd-monomers) on Au(111) is 4.08 Å, which is close enough for coupling of the adsorbed surface species (Fig. 1.2) and small particles are favorable for this reaction [56]. The same authors supposed that reaction rate and selectivity were depending on the particle size (small particles favor the reaction). This indicates a certain degree of structure sensitivity.

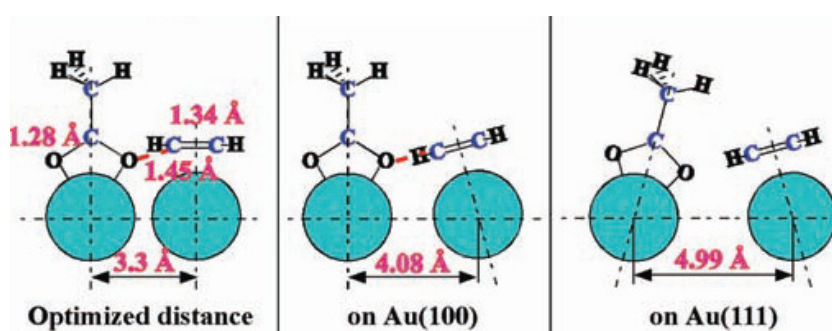


**Fig. 1.2** Coupling of an ethylene and acetate species on a Pd-monomer pair on Au(100) on Au(111). Figure adapted from ref.[56].

The restructuring of the alloyed noble metal particles, with time on stream, led to the deactivation of the PdAu catalyst [16]. Migration of Au into the Pd-particle bulk leading to a separation of active Pd-Au surface sites has been regarded as one possible reason among others for activity loss [64]. However, it should be noted that the deactivation of this catalyst

was observed after a long period of time (~ 6 month). This shows that Au as co-component remarkably improved the stability by maintaining the high selectivity in the VAM synthesis.

Moreover, promoters can also influence the electronic nature of the active component. In oxidation reactions, less noble metals such as bismuth located in the vicinity of active Pd-species are preferentially oxidized and, therefore, can stabilize metallic Pd<sup>0</sup> and enhance the life time of the catalyst [65]. Recently, it was reported that alloy formation between Au and Pd promotes the decomposition of PdO and can improve the catalytic performance in the CO oxidation reaction [66].

Such kind of beneficial influence of co-components is also observed in the investigations presented in this thesis. For this purpose, co-components with lower (Mn, Co, Sb) and higher reduction potential (Au) than Pd were used. Profound influence of co-components especially on the electronic state of Pd and, consequently on activity, selectivity and stability in the gas-phase acetoxylation of toluene to BA is observed [15].

### 1.3.6 Role of supports for Pd-particles

The performance of catalysts is often changed by the use of different supports because of their different physical and chemical properties like thermal stability, acid-base properties, high surface area, oxygen storage capacity and reducibility. The selection of a particular support for the metal particles is often based on the point of zero charge PZC of the support [67]. The increasing order of PZC of the some common supports is as follows: MoO<sub>3</sub> > Nb<sub>2</sub>O<sub>3</sub> > SiO<sub>2</sub> > TiO<sub>2</sub> > CeO<sub>2</sub> > ZrO<sub>2</sub> > Co<sub>3</sub>O<sub>4</sub> > Al<sub>2</sub>O<sub>3</sub> > activated carbon ≈ carbon black. MoO<sub>3</sub> or NbO<sub>3</sub> have high acidic PZC, i.e., a negatively charged surface is good for adsorption of cationic metal precursors, whereas carbon supports with high PZC are useful to support the metal particles in the reduced state. Supports from TiO<sub>2</sub> to Al<sub>2</sub>O<sub>3</sub> are useful for both cationic and anionic species. However, sometimes, modifications in the preparation conditions, thermal pretreatments can also dominate the role of supports.

Pd-catalysts supported on activated carbon, Al<sub>2</sub>O<sub>3</sub> and MgO were studied for cumene hydroperoxide (CHP) hydrogenation by Q. C. Zhu et al. [68]. Among them, Pd supported especially on Al<sub>2</sub>O<sub>3</sub> showed a better performance in terms of activity and stability, because of high surface acidity and hydrothermal stability. However, drop in the activity was noticed due to a change in the support structure and Pd sintering. Acidity of the support is also found to be useful in hydrocracking reactions, for example in the hydrocracking of paraffin wax to middle distillate in which the optimum acidity of SiO<sub>2</sub>-Al<sub>2</sub>O<sub>3</sub> xerogel is useful for the Pd-catalyst to show the highest yield [69]. A catalyst, in which the palladium component was

supported on ligand-functionalized amorphous or ordered mesoporous silica, was used for oxidation of a variety of alcohols using molecular oxygen [70]. It was found that the amorphous silica, the nature of the ligand and the solvent could effectively control the generation of Pd-nanoparticles, which are highly active for aerobic oxidation of alcohols.

There are several reactions in which the nature of the support influences the properties of metal particles and, thus, the catalyst performance. In some reactions the adsorbed oxygen on the support was found to be useful for activity. For example, high activity for CO oxidation was observed on Pd,Pt catalysts suspended on a series of  $\text{FeO}_x$  and  $\text{Al}_2\text{O}_3$  supports. This is due to the adsorption of a large amount of oxygen on  $\text{FeO}_x$  support, which reduced the apparent activation energies [71]. A similar kind of mechanism related to oxygen transfer from  $\text{CeO}_2$  is also useful in catalytic wet air oxidation (CWAO) of aniline, phenol, carboxylic acids and ammonia over Ru, Pd, Pt [72] catalysts.

The catalyst design can be markedly supported by understanding the nature of metal-support surface interactions and/or strong metal-support interaction (SMSI), which strongly affect the dispersion and morphology of the metal particles [73]. Generally, SMSI can be observed between transition metals and reducible oxide supports like  $\text{TiO}_2$ ,  $\text{ZrO}_3$ ,  $\text{V}_2\text{O}_5$  and  $\text{CeO}_2$  [74]. In broader prospective, defects such as oxygen vacancies play a crucial role in the surface properties of transition metal oxides [75] in addition to terraces and steps [76]. The oxygen vacancies themselves diffuse on the surface in the presence of oxygen in the gas phase [75]. Such oxygen defects on the  $\text{TiO}_2$  supports are also useful for the good dispersion and morphology of nanosized metal particles [77, 78]. Even a clean rutile- $\text{TiO}_2(110)$  surface contains 5-10 % surface oxygen defects [77, 79-81].

DFT calculation of an anatase  $\text{TiO}_2(101)$  and rutile  $\text{TiO}_2(110)$  surface [82] revealed that defects are significantly more stable in the subsurface in case of anatase, but on the surface in rutile. Therefore, due to low defect concentration of the anatase surface, metal-support interaction was diminished and in turn, led to eventual sintering of metal particles. In addition, mostly bridging oxygen sites are favored for O vacancies in rutile, and due to the corrugated surface structure, they promote the anisotropic growth of the metal particles.

Several studies were done to explore the interaction between the  $\text{TiO}_2$  (rutile) support and other noble metals like Pt, Pd, Rg and Au. Especially, the gold particles, sufficiently attached to oxygen vacancies are generally free from sintering [77]. Hydrogenation of acetylene (in excess ethylene) to ethylene is favorable if such SMSI exists between Pd and rutile support [83].

In general, among anatase and rutile, anatase is the more widely used as a support mostly for nanosize metal particles, particularly in gas phase reactions due to the strong metal support interactions (SMSI) and high surface area, whereas, rutile is the favorite support for the surface science community because of high thermodynamic stability of its phases and more over the presence of a similar kind of oxygen vacancies [75, 84] which supports the anisotropic growth of the metal particles [78].

In this thesis we present a comparative study about the role of anatase and rutile as supports for a 10Pd,16Sb catalyst in the gas phase acetoxylation of toluene. A clear difference between anatase and rutile supported Pd,Sb catalysts in terms of growth, valance and composition of Pd-particles as well as catalytic performance was observed.

#### **1.4 Liquid-phase reactions for acetoxylation of toluene**

In 1968, J.M. Davidson et al. studied for the first time the acetoxylation of toluene in acetic acid with Pd(OAc)<sub>2</sub> and Pb(OAc)<sub>4</sub> catalyst systems. In the initial developments of this reaction, most of the studies were related to liquid phase processes on solid Pd-catalysts and carried out in batch reactors. Several modifications were introduced to improve the performance of the catalysts by choosing different Pd-precursors like hydroxides, chlorides, clusters or complexes. Moreover, nearly every catalyst system contained one or more co-components. Most importantly, Sn was used as a co-component for Pd-supported catalysts and NaOAc or KOAc salts were added to the reaction mixture. Sn as co-component is useful to reduce the palladium to the active metallic form, whereas acetate salts facilitated the adsorption of the reaction mixture on the solid catalyst. Some of the major investigations related to the acetoxylation of toluene (Tol) to benzyl acetate (BA) and to some other byproducts especially in liquid phase are summarized in Table 1.1.

Formation of metallic Pd was observed in most of the reactions and considered as active phase by many authors. In addition, the presence of oxidized Pd in the vicinity to metallic Pd was also believed to increase the activity [17]. Co-components like Sn [7], Cu [85] and K [86] or Na [87] (from KOAc or NaOAc) seem to assist for the formation of the desired Pd-phase. Among them, Cu or Sn improved the oxygen adsorption on the surface and in subsurface layers of Pd-particles, which led to improve the performance of the catalyst. Apart from co-components, the supports such as SiO<sub>2</sub> [88], charcoal [7] and TiO<sub>2</sub> [17] with a high dispersion of the supported metal particles were also found to improve the performance of the catalysts. Studies of K. Ebitani et al. revealed that TiO<sub>2</sub> as a support stabilized the metallic Pd-clusters. On the other hand, thermal treatments of a Pd,Sn/SiO<sub>2</sub> catalyst especially in helium was



useful to get the metallic Pd-particles, instead of intermetallics, prior to the reaction [88]. These studies also revealed the importance of co-components, supports and finally thermal pretreatments.

**Table 1.1** Some important studies related to acetoxylation of toluene in the liquid phase and necessary remarks.

Catalyst	Conditions			Performance	Remarks	Year / Ref.
	T / °C	P / atm	Time / h			
Pd(OAc) <sub>2</sub> or Pd(OAc) <sub>4</sub>	100	1 and 100	4	BA and 3,3'-dimethylbiphenyl	Reduction of precursors to Pd <sup>0</sup>	1968/[89]
Pd(OAc) <sub>2</sub> /Sn(OAc) <sub>4</sub> , charcoal	100	1	5	91.4 % of BA with 79.7 % Tol conversion	Charcoal indirectly acted as support and enhances the dispersion of Pd <sup>0</sup>	1968/[7]
Pd(OAc) <sub>2</sub> , KOAc PdCl <sub>2</sub> , NaOAc	100	1	5	92.5 % of BA 62.5 % of BA	Pd-species of lower aggregation is favorable and formed from Pd(OAc) <sub>2</sub> rather PdCl <sub>2</sub> .	1968/[86]
Pd/Al <sub>2</sub> O <sub>3</sub> , KOAc	120	50	0.16	92.6 % of BA with 19 % Tol conversion	Pre reduction of Pd with N <sub>2</sub> H <sub>4</sub> •H <sub>2</sub> O	1968/[90]
Pd/Al <sub>2</sub> O <sub>3</sub> , NaOAc	145	1	-	12.4% BA and 12.2% Benzyl diacetat	NaOAc improves the adsorption of acetic acid	1972/[87]
Pd(OAc) <sub>2</sub> (H <sub>5</sub> PMo <sub>10</sub> V <sub>2</sub> O <sub>40</sub> , H <sub>9</sub> PMo <sub>6</sub> V <sub>6</sub> O <sub>40</sub> )	70 - 100	1.6	-	PhOAc, o-, m-, p-MeC <sub>6</sub> H <sub>4</sub> OAc	OAc substitution on ring rather acetoxylation of toluene	1977/[91]
Pd <sup>+</sup> , Pd <sup>2+</sup> complexes, Pd <sup>0</sup> , and Pd-clusters	-	-	-	BA	Pd <sup>0</sup> were active species are especially in clusters	1979/[92]
Co-Cu-NaBr	100	1	20	50-70 % BA with 12-98 % Tol conversion	Optimum ratio (Cu:Cu:Br = 1:1:5-10)	1979/[85]
Pd <sub>4</sub> (CO) <sub>4</sub> (OAc) <sub>4</sub> o-phenanthroline ligands	-	-	-	BA	Pd <sup>2+</sup> are inactive and active Pd <sup>0</sup> formed during the reaction	1980/[93]
Pd/Sn/K From acetate precursors	100	1.2	3	BA 77 % selectivity of BA at 100 % Tol conversion	Sn <sup>2+</sup> , K <sup>+</sup> and charcoal lead to Pd(OAc) <sub>2</sub> decomposition Pd <sup>0</sup>	1991-93 / [94, 95]
PdSn/SiO <sub>2</sub> (Cl) KOAc	70	1	3	BA and Benzyl diacetate	He / 300 °C / 2 h prior to the reaction	1993/[88]
Pd(OAc)/ Sn(OH)/KOAc on Si gel	70	1	3	90 % selectivity of BA, with ~1.2 mol of Tol conversion	Oxygen on surface and subsurface layers of Pd in Sn presence	1994/[96]
(Pd <sub>4</sub> (CO) <sub>4</sub> (OAc) <sub>4</sub> •2AcOH Cluster alone and on TiO <sub>2</sub> support.	90	1	3	94 % yield of BA	Pd-cluster of Pd <sup>0</sup> / Pd <sup>2+</sup> are surface active phase	2002/[17]

## 1.5 Gas-phase reactions for acetoxylation of toluene

Gas phase reactions are industrially more profitable because the separation of the products is easy, the problem of leaching of active components from the catalyst (usually observed in liquid phase reactions) is less and the reaction can be carried over a long period of time.

First, gas phase acetoxylation of toluene was studied by Ebersson et al. over Pd/Al<sub>2</sub>O<sub>3</sub> promoted with Ag, Bi and Cr [97] in 1974. In fact, their goal was to achieve nucleophilic substituted compounds like ortho, meta and para-acetoxytoluene. However, benzyl acetate was formed as a major product. More importantly, it was formed only in the presence of co-components. XPS analysis from spent samples revealed that in the presence of promoters, especially of Cr in addition to Bi, Pd (II) was formed besides Pd (0) on the surface. XPS Pd3d<sub>5/2</sub> spectra of the Pd/Al<sub>2</sub>O<sub>3</sub> catalyst with a) Bi and b) Ag/Bi/K<sub>2</sub>Cr<sub>2</sub>O<sub>3</sub> can be seen in Fig. 1.3.

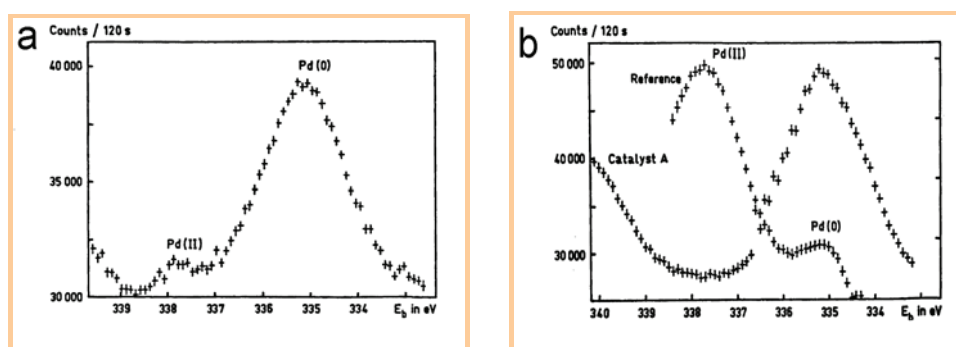


**Fig. 1.3** XPS Pd3d<sub>5/2</sub> spectra of spent Pd/Al<sub>2</sub>O<sub>3</sub> catalyst promoted with a) Bi, b) Ag, Bi, K<sub>2</sub>Cr<sub>2</sub>O<sub>3</sub> (Figure is adapted from ref.[97]).

They supposed that the redox system Cr<sup>3+</sup>/Cr<sup>4+</sup> was acting as mediator between O<sub>2</sub> and Pd (0) and hence possibly promotes the formation of Pd (II) on the catalyst surface during the reaction. This shows that co-component with low reduction potential (E<sup>0</sup>) are useful to maintain the oxidized Pd besides metallic Pd during the reaction.

Later T. Komatsu et al. studied the role of intermetallic compounds on the gas phase acetoxylation of toluene [18]. They deposited the desired particles on a SiO<sub>2</sub> support by successive hydrogen treatment at high temperatures. Among PdFe, Pd<sub>5</sub>Ge, Pd<sub>5</sub>Ga<sub>2</sub>, Pd<sub>2</sub>Ge, PdZn, PdIn, Pd<sub>3</sub>Tl, PdCd, Pd<sub>3</sub>Pb and Pd<sub>3</sub>Bi intermetallics used, Bi, Pb, Cd and Tl containing catalysts showed high selectivity for benzyl acetate, whereas palladium metal alone was not selective for this reaction, however, it was active (showed high toluene conversion). Mainly two reasons have been proposed to explain the performance of the catalysts: 1) an oxide layer of the second element (co-component) formed during time on stream and acted as a support of fine palladium particles; 2) catalysts containing co-component with covalent radii of about



0.15 nm showed high yield of benzyl acetate. Authors observed that the yield increased with increasing covalent radius, reached the maximum at about 0.15 nm for bismuth and lead, and decreased for the larger radii of cadmium and thallium. They supposed that the distance between palladium atoms in Pd<sub>3</sub>Bi and Pd<sub>3</sub>Pb might be appropriate for the formation of a reaction intermediate during acetoxylation; however adequate explanation was missing. In any case, the selectivity is improved only until 36 % with Bi with only a low toluene conversion ( $\approx 18$  %).

Later, Q. Shu et al. investigated the gas-phase acetoxylation of toluene with acetic acid to benzyl acetate over Pd/SiO<sub>2</sub> promoted with Sn and K [98]. Initially, they focused their study to remove Cl from the catalyst system during its preparation. They found that the removal of Cl was very important for the catalyst performance because it promotes the Pd-particle growth. Furthermore, they studied the effect of thermal treatment and the influence of the promoter (Sn) [99] on the catalyst performance. Higher activity was observed when the catalyst was prepared by reduction of the palladium component on SiO<sub>2</sub> in H<sub>2</sub> before Sn loading. Almost 25.3 % of toluene conversion with 91 % of selectivity for benzyl acetate was achieved over the Pd-Sn-K/SiO<sub>2</sub> catalyst, whereas lower activity and selectivity were obtained when Pd was replaced with other noble metals. Another important observation was that reduction treatments after Sn addition led to the formation of intermetallic compounds like Pd<sub>1</sub>Sn<sub>1</sub> or Pd<sub>20</sub>Sn<sub>13</sub> and as consequence the catalyst lost its activity predominantly. Thus, from the current studies of Shu et al. [98] and Komatsu et al. [18], we can say that the co-components are quite useful to improve the catalyst performance; however formation of intermetallics should be avoided because they might not be good candidates for this reaction.

Benhmid et al. paid much attention to improve the activity of the catalysts for gas phase acetoxylation of toluene. Their study included the role of different promoters (Sb, Sn, Cu, Bi) and supports (TiO<sub>2</sub> (anatase), ZrO<sub>2</sub>, Al<sub>2</sub>O<sub>3</sub>, SiO<sub>2</sub>) on the Pd-catalyst performance [2-6, 8-11]. The major findings from their investigations are as follows

Initially, single metals (Pd or Sb) supported on TiO<sub>2</sub> anatase showed only < 5 % toluene conversion. However, the combination of both Pd and Sb significantly enhanced the activity of the Pd and Sb supported catalysts. Initially, a model catalyst with 5 wt.-% Pd and 8 wt.-% Sb on TiO<sub>2</sub> was tested and showed nearly 16 to 18 times higher activity (X-Tol  $\sim 37$ %; Y-BA  $\sim 32$ %) than that containing TiO<sub>2</sub>-supported monometallic Pd or Sb. Then, catalysts with different weight contents have been tested for this reaction.

Afterwards, Pd/TiO<sub>2</sub> catalyst was modified by adding other promoters like Cu, Bi [4] and Sn and the activity was compared with the Sb catalyst. Among them, the 10Pd,8Sb/TiO<sub>2</sub>

catalyst showed high toluene conversion (68.5 %) and yield of benzyl acetate (58.3 %). However, the catalyst needed a 10-12 h induction period to reach maximum activity and deactivated further on stream, whereas the catalyst with Cu as co-components showed high selectivity ( $\sim 90$  %) without deactivation. However this catalyst needed even longer conditioning time of 60 h. On the other hand, the Sn catalysts also suffered from long conditioning time. One common property among all the samples is that Pd-particles grew during the conditioning time along with the toluene conversion and yield of benzyl acetate from few nanometers to  $\approx 80$ -100 nm and slight size variations are depending on the co-component used. This shows that the catalysts needed a certain time, temperature and atmosphere for the growth of the Pd-particle up to the optimum size. Among all the samples, bigger Pd-particles were formed in Sb catalyst, followed by Sn, Cu and Bi, whereas the order of activity (toluene conversion) is  $\text{Sb} > \text{Cu} > \text{Sn} > \text{Bi}$ .

Simultaneous investigations have been done for Pd,Sb supported on different support like  $\text{ZrO}_2$ ,  $\text{Al}_2\text{O}_3$ ,  $\text{SiO}_2$ . Among all,  $\text{TiO}_2$  anatase was found to be the most suitable support. The key parameters which influenced the performance of the catalyst were the Pd-particle size (*from* TEM), valence states of Pd (*from* XPS) and acidity characteristics (*from* FT-IR pyridine adsorption). They emphasized that bigger Pd-particles were active for this reaction. The trend in the Pd-particle size and the activity is as follows:  $\text{TiO}_2 > \text{SiO}_2 > \text{ZrO}_2 > \gamma\text{-Al}_2\text{O}_3$ . The yields of products obtained over 10Pd,8Sb/MeOx (MeOx =  $\text{TiO}_2$ ,  $\text{SiO}_2$ ,  $\text{ZrO}_2$ ,  $\gamma\text{-Al}_2\text{O}_3$ ) catalysts and TEM images of the  $\text{TiO}_2$ ,  $\gamma\text{-Al}_2\text{O}_3$  supported 10Pd,8Sb catalysts after time on stream are shown in Fig. 1.4.

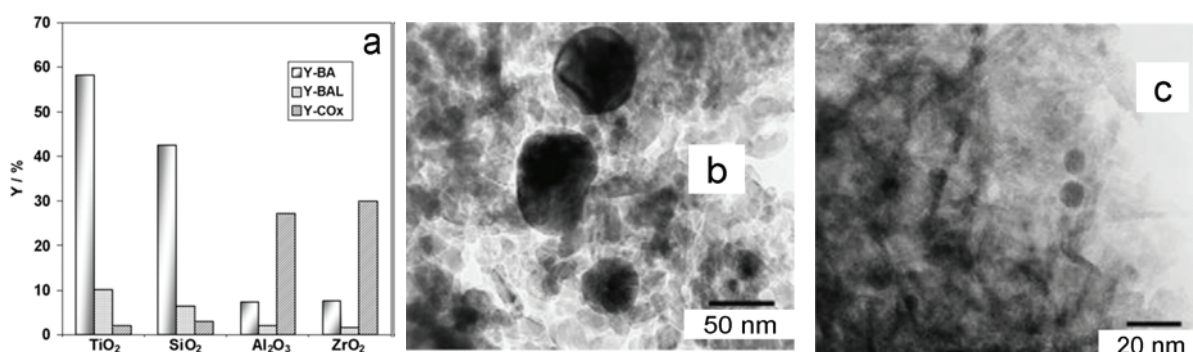


**Fig. 1.4:** a) Comparison of the yields of products obtained over 10Pd,8Sb/MeOx (MeOx =  $\text{TiO}_2$ ,  $\text{SiO}_2$ ,  $\text{ZrO}_2$ ,  $\gamma\text{-Al}_2\text{O}_3$ ) catalysts; b, c) electron micrographs of the spent 10Pd8Sb catalysts on different supports (b:  $\text{TiO}_2$ ; c:  $\gamma\text{-Al}_2\text{O}_3$ ). Figure is adopted from ref.[9].

## Chapter 2

### **Preparation and testing of the catalysts, principle and applications of the characterization methods**

---

---

Chapter 2 covers a complete description about the preparation of supported Pd-catalysts by using different metal precursors, co-components, additives as well as supports. The experimental conditions used to test the solid catalysts for the gas phase acetoxylation of toluene are mentioned. Finally, the principle and applications of various characterization methods used in the present investigation are described.

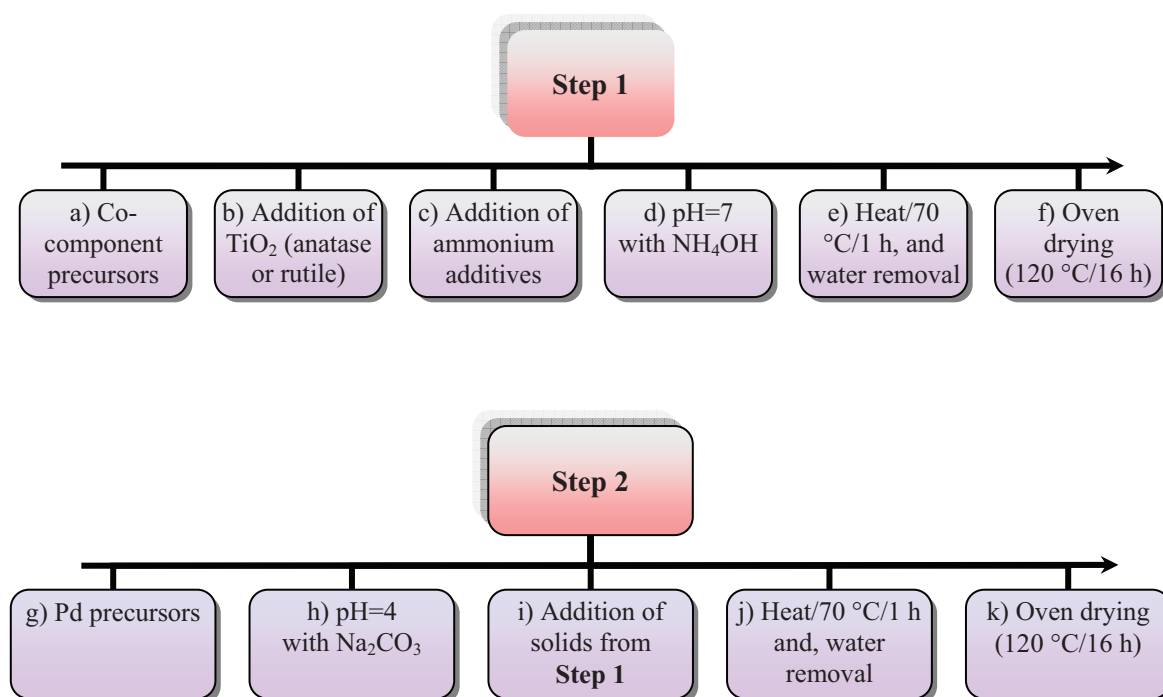
---

---

## 2.1 Catalysts preparation and testing

### 2.1.1 General procedure

A scheme of the general preparation procedure of solid samples involving a two step impregnation process is given in Scheme 2.1. Several Pd-catalysts were prepared by using different co-components (Cu, Sb, Mn, Co and Au), metal precursors (chlorides, nitrates, acetates and in case of Sb also  $\text{Sb}_2\text{O}_3$ ), supports (anatase, rutile) and additives ( $(\text{NH}_4)_2\text{SO}_4$ ,  $\text{NH}_4\text{NO}_3$ ,  $(\text{NH}_4)_2\text{CO}_3$  and urea). The latter have been added to facilitate the removal of chloride as volatile  $\text{NH}_4\text{Cl}$ .



**Scheme 2.1.** Several stages (from a to k) involved in the preparation of solid samples by two step impregnation process. Preparation method is adapted from ref.[10].

The procedure comprises the deposition of the co-components in the first step followed by deposition of palladium in the second step. For example, a catalyst with a nominal content of 10 wt.-% Pd and 8 wt.-% of Sb using chloride precursors and  $(\text{NH}_4)_2\text{SO}_4$  as an additive was prepared as follows. To get 10 g of the final catalyst,  $\approx 8.2$  g of  $\text{TiO}_2$  was added to the aqueous slurry of  $\text{Sb}_4\text{O}_5\text{Cl}_2$  (it was prepared by the addition of water to  $\text{SbCl}_3$  and the formation of  $\text{Sb}_4\text{O}_5\text{Cl}_2$  was confirmed by XRD, FT-IR analysis), and stirred for 1 h at room temperature. Then, 13.2 ml of a 2.75 M aqueous solution of the  $(\text{NH}_4)_2\text{SO}_4$ , was introduced and stirred for 1 h at 70 °C. By adding the required amount of 25 %  $\text{NH}_4\text{OH}$ , a value of pH = 7 was adjusted. Then, the resulting suspension was further stirred for 1 h at 70 °C and finally water was removed with a rota evaporator at the same

temperature. The obtained solid was dried at 120 °C for 16 h.

The second step deals with the impregnation of Pd on the above solid obtained from Step 1. A value of pH = 4 was adjusted by drop wise addition of 1N Na<sub>2</sub>CO<sub>3</sub> to the acidified aqueous PdCl<sub>2</sub> solution. Thereafter, the solid from Step 1 was added to the above solution. The resultant suspension was stirred for 1 h at 70 °C, and a water evaporation step is followed. The final sample was dried at 120 °C for 16 h.

The oven dried sample was calcined (300 °C-air) in situ in the reactor or externally treated in helium at 600 °C before testing the catalyst for gas phase acetoxylation of toluene. Comprehensive characterization of the catalysts revealed that some sulfide remains in the samples, which were prepared using (NH<sub>4</sub>)<sub>2</sub>SO<sub>4</sub>. Since these sulfide species may be reason for the low catalytic activities observed in certain cases, SO<sub>4</sub>-free additives have been used for the preparation of further catalysts.

A list of 10 wt.-% Pd,8 wt.-% Sb/TiO<sub>2</sub> catalysts prepared by the above mentioned procedure by using different metal precursors and additives, is shown in Table 2.1. In addition, similar catalysts however with Cu as co-component instead of Sb were also prepared, as shown in Table 2.1. The influence of the above mentioned parameters and thermal treatments (helium and 10 %H<sub>2</sub>/He) on the structural phases and Pd-particle formation is described in Chapter 3.

**Table 2.1** List of the 10Pd,8Sb/TiO<sub>2</sub> and 10Pd,8Cu/TiO<sub>2</sub> catalysts prepared using different precursors and additives. (Catalysts of Chapter 3).

Catalyst composition (amount of support)	Pd-Precursor solution	Co-component solution / slurry	Additive solution (13.2 ml of 2.75 M)
10 wt.-% Pd,8 wt.-% Sb/TiO <sub>2</sub> (8.296 g)	Pd(CH <sub>3</sub> COO) <sub>2</sub> (1.9290 g + 2 M HCl)	Sb(CH <sub>3</sub> COO) <sub>3</sub> (1.9659 g + 10 ml H <sub>2</sub> O)	(NH <sub>4</sub> ) <sub>2</sub> SO <sub>4</sub>
(8.2492 g)	PdCl <sub>2</sub> (1.6712 g + 10 ml 2 M HCl)	Sb <sub>4</sub> O <sub>5</sub> Cl <sub>2</sub> (1.4998 g SbCl <sub>3</sub> + 10 ml H <sub>2</sub> O)	(NH <sub>4</sub> ) <sub>2</sub> SO <sub>4</sub>
(8.20 g)	(1.6675 g + 10 ml 2 M HCl)	(1.4528 g SbCl <sub>3</sub> + 10 ml H <sub>2</sub> O)	(NH <sub>4</sub> ) <sub>2</sub> CO <sub>3</sub>
(8.2010 g)	(1.6681 g + 10 ml 2 M HCl)	(1.5110 g SbCl <sub>3</sub> + 10 ml H <sub>2</sub> O)	NH <sub>4</sub> NO <sub>3</sub>
(8.210 g)	(1.6671 g + 9.4 ml 2 M HCl)	(1.5111 g SbCl <sub>3</sub> + 10 ml H <sub>2</sub> O)	Urea
(8.20 g)	(1.6700 g + 10 ml 2 M HCl)	(1.4999 g SbCl <sub>3</sub> + 10 ml H <sub>2</sub> O)	No additive
10 wt.-% Pd,8 wt.-% Cu/TiO <sub>2</sub> (8.292 g)	Pd(NO <sub>3</sub> ) <sub>2</sub> •2 H <sub>2</sub> O (2.5040 g + 16 ml H <sub>2</sub> O)	Cu(NO <sub>3</sub> ) <sub>2</sub> •3H <sub>2</sub> O (3.0446 g + 10 ml H <sub>2</sub> O)	(NH <sub>4</sub> ) <sub>2</sub> SO <sub>4</sub>
(8.292 g)	Pd(CH <sub>3</sub> COO) <sub>2</sub> (1.9289 g + 2 M HCl)	Cu(CH <sub>3</sub> COO) <sub>2</sub> •H <sub>2</sub> O (2.5860 g + 10 ml H <sub>2</sub> O)	(NH <sub>4</sub> ) <sub>2</sub> SO <sub>4</sub>

(8.286 g)	<b>PdCl<sub>2</sub></b> (1.6675 g + 11 ml 2 M HCl)	<b>CuCl<sub>2</sub>•2 H<sub>2</sub>O</b> (2.4174 g + 10 ml H <sub>2</sub> O)	(NH <sub>4</sub> ) <sub>2</sub> SO <sub>4</sub>
(8.20 g)	(1.6671 g + 10 ml 2 M HCl)	(2.1513 g + 10 ml H <sub>2</sub> O)	<b>(NH<sub>4</sub>)<sub>2</sub>CO<sub>3</sub></b>
(8.0 g)	(1.6842 g + 10 ml 2 M HCl)	(2.1513 g + 10 ml H <sub>2</sub> O)	<b>NH<sub>4</sub>NO<sub>3</sub></b>
(8.20 g)	(1.6670 g + 9 ml 2 M HCl)	(2.1470 g + 10 ml H <sub>2</sub> O)	<b>Urea</b>
(8.2352 g)	(1.6671 g + 10 ml 2 M HCl)	(2.1476 g + 10 ml H <sub>2</sub> O)	<b>No additive</b>

### 2.1.2 Preparation of 10 wt.-% Pd,16 wt.-% Sb/TiO<sub>2</sub> (anatase, rutile) using Sb<sub>2</sub>O<sub>3</sub>, without additives

Alternatively, Sb<sub>2</sub>O<sub>3</sub> has been used as co-component precursor for catalysts with nominal amounts of 10 wt.-% Pd, 16 wt.-% Sb. In this case, neither ammonium containing agents nor urea was used.

In addition, an intermediate calcination step (400 °C / air / 3 h) was also performed for the oven dried samples after first step of the preparation (i.e. after impregnation of Sb<sub>2</sub>O<sub>3</sub> on the support).

Especially, anatase supported 10Pd,16Sb catalyst, after conventional in situ calcination (300 °C in air for 2 h) in the reactor, showed deactivation in the acetoxylation reaction. Therefore, to improve the catalyst stability and product selectivity high temperature thermal pretreatment at 600 °C in air, He and 10 % H<sub>2</sub>/He was done prior to the testing. Impact of thermal treatments on the structure of Pd and its influence on the catalyst performance is described in Chapter 4, whereas the comparison between the activity of anatase and rutile supported catalysts after conventional activation is described in Chapter 6. Table 2.2 shows the preparation details of TiO<sub>2</sub> anatase and rutile supported 10Pd,16Sb catalysts as well as conditions of the thermal pretreatments (300 °C and 600 °C) and atmosphere (air, He, 10 % H<sub>2</sub>/He).

**Table 2.2** TiO<sub>2</sub> anatase and rutile supported 10Pd,16Sb catalysts prepared using Sb<sub>2</sub>O<sub>3</sub> and PdCl<sub>2</sub>, and without additives. (Catalysts of Chapter 4 & 6\*)

Catalyst composition (amount of support)	Pd-Precursor Solution	Co-component slurry	Thermal pretreatment
10 wt.-% Pd,16 wt.-% Sb/Antase (8.2061 g)	PdCl <sub>2</sub> (1.6682 g + 12.3 ml 2 M HCl)	Sb <sub>2</sub> O <sub>5</sub> (1.9171+ 15 ml H <sub>2</sub> O)	300 °C-air / 2 h*
”	”	”	600 °C-air / 4 h
”	”	”	600 °C-He / 4 h
10 wt.-% Pd,16 wt.-% Sb/Rutile (8.2015 g)	PdCl <sub>2</sub> (1.6762 g + 12.1 ml 2 M HCl)	Sb <sub>2</sub> O <sub>5</sub> (1.9251+ 15 ml H <sub>2</sub> O)	300 °C-air / 2 h*

### 2.1.3 Preparation of 10 wt.-% Pd,8 wt.-% M/TiO<sub>2</sub> anatase (M=Sb, Mn, Co, Au) with oxide and chloride precursors, without additives

To explore the effect of co-components (Mn, Co, Au) with a wide range of standard reduction potentials ( $E^0$ : Mn<sup>2+</sup>/Mn = -1.18 eV, Co<sup>2+</sup>/Co = -0.28 eV and Au<sup>3+</sup>/Au = +1.52 eV) on the catalyst performance, 10 wt.-% Pd,8 wt.-% M/TiO<sub>2</sub> (anatase) (M=Mn, Co, Au) catalysts were prepared from chloride precursors. For comparative study of the role of co-components, additionally, 10Pd,8Sb/TiO<sub>2</sub> catalyst was also taken into account. An intermediate calcination step (400 °C / air / 3 h) was performed also for the present samples. In Table 2.3, list of the catalysts prepared with different co-components and after final thermal pretreatment (300 °C-air) are summarized.

**Table 2.3** List of the 10Pd,8M/TiO<sub>2</sub> anatase (M=Sb, Mn, Co, Au) catalysts prepared using oxide and chloride precursors, and without additives. (Catalysts of Chapter 5)

Catalyst (amount of support)	Pd-Precursor solution	Co-component solution /slurry	Thermal pretreatment
10 wt.-% Pd,8 wt.-% Sb/TiO <sub>2</sub> (8.2061 g)	PdCl <sub>2</sub> (1.6671 g + 12.2 ml 2 M HCl)	Sb <sub>2</sub> O <sub>5</sub> (0.9511+ 15 ml H <sub>2</sub> O)	300 °C-air / 2 h
10 wt.-% Pd,8 wt.-% Mn/TiO <sub>2</sub> (8.2041 g)	(1.7045 g + 12.1 ml 2 M HCl)	MnCl <sub>2</sub> (1.8447+ 10 ml H <sub>2</sub> O)	300 °C-air / 2 h
10 wt.-% Pd,8 wt.-% Co/TiO <sub>2</sub> (8.2068 g)	(1.7019 g + 12.1 ml 2 M HCl)	[Co(NH <sub>3</sub> ) <sub>6</sub> ]Cl <sub>3</sub> (3.6384+ 10 ml H <sub>2</sub> O)	300 °C-air / 2 h
10 wt.-% Pd,8 wt.-% Au/TiO <sub>2</sub> (8.3029 g)	(1.6853 g + 12.1 ml 2 M HCl)	HAuCl <sub>4</sub> (1.3854+ 10 ml H <sub>2</sub> O)	300 °C-air / 2 h

### 2.1.4 Catalyst testing

Catalytic tests were performed in a fixed-bed Hastelloy C micro reactor at 210 °C and 2 bar total pressure with 0.8 g catalyst particles (0.425–0.6 mm). The catalyst particles were diluted with the fivefold amount of corundum particles to avoid hot spot formation during the

reaction. Prior to the catalytic tests, the samples were calcined in situ in the catalytic reactor in a flow of 27.6 ml/min air at 300 °C for 2 h or externally treated in the oven in presence of air He or 10 % H<sub>2</sub>/He (50 ml/min) at 600 °C for 4 h. The liquid reactants toluene (>99.9 %, Roth, Germany) and acetic acid (>99.9 %, Walter CMP, Germany) in a molar ratio of 1:4 were dosed by a HPLC pump, while highly purified gases (>99.99) were metered by mass flow controllers, resulting in a total feed mixture of toluene:acetic acid:oxygen:nitrogen = 1:4:3:16. Tests were performed with a gas hourly space velocity (GHSV) of 2688 h<sup>-1</sup> and a residence time of  $\tau = 1.34$  s. The product stream was collected in a cold trap and analyzed off-line by gas chromatography (Shimadzu GC-2010) using an WCOT fused silica capillary column. The column outlet was connected to a methanizer (30% Ni/SiO<sub>2</sub> catalyst) for conversion of CO<sub>x</sub> into methane, detected by a Flame Ionization Detector (FID). A more detailed description of the testing setup is given in ref.[100].



## 2.2 Principle and applications of the characterization methods

### 2.2.1 Inductively coupled plasma-optical emission spectroscopy (ICP-OES)

ICP-OES is an analytic technique in which atoms or ions present in the sample are excited electronically in Ar plasma and emit electromagnetic radiation at wavelengths characteristic of a particular element. The intensity of the signal is proportional to the concentration of the element present in the sample [101-103].

[ICP torch used as an excitation source consists of concentric quartz glass tubes and a radio frequency (RF) generator that surrounds a part of this quartz torch (Fig. 2.2.1). When the ICP torch is ignited by Tesla discharge, an intense electromagnetic field is created within the induction coils which ionizes the Ar gas at a temperature of 5000 to 8000 K. The Nebulizer introduces the sample directly in the

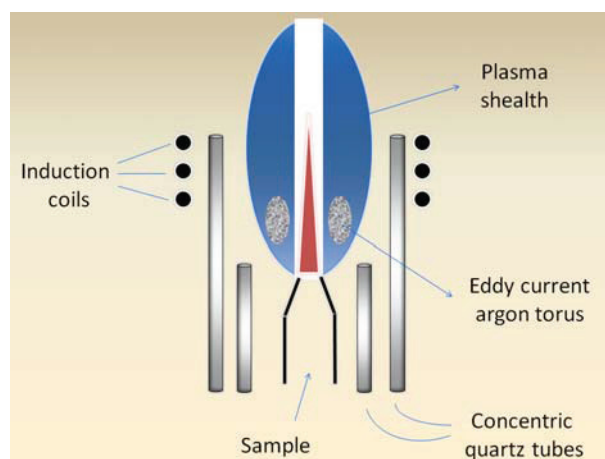


Fig. 2.2.1 Basic structure of ICP plasma.

plasma flame, in which atoms in the sample are excited electronically. Generally, a diffraction grating is used to separate the wavelengths emitted during relaxation of the atoms. Semiconductor photo detectors such as charge coupled devices (CCDs) measure intensity at different wavelengths.

ICP-OES is used for quantitative determination of elements. Practically, most samples are liquids, whereas solid samples are dissolved prior to the analysis. Halogens, some non-metals, noble gases are difficult to measure.

#### 2.2.1.1 Experimental description

A Varian 715-ES ICP-emission spectrometer was used for analysis. 10 mg of the sample was mixed with 5 ml of aqua regia and 3 ml HF and treated in a microwave-assisted sample preparation system "MULTI WAVE" (Anton Paar/Perkin-Elmer) at  $\approx 200^\circ\text{C}$  and  $\approx 60$  bar. The digested solution was filled up to 100 ml with deionized water. The ICP Expert software was used for analysis.

### 2.2.2 X-ray fluorescence (XRF) spectroscopy

When X-rays strike a sample with sufficient energy, electrons are ejected from inner shells by creating vacancies. These vacancies are filled by outer-shell electrons. During this process, characteristic X-rays of the atoms are emitted. The energy of the emitted X-rays is equal to the difference between the two binding energies of the corresponding shells. XRF is a fast and non-destructive method widely used to measure the elemental composition of materials often for qualitative analysis. Not suitable for elements of atomic number less than 11 unless special equipment is available, in which the elements down to atomic number 6 may be determined.

In the most cases, the inner K and L shells are involved in XRF detection. The X-ray fluorescence spectrum of Ti atoms in anatase and rutile and the processes involved in XRF can be seen in Fig. 2.2.2.

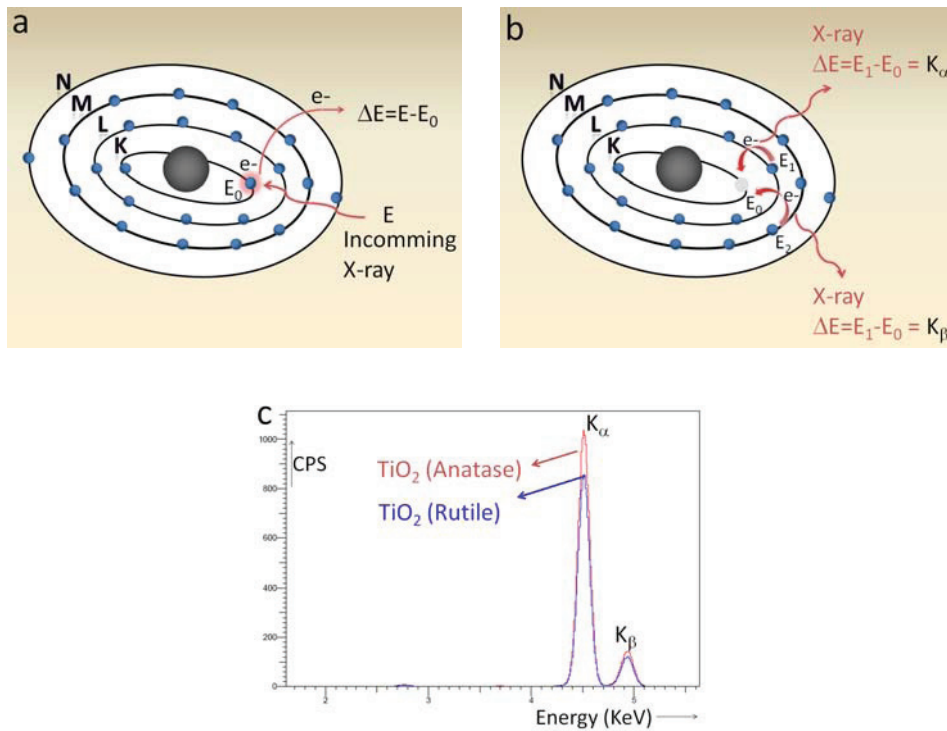


**Fig. 2.2.2** X-ray fluorescence process for Ti atoms. a) An electron in the K shell is ejected from the atom by external primary excitation, b) an electron from L or M shell jumps into vacancy, emitting a characteristic X-ray of an atom, c) spectra taken using XRF spectrometer for TiO<sub>2</sub> anatase and rutile.

#### 2.2.2.1 Experimental description

XRF elemental analyses were carried out by an Energy-dispersive X-ray fluorescence (XRF) spectrometer (ED 2000, Oxford, Instruments) with an Ag anode. High voltage from 4 kV up

to 50 kV was used. For semi quantitative estimation of the composition of the samples, the software package XpertEase (Oxford Instruments) was used.

### 2.2.3 Elemental analysis (CHNS)

For the CHNS analysis, generally the solid samples are mixed with oxidation reagents like vanadium pentoxide ( $V_2O_5$ ) and packed into lightweight containers of oxidisable metals like Sn, which are then combusted in a reactor at 1050 °C. Sn promotes a violent reaction (flash combustion) in an enriched oxygen atmosphere. The exothermic oxidation of Sn raises the temperatures to nearly 1700 °C at which a complete combustion of the sample takes place. The combustion products  $CO_2$ ,  $H_2O$ ,  $NO_2$  and  $SO_2$  are carried by a constant flow of carrier gas (helium) that passes through a glass column packed with an oxidation catalyst of tungsten trioxide ( $WO_3$ ) and a copper reducer, both kept at 1000 °C. Cu removes the excess oxygen and reduces the nitrogen oxides to  $N_2$ . The  $CO_2$ ,  $H_2O$ ,  $N_2$  and  $SO_2$  are then transported by the helium to, and separated by, packed column and quantified with a TCD (set at 290 °C.) [104]. The course of action in the CHNS elemental analysis is shown in Fig. 2.2.3.

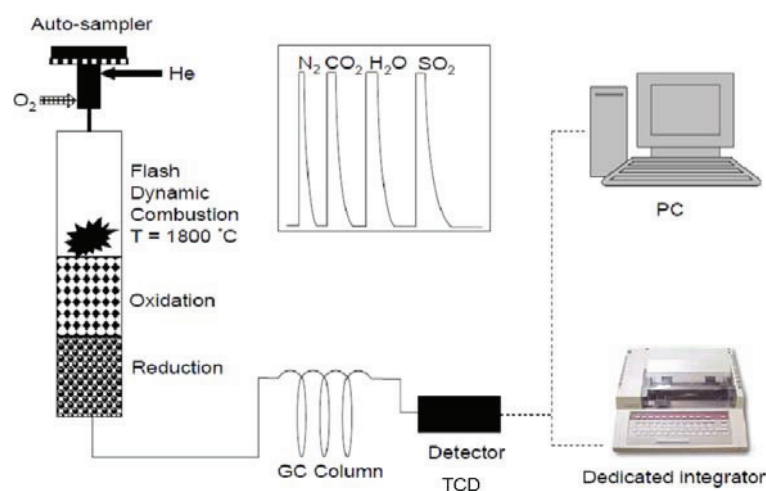


**Fig. 2.2.3** The processes involved in the CHNS elemental analysis. The figure is adapted from ref.[105]

The chromatographic responses are calibrated against pre-analyzed standards, and the CHNS elemental contents are reported in weight percent.

#### 2.2.3.1 Experimental description

CHNS microanalyser TruSpec (Leco) is used for the present investigations. 10 mg of the solid sample was mixed with  $V_2O_5$  and proceed as described above for the quantitative analysis of the C, H, N and S present in the samples.

### 2.2.4 N<sub>2</sub>-physorption (BET-surface area and pore size distribution)

The measurement of adsorption at the gas/solid interface is the basis for these investigations which gives information about surface area and pore properties by physical adsorption of gas molecules [106]. In 1938 Stephen Brunauer, Paul Emmett, and Edward Teller developed a model isotherm to measure the surface area of solid sample by modifying the Langmuir's mechanism [107]. It is as follows.

$$S = \frac{1}{[V(P_0/(P-1))]} = \frac{c-1}{V_m c} (P/P_0) + \frac{1}{V_m c} \quad \text{and} \quad c = (E_1 - E_L)/RT \quad \text{Eq (1)}$$

$P$  = Equilibrium,  $P_0$  = Saturation pressure of adsorbates at the temperature of adsorption

$V$  = Volume of adsorbed gas

$V_m$  = Monolayer adsorbed gas quantity

$c$  = BET constant

$E_1$  = heat of adsorption for the first layer and  $E_L$  = second and higher layers and is equal to the heat of liquefaction.

According to BET method, a plot of  $1/[V_a(P_0/P - 1)]$  Vs  $P/P_0$  is a straight line (when  $P/P_0$  is in the range of 0.05 to 0.30). Such plot is obtained for 10Pd,16Sb/TiO<sub>2</sub> (rutile) catalyst is evident from Fig. 2.2.4.

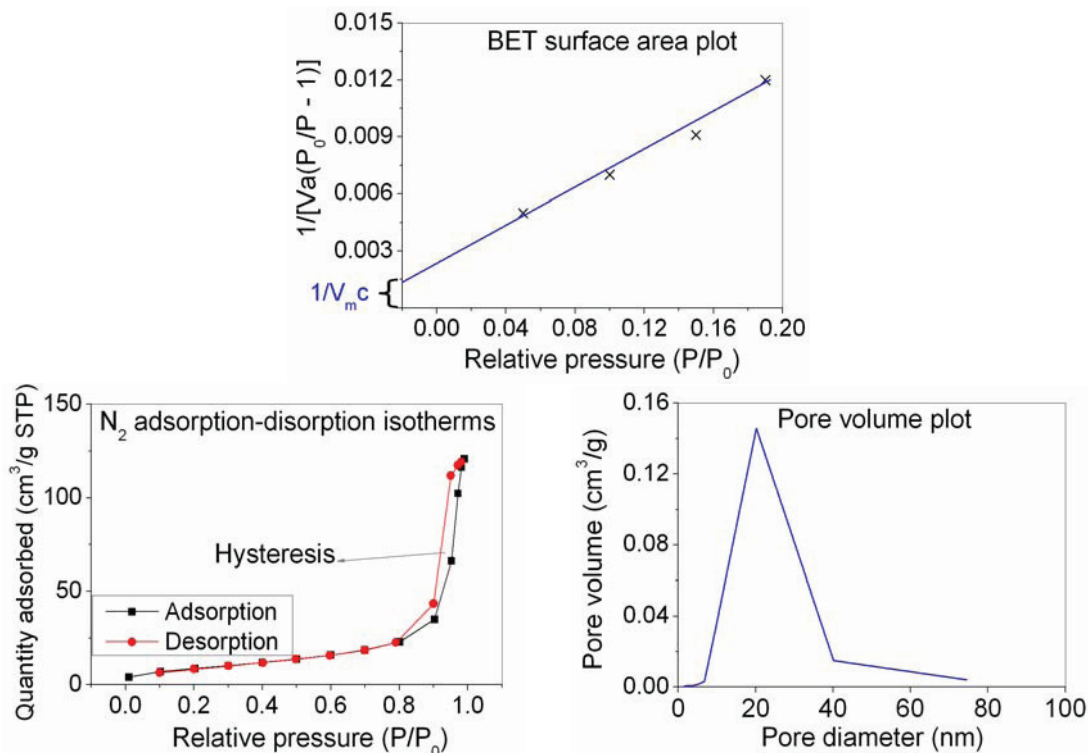


Fig. 2.2.4 BET surface area and pore volume plots derived from N<sub>2</sub>-physorption experiments.

From the value of slope ( $s = (c-1)/V_m c$ ) and intercept ( $I = 1/V_m c$ ),  $V_m$  (the number of gas molecules adsorbed in a monolayer) can be calculated, which is used in calculating the specific surface area of the catalyst by the following equation.

$$S = \frac{V_m N_A}{22414 W A_m} \quad \text{Eq (2)}$$

$V_m$  = Monolayer volume in ml at STP

$N_A$  = Avogadro number

$W$  = Weight of the catalyst sample (g)

$A_m$  = Mean cross sectional area occupied by adsorbate molecule (e.g. for  $N_2$ , it is  $16.2 \text{ \AA}^2$ ).

In addition to BET surface area,  $N_2$ -physisorption experiments provide the information about the pore properties as well (Fig. 2.2.4).

From Fig. 2.2.4, based on the shape of the hysteresis, it is also possible to distinguish different types of pores present in the solid samples. Generally, pores are classified into three categories on the basis of pore width: macropores ( $> 50 \text{ nm}$ ), mesopores ( $2\text{-}50 \text{ nm}$ ) and micropores ( $< 2 \text{ nm}$ ). Usually Kr or Xe are used to measure micropores.

#### 2.1.4.1 Experimental description

About 200 mg of the powder sample ( $\approx 1/3$  full) is taken in glass tube. Before the measurement, tube was evacuated for 2 h at  $150 \text{ }^\circ\text{C}$  to remove physisorbed water. The surface area ( $S_{\text{BET}}$ ) and pore size distribution of the catalysts were determined on an ASAP - 2010 (Micromeritics) by  $N_2$  physisorption at  $-196 \text{ }^\circ\text{C}$ .

### 2.2.5 CO-adsorption analyzed by Fourier transform infrared (FT-IR) spectroscopy

The study of CO adsorption by FTIR spectroscopy is widely used for the analysis of surface sites, in particular the state of supported metals [108]. CO adsorption gives information about the oxidation and coordination state of the metal surface species on the mono layer. Number of active sites can be calculated by normalizing the intensity of individual peaks in the spectrum to BET surface area.

Depending on the kind of interaction of CO with different surface sites the  $\nu_{\text{CO}}$  frequency shifts relative to the frequency of the gaseous CO molecule at  $2143\text{ cm}^{-1}$ . If there is a donor-acceptor interaction via a  $\sigma$ -bond between the filled CO  $\sigma$ -orbitals and the empty metal d-orbitals, a shift of  $\nu_{\text{CO}}$  to higher wavenumbers compared to  $\nu_{\text{CO(gas)}}$  is observed. This frequency shift rises when the ratio of the metal ion charge to the metal

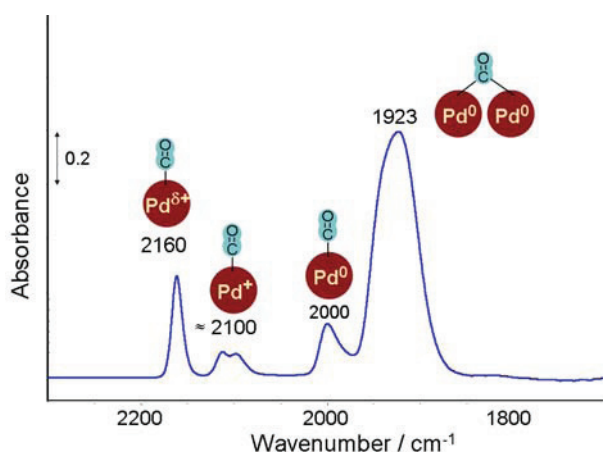


**Fig. 2.2.5** FT-IR spectra of CO-adsorption on 10Pd,8Sb/TiO<sub>2</sub> anatase catalyst after calcination at 300 °C.

ion radius increases. If the CO molecule is partially bound to adsorption sites by the use of occupied d-orbitals via back-donation, then typical carbonyl complexes will be formed and a drop of the  $\nu_{\text{CO}}$  frequency can be observed compared to  $\nu_{\text{CO(gas)}}$ . Fig. 2.2.5 shows the FT-IR spectra of CO adsorption on a 10Pd,8Sb/TiO<sub>2</sub> catalyst, different states can be assigned to Pd depends on the peak position.

#### 2.2.5.1 Experimental description

CO adsorption studies in transmission mode were carried out on a Bruker Tensor 27 FTIR spectrometer equipped with a heatable and evacuable homemade reaction cell with CaF<sub>2</sub> windows connected to a gas-dosing and evacuation system. The sample powders were pressed into self-supporting wafers with a diameter of 20 mm and a weight of 50 mg. Adsorption of 5 % CO/He was carried out at room temperature after pretreatment of the samples in air at 300 °C for 2 h, subsequent cooling to room temperature and evacuation. Generally, difference spectra were evaluated, obtained by subtracting the respective spectrum of the pretreated sample from the adsorbate spectrum.

### 2.2.6 Thermo gravimetriy-Differential thermal analysis (TG-DTA)

TG is the measure of mass changes of a sample as a function of temperature. It is often related to physical changes in the sample, however chemical information can be obtained by coupling with differential thermal analysis (DTA), differential scanning calorimetry (DSC) and mass spectrometry [109]. TG-DTA is routinely applied in a wide range of studies such as identification, quantitative composition analysis, phase diagrams, hydration-dehydration, thermal stability, polymerisation, purity, and reactivity. Generally, measurements can be carried out up to 1200 °C in different atmospheres. TG is related to a change of mass, involves desorption of physisorbed or chemisorbed water as well as degradation of materials. On the other hand, the DTA signal is the temperature difference between an inert reference and the sample which gives information about the oxidation or reduction, phase changes and chemical transformations. As an example, TG-DTA curves of a 10Pd,8Sb/TiO<sub>2</sub> catalyst until 600 °C in air can be seen in Fig. 2.2.6.

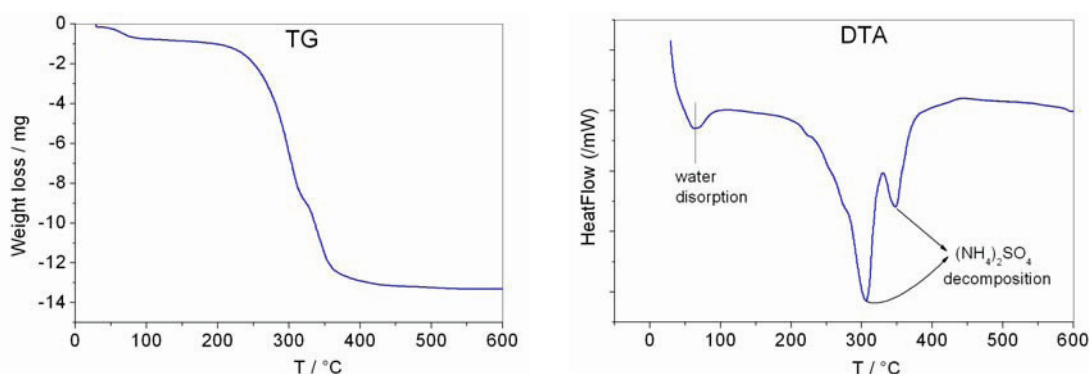


**Fig. 2.2.6** Simultaneous TG-DTA spectra of 10Pd,8Sb/TiO<sub>2</sub> catalyst contains (NH<sub>4</sub>)<sub>2</sub>SO<sub>4</sub>.

From Fig. 2.2.6, TG indicates the mass loss of nearly 13 mg during heating until 600 °C. Simultaneous measurement of DTA gives the information about the exact temperature at which the transformations occurred. This 10Pd,8Sb/TiO<sub>2</sub> catalyst contains (NH<sub>4</sub>)<sub>2</sub>SO<sub>4</sub>, which showed two distinct peaks ~ 300 °C and 350 °C related to its decomposition and subsequent evaporation of decomposed products, respectively. Coupling with mass spectrometry also provide the valuable information about the decomposed products.

#### 2.2.6.1 Experimental description

Thermo gravimetric analysis and differential thermal analysis (TG-DTA) has been done with a TGA 92 (Setaram) until 600 °C in air or He flow (3 Lt/h). The heating rate was 10 °C/min. 20-50 mg of the sample was used for the analysis.



### 2.2.7 X-ray diffraction (XRD)

When X-rays strike a sample, several processes take place like absorption, photo emission, fluorescence, as well as the emission of X-rays of high wavelength. Coherent and incoherent scattering from a crystal lattice can be observed from diffracted beams when the energy of the source X-rays is lower (1 keV-100 keV). Bragg's law is the basis for X-ray diffraction (XRD), because it is related to the coherent and incoherent scattering. The Bragg's equation is as follows.

$$n\lambda = 2d \sin \theta \quad \text{Eq (3)}$$

$n$  = Order of a reflection ( $n = 1, 2, 3 \dots$ )

$\lambda$  = wavelength

$d$  = Distance between parallel lattice planes

$\theta$  = Angle between the incident beam and a lattice plane, known as the Bragg angle (Fig. 2.2.7).

After diffraction, the X-rays can be recorded using digital methods and the final data can be displayed as a graph of intensity, as a function of interplanar distance  $d$ , or as function of diffraction angle  $2\theta$ . The intensity of diffracted beam depends on the arrangement of the atoms on these planes. The basic representation of interactions of two X-rays which are in phase, constructive interference and a diffractogram of 10Pd/TiO<sub>2</sub> catalyst contained metallic Pd and TiO<sub>2</sub> phases can be seen in Fig. 2.2.7.

XRD is generally used for identification of crystalline phases contained in sample, characterization of phase transformations and determination of lattice parameters. Samples must be crystalline for phase identification. Assignment of the particular phase compound or phase present in the sample can be done by comparing with data base.

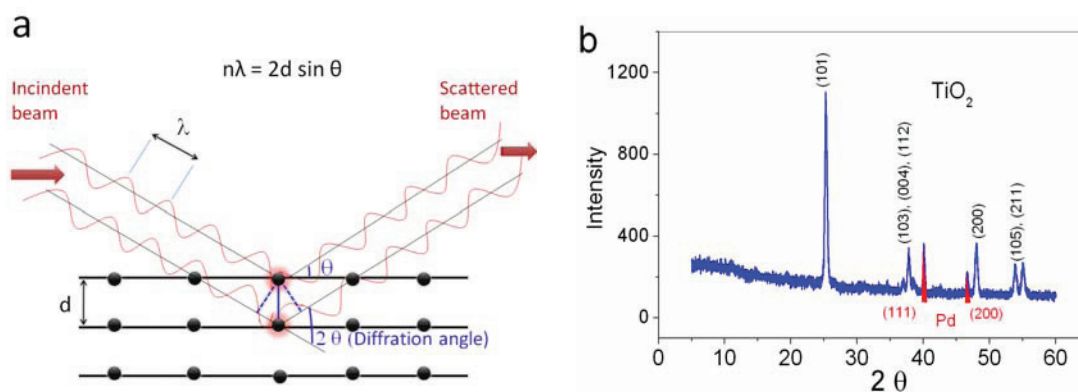


Fig. 2.2.7: a) Interaction of X-rays with atoms of crystal, b) interference, c) diffractogram of 10Pd/TiO<sub>2</sub>.

With the analysis of X-ray diffraction line broadening (XLB) of the peak shape of one or more diffraction lines crystallite size can be calculated using the Scherrer equation.

$$D_B = \frac{K\lambda}{\beta \cos \theta} \quad \text{Eq (4)}$$

$D_B$  = Mean crystallite diameter

$K$  = Scherrer's constant

$\lambda$  = X-ray wave length (1.5418 Å for CuK $\alpha$  radiation)

$\beta$  = Full width at half maximum (FWHM)

### 2.2.7.1 Experimental description

XRD powder patterns at ambient conditions were recorded in transmission geometry with Cu K $\alpha$  radiation ( $\lambda = 1.5406$  Å) in the  $2\theta$  range of 10-55° (step width = 0.25°, time per step 25 s) on a Stoe STADI P diffractometer, equipped with a linear Position Sensitive Detector (PSD).

*In situ*-XRD patterns during thermal pretreatment were measured in Bragg-Brentano geometry with Cu K $\alpha$  radiation ( $\lambda = 1.5418$  Å) between 100 and 650 °C at a heating rate of 10 K/min in a Bühler-XRD-chamber. Samples were placed on a Pt-Rh sample holder (or ceramic samples holder) in He and 10 % H<sub>2</sub>/He flow, respectively, with the flow rate of 30 mL/min. Spectra were recorded every 25 °C at an isothermal hold of 90 min.

Processing and assignment of the powder patterns was done using the software WinXpov (Stoe) and the Powder Diffraction File (PDF) database of the International Centre of Diffraction Data (ICDD). Crystallite sizes were calculated using the Scherrer equation.

### 2.2.8 X-ray absorption near edge structure (XANES)

The principle of XANES spectroscopy is the absorption of X-rays at certain energies leading to sharp rises in the absorption spectra. The sharp rises are called absorption edges. At these edges electrons are excited from the core levels to the lowest empty states. The energy of such absorption edges depends on the kind of atom which is excited and its valance state. Such experiments performed at synchrotron facilities offering variable monochromatic X-ray radiation. Often the absorption edge is measured in a direct by comparing the photon intensity before and after the irradiation on the sample. To improve the sensitivity of the measurements, decay products like fluorescence photons or Auger electrons are measured. The fundamental process contributing to XANES and the spectrum of Pd-foil measured in fluorescence mode are shown in Fig. 2.2.8.

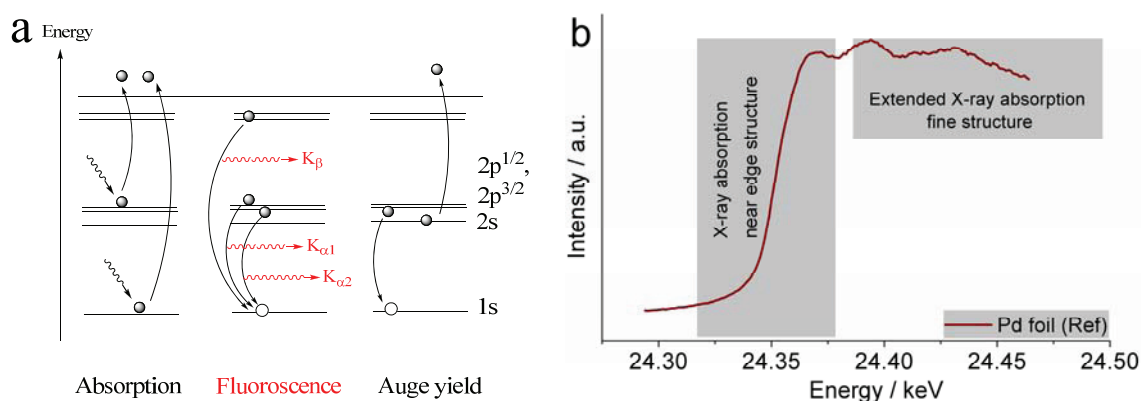


**Fig. 2.2.8** a) The fundamental processes which contribute to XANES like absorption (photoelectron mission), fluorescence (filling of the core hole by an electron in another level) leaving the photon and auger (filling of the core hole by an electron in another level followed by emission of an auger electron), b) XANES pattern of the metallic foil.

In the experimental setup used in the present investigations the fluorescence photon were detected allowing the determination of the valance state of the bulk atoms. Therefore, it was possible to investigate the difference of the valance states between the bulk atoms detected by XANES and the atoms in the near-surface region investigated with XPS.

#### 2.2.8.1 Experimental description

The X-ray absorption experiments were performed at the BAMline at BESSY II of the Helmholtz Centre Berlin for Materials and Energy. The X-ray fluorescence of the Pd K<sub>α</sub> line was detected with a silicon drift detector.

### 2.2.9 X-ray photoelectron spectroscopy (XPS)

XPS is also often called as electron spectroscopy for chemical analysis (ESCA), and is based on the photoelectric effect in which electrons are ejected from core levels of atoms by irradiation with X-rays. In XPS, a material is irradiated with a beam of X-rays of known energy, and the kinetic energy and number of electrons that escape from a surface layer of 1 to 10 nm depth is analyzed [110]. Since the energy of the X-rays with a particular wavelength is known, the electron binding energy of each of the emitted electrons can be determined by using an equation that is based on the work of Ernest Rutherford (1914).

$$E_{\text{binding}} = E_{\text{photon}} - (E_{\text{kinetic}} + \phi) \quad \text{Eq (5)}$$

where  $E_{\text{binding}}$  is the binding energy of the electron,  $E_{\text{photon}}$  is the energy of the X-ray photons being used,  $E_{\text{kinetic}}$  is the kinetic energy of the electron as measured by the instrument and  $\phi$  is the work function of the spectrometer (not the material).

XPS measures the chemical or electronic state and elemental composition of the surface (top 1-10 nm usually) of the samples. XPS is one of the most important methods used to characterize the catalysts of heterogeneous catalysis. A basic representation of the XPS process and the spectrum of Ti in 10Pd/TiO<sub>2</sub> catalyst are shown in Fig. 2.2.9.

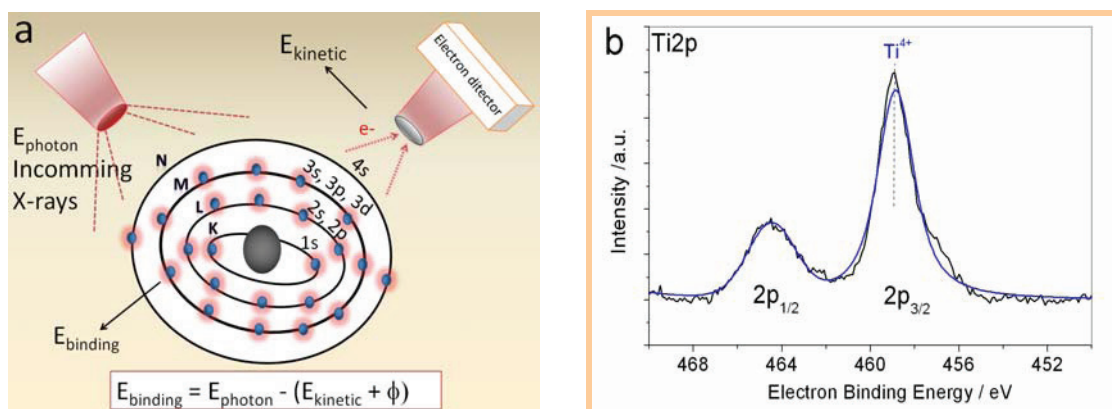


Fig. 2.2.9: a) Rough diagram of XPS process and b) Ti2p spectra from XPS analysis of Pd/TiO<sub>2</sub>.

#### 2.2.9.1 Experimental description

XP spectra were recorded on a VG ESCALAB 220iXL instrument with monochromatic Al K $\alpha$  radiation ( $E = 1486.6$  eV). The samples were fixed with a double adhesive carbon tape on a stainless steel sample holder. The peaks were fitted by Gaussian-Lorentzian curves after Shirley background subtraction. The electron binding energy was referenced to the Ti  $2p_{3/2}$  peak of TiO<sub>2</sub> at 458.8 eV. For quantitative analysis of the near-surface region the peak areas

were determined and divided by the element-specific Scofield factors and the analyser-dependent transmission function.

### 2.2.10 Transmission electron microscopy (TEM)

The TEM is useful for indicating the size of the particles present in the samples in nm range and it gives the information related the morphology, composition and distribution. It has now become capable of observing specimens at atomic resolution and is making valuable contribution to research and development in the academic and industry. In transmission electron microscope, a sample in the form of thin foil is irradiated by electrons having energy of hundred of eV. In the interior of the crystal the electrons are transmitted, scattered, or reflected. The schematic geometry of the electron microscopy, the TEM micrograph of the 10Pd,16Sb/TiO<sub>2</sub> (rutile) sample is shown in Fig. 2.2.10.

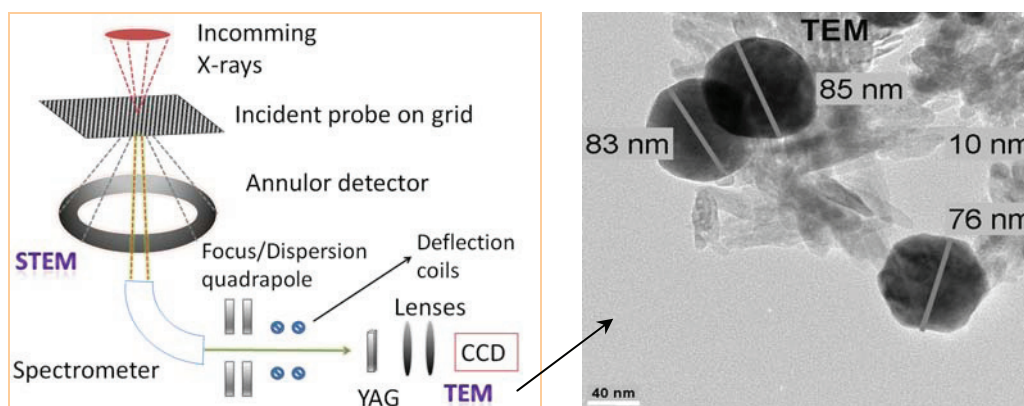


**Fig. 2.2.10** Schematic geometry of the electron microscopy, the TEM micrograph of the 10Pd,16Sb/TiO<sub>2</sub> (rutile) after 30 h stream in gas phase acetoxylation of toluene.

After the interaction with the specimen, the electrons enter the imaging system of the microscope, composed of the objective, intermediate and projector magnetic lens. The image is visualized on a fluorescent screen and recorded on a photographic film or on a CCD-camera. Objective lens is the most important lens of TEM, because its aberrations limit the resolution of the microscope. An electron diffraction pattern is formed in its back focal plane. A removable aperture situated in this plane is used to select different electron beams to form different images, thus manipulating the image contrast.

The non-transmitted components may be obtained either by beam tilting or by the use of annular dark field detectors. EDXS (energy-dispersive x-ray spectroscopy) elemental mapping with STEM provides the apparent distribution of the different metal components in the sample.

### **2.2.10.1 Experimental description**

TEM measurements were performed at 200 kV on a JEM-ARM200F (JEOL) which is aberration-corrected by a CESCOR (CEOS) for the scanning transmission (STEM) applications. The microscope is equipped with a JED-2300 (JEOL) energy-dispersive X-ray-spectrometer (EDXS) for chemical analysis. High-angle annular dark field (HAADF) and EDXS imaging was operated with spot size 6 c and a 40  $\mu\text{m}$  condenser aperture. Preparation of the TEM sample: the sample was deposited on a holey carbon supported grid (mesh 300) and transferred to the microscope.





## Chapter 3

### **Exploring the synthesis conditions for supported Pd-particles of optimum size and composition**

---

As mentioned in the earlier section (1.1 Motivation), highest catalytic performance has been obtained so far with TiO<sub>2</sub> supported Pd-catalysts containing Sb, Cu or Bi as co-components. All these catalysts had in common that the catalytic performance rises strongly within an initial activation period (which was shortest for Sb but longest for Cu containing catalysts) and this went along with a significant growth of the Pd-particles. Given that Pd-particles of optimum size and composition must exist before the catalysts can reach their maximum performance, it should be possible to pre-form such particles by tailored synthesis and pretreatment protocols and, thus, to shorten the unacceptably long equilibration times.

With this challenge in mind, the influence of different metal precursors (chlorides, nitrates, acetates) and additives (ammonium sulfate, carbonate, nitrate and urea), as well as different thermal pretreatment conditions has been investigated and described in this section. For this purpose, the two catalysts with the most different properties, namely 10Pd,8Sb/TiO<sub>2</sub> (rather short conditioning but fast deactivation) and 10Pd,8Cu/TiO<sub>2</sub> (very long conditioning but much higher stability) have been selected [10, 11].

---

### 3.1 Influence of different metal precursors

To test the impact of different metal precursors (chlorides, nitrates and acetates), catalysts containing nominal amounts of 10 wt.-% Pd and 8 wt.-% Sb or Cu, on TiO<sub>2</sub> (anatase) were prepared according to the Scheme 2.1 of Chapter 2. The complete details about the catalysts preparation is described in the Section 2.1.1 and Table 2.1.

#### 3.1.1 Thermal analysis (TG-DTG)

To elucidate optimum thermal pretreatment conditions, TG and DTG analysis was done in helium flow up to 600 °C and the respective results are shown in Fig. 3.1. Most pronounced weight loss (around 40 %) was observed for chloride-based Pd,Cu/TiO<sub>2</sub> and Pd,Sb/TiO<sub>2</sub> samples, while the acetate samples show the lowest loss (20 %). Especially for the chloride samples, the TG curves for both the Cu and Sb containing catalysts are similar (Fig. 3.1a). In contrast, for the acetate samples, some differences are found concerning the characteristic temperatures for the weight loss, where as the nitrate (Cu) sample showed the major weight loss around 300 °C. For a more detailed analysis of the characteristic temperature of the weight loss, DTG analysis was done simultaneously and the results are shown in Fig. 3.1b.

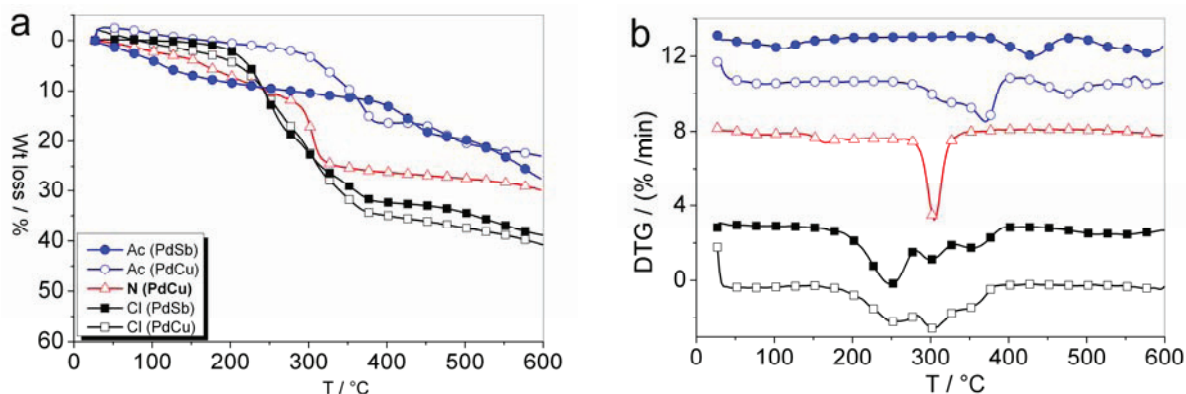


**Fig. 3.1:** a) Thermogravimetric (TG), b) differential thermogravimetric (DTG) analysis in helium flow up to 600 °C of the samples prepared from various metal precursors: □ Pd,Cu/TiO<sub>2</sub> (chlorides), ■ Pd,Sb/TiO<sub>2</sub> (chlorides), △ Pd,Cu/TiO<sub>2</sub> (nitrates), ○ Pd,Cu/TiO<sub>2</sub> (acetates), ● Pd,Sb/TiO<sub>2</sub> (acetates).

DTG effects for chloride samples are observed mainly in the 200 and 400 °C temperature region. The DTG curves in the range of 200 to 310 can be assigned to the decomposition of NH<sub>4</sub>Cl (it is formed due to the reaction between ammonium sulfate and chloride precursors), while the peaks in the range from 260 to 400 °C are related to (NH<sub>4</sub>)<sub>2</sub>SO<sub>4</sub> decomposition [111]. In Pd,Cu/TiO<sub>2</sub> (nitrates) sample, a sharp peak pronounced at 300 °C represents the characteristic decomposition temperature of Pd(NO<sub>3</sub>)<sub>2</sub>•2H<sub>2</sub>O. In addition, (NH<sub>4</sub>)<sub>2</sub>SO<sub>4</sub> decomposition at this temperature can not be ruled out. Additionally, a small peak at 170 °C

can be assigned to  $\text{Cu}(\text{NO}_3)_2 \cdot \text{H}_2\text{O}$  decomposition [112]. On the other hand, Pd,Cu/TiO<sub>2</sub> (acetate) sample showed a major decomposition in the range of 300 to 400 °C. This includes the decomposition of  $\text{Cu}(\text{CH}_3\text{COO})_2 \cdot \text{H}_2\text{O}$  [113],  $\text{Pd}(\text{CH}_3\text{COO})_2$  [114] and  $(\text{NH}_4)_2\text{SO}_4$  as well, whereas the decomposition curve observed at ~ 470 °C is assigned to thermally produced sulfuric acid from  $(\text{NH}_4)_2\text{SO}_4$  and possibly evolution of sulfur trioxide and water [115]. In contrast to the Pd,Cu/TiO<sub>2</sub> (acetate) sample, where a major decomposition observed in certain range, the TG results of the Pd,Sb/TiO<sub>2</sub> (acetate) indicate a gradual decomposition until 400 °C and a sharp decrease at 420 °C (Fig. 3.1a) which includes decomposition products from precursors and ammonium additives. Afterwards, the formation of the Pd-phase was checked by XRD measurements.

### 3.1.2 X-ray diffraction (XRD)

In Fig. 3.2 the XRD patterns obtained after 4 h thermal pretreatment at 600 °C are presented. A clear influence of the nature of the metal precursor on the crystallinity of the samples could be observed. Most crystalline materials were observed for the chloride precursors (Fig. 3.2a and b).

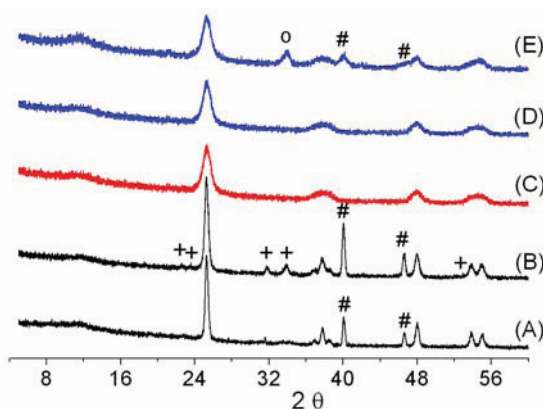


**Fig. 3.2** XRD patterns of the samples after thermal pretreatment in helium at 600 °C for 4 h prepared from various metal precursors: (A) Pd,Cu/TiO<sub>2</sub> (chlorides), (B) Pd,Sb/TiO<sub>2</sub>(chlorides), (C) Pd,Cu/TiO<sub>2</sub> (acetates), (D) Pd,Sb/TiO<sub>2</sub> (acetates) and (E) Pd,Cu/TiO<sub>2</sub> (nitrates). o PdO, ++ Na<sub>2</sub>SO<sub>4</sub>, # Pd, remaining reflections from TiO<sub>2</sub> (anatase).

Sharp Pd and anatase reflections were found for these samples. All other precursors lead to less crystalline samples with broad reflections. For samples prepared from nitrates, PdO was detected besides Pd (Fig. 3.2E). Due to the formation of this undesired PdO-phase and the loss of copper (as observed by XRF investigations) using the metal acetates as precursors, the following investigations were performed with samples prepared from metal chlorides. The more similarities between the XRD patterns of the chloride-based solids shown in Fig. 3.2 and

those obtained from equilibrated catalysts [10, 11]; suggest that thermal pretreatment in helium might be a suitable method to create active catalysts.

Based on the above TG-DTG and XRD investigations it could be concluded that  $(\text{NH}_4)_2\text{SO}_4$  had considerable impact especially on the chloride precursors in terms of weight loss, as well as on chemical interactions. Unfortunately, it may be the reason for the formation of sulfide species on the catalysts surface that can acts as poison. Therefore, we explored the impact of other  $\text{SO}_4$ -free additives on the chloride precursors, such as  $\text{NH}_4\text{NO}_3$ ,  $(\text{NH}_4)_2\text{CO}_3$  and urea as substituents for  $(\text{NH}_4)_2\text{SO}_4$ . This is described in the next section.

### 3.2 Effect of various ammonium additives

#### 3.2.1 Thermal analyses (TG-DTA)

To check, in addition to  $(\text{NH}_4)_2\text{SO}_4$ , the influence of different ammonium additives on the weight loss, TG and simultaneous DTA (differential thermal analysis) measurements were performed with  $\text{NH}_4\text{NO}_3$ ,  $(\text{NH}_4)_2\text{CO}_3$  and urea in comparison to a sample prepared without any additive. The TG results for the Pd,Cu/TiO<sub>2</sub> and Pd,Sb/TiO<sub>2</sub> samples (with chloride precursors) are displayed in Fig. 3.3.

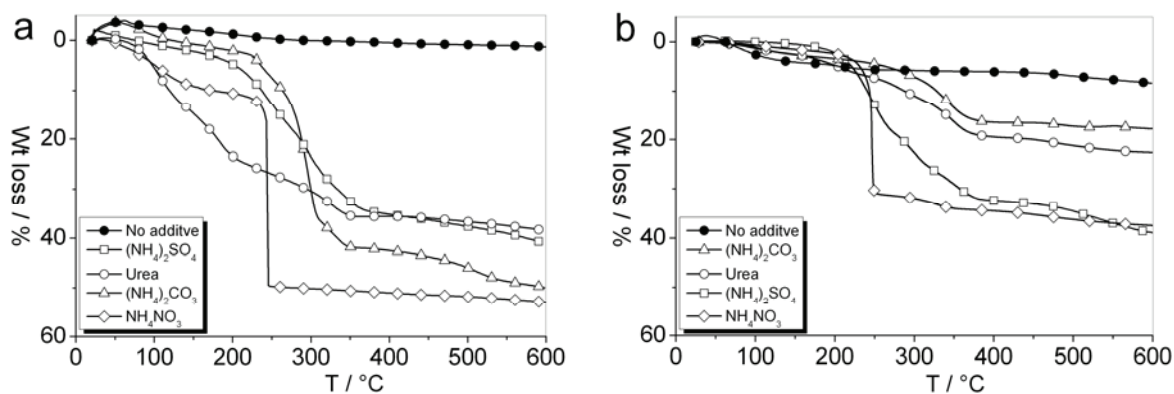


**Fig. 3.3** Thermogravimetric analysis (TG) in helium flow up to 600 °C of a) Pd,Cu/TiO<sub>2</sub>, b) Pd,Sb/TiO<sub>2</sub> samples prepared from chloride metal precursors and by the addition of different additives. TG spectra of the samples prepared without additives are also shown.

In the case of the Cu sample, free of ammonium additive, only a slight loss of 1.2 % was found, while this is 8.2 % in Sb sample. This suggests a rather high volatility of the Sb components in the sample. Thus,  $\text{SbCl}_3$  precursor might be responsible for corresponding weight loss because of its low thermal stability [116, 117].

The other Cu samples which contain ammonium additives show a loss between 39 and 51 % and the order is:  $\text{NH}_4\text{NO}_3 > (\text{NH}_4)_2\text{CO}_3 > \text{urea} \approx (\text{NH}_4)_2\text{SO}_4$ , whereas Sb samples lost 17 to 39 % of their weight and the additives are effective in the following order:  $\text{NH}_4\text{NO}_3 \approx$

$(\text{NH}_4)_2\text{SO}_4 > (\text{NH}_4)_2\text{CO}_3 \approx \text{urea}$ . The decomposition temperature merely depends on the various ammonium additives used. TG analysis reveals a sharp decrease at 250 °C for  $\text{NH}_4\text{NO}_3$  [118] containing samples, while the range was broader between 200 and 360 °C for the carbonate- and sulfate-containing samples. For urea additive a continuous decomposition between ca. 80 and 350 °C was detected, which is according to the literature [119]. For all samples, above 400 °C only slight changes were observed.

### 3.2.2 X-ray fluorescence (XRF)

The aim of using the additives was to remove chloride from the samples, since residual chloride may have a negative influence on the catalytic properties of the system. Therefore, XRF measurements were performed for the non-pretreated samples and after 4 h thermal pretreatment at 400 °C and 600 °C in helium flow to check for residual chloride (Fig. 3.4).

As expected, Cl removal is negligible without any ammonium compound even after 600 °C thermal treatment. In case of the Pd,Sb sample, chloride is removed at lower temperatures in comparison to Pd,Cu samples. Above 400 °C, significant changes of the Cl amount were not detected anymore for Pd,Sb samples. When Cu is used as co-component, Cl removal is not yet completed after thermal pretreatment at 400 °C but continues until about 600 °C. The differences in the chloride amount for the non-pretreated samples can be explained by loss of chloride during drying (120 °C, 16 h) in some samples.

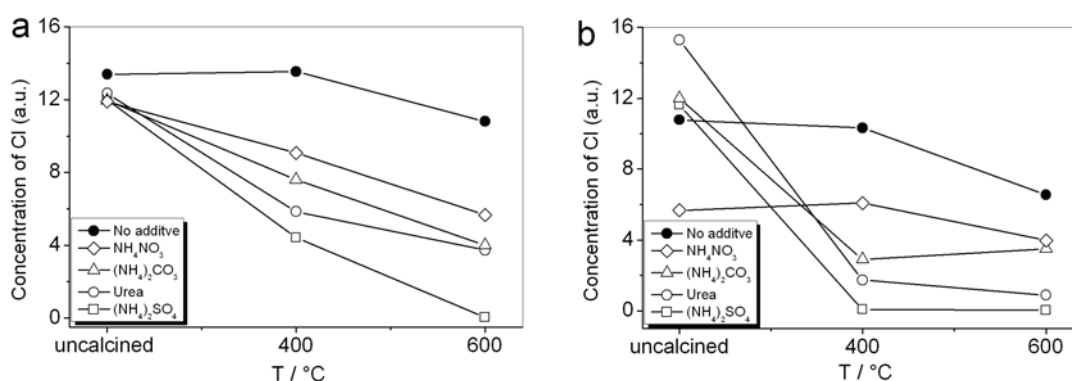


**Fig. 3.4** Cl peak intensity measured by XRF before and after thermal pretreatment in helium at 400 and 600 °C of a) Pd,Cu/TiO<sub>2</sub>, b) Pd,Sb/TiO<sub>2</sub> samples prepared with and without different additives.

These results indicate that the efficiency of chloride removal increases in the following order:  $\text{NH}_4\text{NO}_3 < (\text{NH}_4)_2\text{CO}_3 < \text{urea} < (\text{NH}_4)_2\text{SO}_4$ . The poor ability of  $\text{NH}_4\text{NO}_3$  to remove chloride might be due to the fact that it is decomposed at too low temperature (*cf* Fig. 3.3). Obviously,  $(\text{NH}_4)_2\text{SO}_4$  is the only ammonium compound which is able to



remove Cl completely from both Pd,Sb/TiO<sub>2</sub> and Pd,Cu/TiO<sub>2</sub> samples. Besides complete chloride removal, the formation of Pd-particles while suppressing PdO formation was tentatively considered to be essential. Therefore, XRD investigations were done for the Pd,Cu/TiO<sub>2</sub> and Pd,Sb/TiO<sub>2</sub> samples after thermal treatment in He at 400 and 600 °C.

### 3.2.3 X-ray diffraction (XRD)

In Fig. 3.5, the XRD patterns of Pd,Cu/TiO<sub>2</sub> and Pd,Sb/TiO<sub>2</sub> samples after thermal pretreatment in He for 4 h at 400 and 600 °C are presented. The major difference between the XRD patterns at 400 and 600 °C is the intensity. Samples pretreated at 400 °C showed relatively low intensity which indicates low crystallinity.

XRD patterns of all the samples contain the reflections of TiO<sub>2</sub> anatase (PDF No. 21-1272) and NaCl (PDF No. 70-2509). However, NaCl was absent in Cu or Sb samples prepared with (NH<sub>4</sub>)<sub>2</sub>SO<sub>4</sub>. In this case, Na<sub>2</sub>SO<sub>4</sub> (+) is present and is more prominent in the Sb sample (Fig. 3.5d). Na ions originate most probably from Na<sub>2</sub>CO<sub>3</sub>, which was used to maintain the pH value during the preparation, while sulfate ions might from the respective ammonium additive.

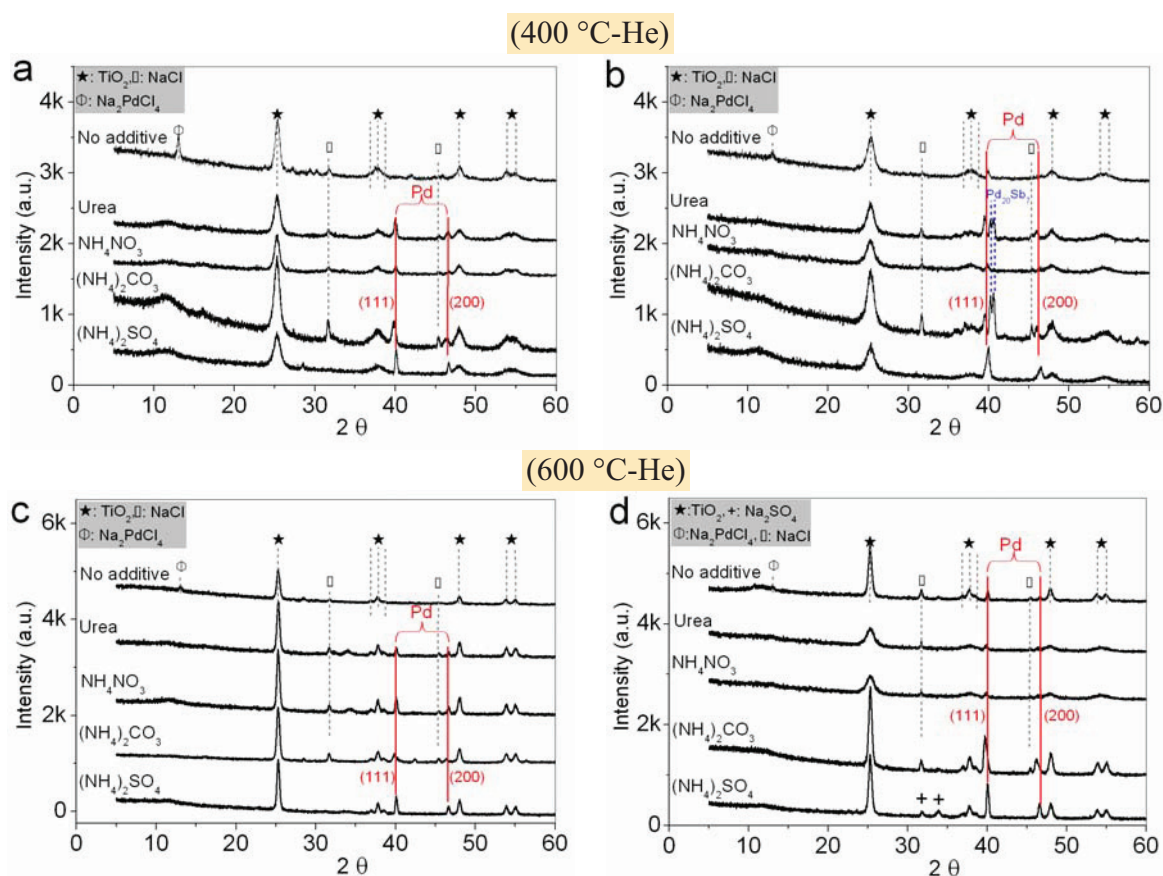


**Fig. 3.5** XRD patterns measured after 4 h thermal pretreatment in helium at 400 and 600 °C of the (a, c): Pd,Cu/TiO<sub>2</sub>, (b, d): Pd,Sb/TiO<sub>2</sub> samples prepared with and without chloride-removing additives.

On the other hand, in the absence of any additive, an additional  $\text{Na}_2\text{PdCl}_4$  phase (PDF No 84-1946) could also be observed. Besides these phases,  $\text{Pd}_{20}\text{Sb}_7$  alloy phase was observed only in Pd,Sb/ $\text{TiO}_2$  samples after thermal treatment at 400 °C in helium, which were prepared by using  $(\text{NH}_4)_2\text{CO}_3$  and urea, however,  $\text{Pd}_{20}\text{Sb}_7$  alloy phase is destabilized with 600 °C treatment.

Reflections corresponding to metallic palladium (PDF No. 88-2335) at  $2\theta = 40.01^\circ$  and at  $2\theta = 46.5$  are related Pd(111) and Pd(200), respectively. They can be seen for the samples containing ammonium additives irrespective of the co-component Cu or Sb (Fig. 3.5). However, especially in the Sb sample metallic Pd-phase is observed even in the absence of ammonium additives. This shows that Sb promotes the reduction of palladium more effectively than Cu. Relatively high intense Pd-reflections are shown by the samples containing  $(\text{NH}_4)_2\text{SO}_4$ , independent on the co-component used. It might be due to high ability of  $(\text{NH}_4)_2\text{SO}_4$  for Cl removal, thus facilitating the formation of crystalline metallic Pd. To study this process in more details, *in situ* XRD investigations were made with the samples starting from the chlorides and using  $(\text{NH}_4)_2\text{SO}_4$  as additive.

### 3.2.4 In situ - XRD investigations

As mentioned above, a major aim of this work is to tailor the thermal pretreatment procedure of Pd-catalysts for the preferential formation of Pd-particles with a size of 80-100 nm identified in active equilibrated catalysts, to avoid long conditioning times in catalysis. This goal can only be reached, when detailed knowledge is available about the influence of thermal pretreatment conditions on the formation of crystalline phases as well as on the growth of Pd-crystallites. Therefore, *in situ*-XRD studies of Pd,Sb/ $\text{TiO}_2$  and Pd,Cu/ $\text{TiO}_2$  precursors during heating in inert (He) and reducing (10 %  $\text{H}_2/\text{He}$ ) atmospheres have been performed. In contrast to thermal pretreatment of 4 h at 400 or 600 °C used for catalyst preparation, the samples were heated stepwise with isothermal holds of 90 min for recording XRD powder patterns different temperatures. The whole thermal pretreatment period took about 28 h. The respective XRD patterns during the thermal treatment in helium from 100 to 650 °C are shown in Fig. 3.6. A detailed description of the experimental procedure is described in Chapter 2.

#### 3.2.4.1 Measurements in He

In helium flow, the *in situ*-XRD patterns of both the Pd,Sb and Pd,Cu precursor compounds in the low-temperature range between 100 and 200 °C show the reflections of  $\text{Pd}_{1.094}(\text{NH}_3)_{1.8}\text{Cl}_{2.06}$  (PDF No. 87-1209) (Fig. 3.6). This indicates that  $(\text{NH}_4)_2\text{SO}_4$  probably



decomposes by generating free ammonia molecules [115] which in turn interact with  $\text{PdCl}_2$  to form a chloroamine complex. Another chloroamine complex,  $(\text{NH}_4\text{Cu}(\text{NH}_3)_2\text{Cl}_3)_{0.3}$  (PDF No. 70-78) is also formed with copper between 100 and 200 °C but not with antimony as a co-component. This is easy to understand, since Cu is well known to form amine complexes, while this property is missing for Sb as a main group element. Instead,  $(\text{NH}_4)_2\text{PdCl}_4$  (PDF No. 73-1507) is formed as an additional ammonium-containing Pd compound besides  $\text{Pd}_{1.094}(\text{NH}_3)_{1.8}\text{Cl}_{2.06}$  in the Pd,Sb catalyst.

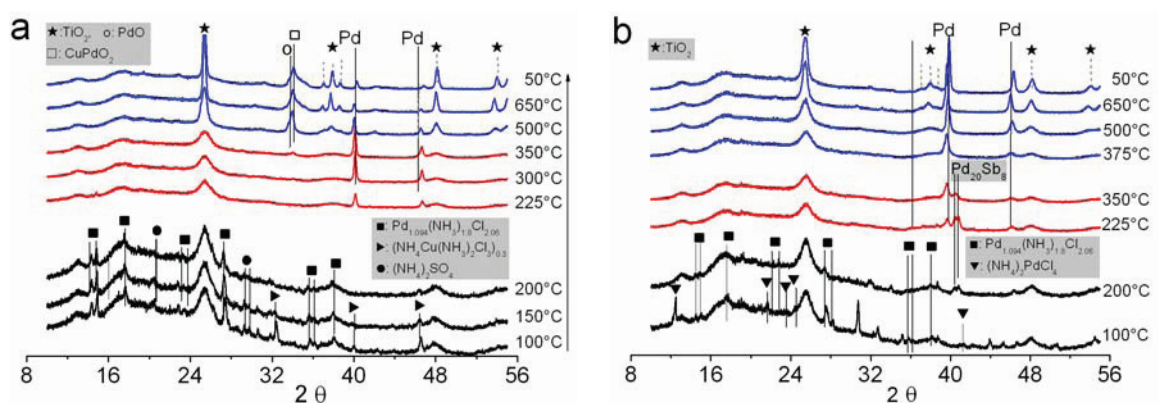


**Fig. 3.6** XRD patterns of a) Pd,Cu/TiO<sub>2</sub>, b) Pd,Sb/TiO<sub>2</sub> samples recorded during thermal pretreatment in helium. Patterns at 100 to 200 °C have been magnified by a factor of 2. Patterns at 50 °C were after cooling.

Above 225 °C, the reflections of the chloroamine complexes as well as of  $(\text{NH}_4)_2\text{PdCl}_4$  disappear for both the solids and reflections of monometallic Pd appeared. This shows clearly that Pd-crystallites are not directly formed from the  $\text{PdCl}_2$  precursor but via intermediate Pd-chloroamine complexes and  $(\text{NH}_4)_2\text{PdCl}_4$  [120]. Based on these observations, it can be stated that the role of  $(\text{NH}_4)_2\text{SO}_4$  is not only to remove chloride, but also to promote the formation of the desired metallic Pd-crystallites already at rather low temperatures. Besides monometallic Pd, a  $\text{Pd}_{20}\text{Sb}_7$  alloy phase is formed in the Pd,Sb sample between 225 and 350 °C, while no such alloying is observed between Pd and Cu. Possibly, complexation of Cu by  $\text{NH}_3$  separates this co-component more effectively from Pd, in comparison to Sb, which in turn could suppress the formation of a Pd,Cu alloy at low temperature.

In the Pd,Sb sample, the reflections of Pd become more pronounced with rising temperature in the range between 375 and 650 °C, while the reflections of the  $\text{Pd}_{20}\text{Sb}_7$  alloy disappear. In contrast, PdO and  $\text{PdCuO}_2$  phases are formed in the Pd,Cu sample. It is well known that Cu(II) can enter into the crystal lattice of PdO to form  $\text{PdCuO}_2$  on supported catalyst systems (Pd,Cu/SiO<sub>2</sub>) [121]. However, the source of oxygen is not clear in the present case. Possibly, O<sub>2</sub> being present in trace amounts in the helium flow

accumulated in this long-term in situ-experiment while this did not play a role in the 4 h thermal pretreatment at 600 °C, in which metallic Pd was formed (Fig. 3.5). In any case, oxidation of Pd during thermal pretreatment at this stage of the work has been considered to be undesired since it proceeds at the expense of the target metallic Pd-phase. To suppress this oxidation and to promote reduction of Pd to the metallic state, thermal pretreatment has been studied in reducing atmosphere.

### 3.2.4.2 Measurements in 10 % H<sub>2</sub>/He

The XRD patterns for Pd,Cu and Pd,Sb samples reveal the presence of the same amine/ammonium-containing chloro complexes as in pure He flow in the range between 100 and 200 °C (Fig. 3.7). Marked influence of the thermal pretreatment atmosphere on the phase composition can clearly be seen only at elevated temperatures above 225 °C. In the Pd,Cu/TiO<sub>2</sub> sample, metallic Pd forms between 225 to 400 °C which is converted to PdH, most probably by dissolution of hydrogen in the Pd-lattice. This effect is well known for non-alloyed Pd-particles [122].

As in helium flow, no alloy formation is observed in the Pd,Cu sample. The PdH reflections vanished upon rising the temperature to 650 °C, possibly due to decomposition. Upon subsequent cooling to 50 °C, the crystallization of sulfur-containing phases such as CuS (PDF No. 3-1090) and Pd<sub>13</sub>Cu<sub>3</sub>S<sub>7</sub> (PDF No. 75-2229) is observed. Obviously H<sub>2</sub> promotes the reduction of (NH<sub>4</sub>)<sub>2</sub>SO<sub>4</sub> and/or of residual sulfate which remained in the TiO<sub>2</sub> support from the titania synthesis process to sulfide. The presence of sulfur-containing compounds was also confirmed by TEM-EDX and XPS results presented below.

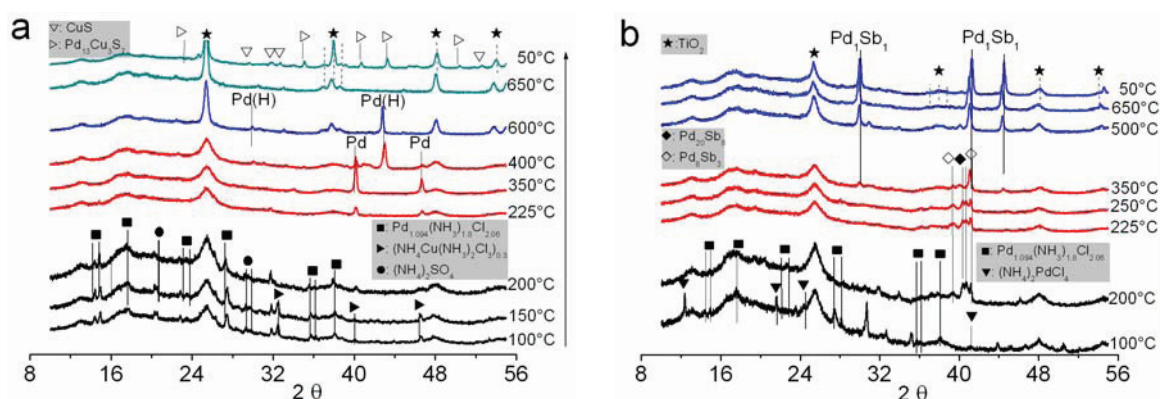


**Fig. 3.7** XRD patterns of a) Pd,Cu/TiO<sub>2</sub>, b) Pd,Sb/TiO<sub>2</sub> samples recorded during thermal pretreatment in 10 % H<sub>2</sub>/He. Patterns at 100 to 200 °C have been magnified by a factor of 2. Patterns at 50 °C were after cooling.

When the Pd,Sb precursor compound is pretreated in 10 % H<sub>2</sub>/He, no monometallic Pd

is observed as formed in pure helium. Instead, three different alloy compounds, namely Pd<sub>20</sub>Sb<sub>7</sub> (PDF No. 89-7603), Pd<sub>8</sub>Sb<sub>3</sub> (PDF No. 65-4354) and Pd<sub>1</sub>Sb<sub>1</sub> (PDF No. 89-2059) are formed. The former alloy (Pd<sub>20</sub>Sb<sub>7</sub>) was also observed in pure helium and disappears above 300 °C in favor of Pd<sub>1</sub>Sb<sub>1</sub>. This suggests that Pd<sub>20</sub>Sb<sub>7</sub> might be the intermediate phase for the formation of the Pd<sub>1</sub>Sb<sub>1</sub> phase. To the best of our knowledge, it is the first time that the formation of alloys between Pd and Sb is observed during this particular thermal pretreatment. In contrast to the Pd,Cu sample, no sulfur-containing phases have been observed in the Pd,Sb sample.

### 3.2.4.3 Crystallite size calculated using the Scherrer equation

Metal crystallite sizes are plotted as a function of temperature for the two different thermal pretreatment atmospheres in Fig. 3.8. When pretreated in helium flow, the mean Pd-crystallite size in the Pd,Cu/TiO<sub>2</sub> sample is about 45 nm and does virtually not change with rising thermal pretreatment temperature, while their number decreases in favor of PdO and CuPdO<sub>2</sub> formation (*cf* Fig. 3.6). In the Pd,Sb/TiO<sub>2</sub> sample, the size of Pd-crystallites increase from about 20 to 40 nm (Fig. 3.8b).

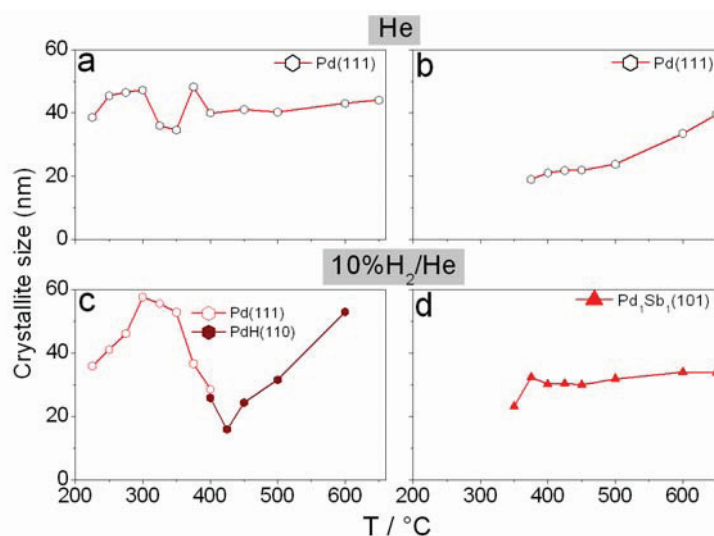


**Fig. 3.8** Crystallite size derived by the Scherrer equation from in situ-XRD measurements in helium and as well as in 10 % H<sub>2</sub>/He flow for (a, c): Pd,Cu/TiO<sub>2</sub> and (b, d): Pd,Sb/TiO<sub>2</sub> samples.

In reducing 10 % H<sub>2</sub>/He atmosphere, Pd-crystallites increase between 200 and 300 °C from about 40 to 60 nm in the Pd,Cu/TiO<sub>2</sub> sample followed by passing a minimum around 450 °C. This is most probably due to the incorporation of hydrogen in the Pd-crystallites to form PdH. The latter crystallites increase again to a final size of about 50 nm at 600 °C, before they decompose suddenly above 650 °C, probably due to the formation of the mixed Pd<sub>13</sub>Cu<sub>3</sub>S<sub>7</sub> phase (Fig. 3.8c and *cf* Fig. 3.7). In contrast, neither Pd nor PdH is observed for the

Pd,Sb/TiO<sub>2</sub> sample pretreated under the same conditions, but Pd<sub>1</sub>Sb<sub>1</sub> alloy crystallites are formed, the size of which stays more or less constant at about 30-35 nm, which is smaller in comparison to that of the pure Pd-particles formed in helium flow.

### 3.2.5 Size and morphological studies with transmission electron microscopy (TEM)

While XRD only provides information on the size of the primary metal crystallites, TEM/EDX enables insight into the morphology, size and composition of the metal particles which are usually built up of several crystallites. In previous investigations, metal particles larger than 100 nm were observed by TEM for catalytically active Pd-containing catalysts, especially in presence of Cu [11]. Electron micrographs of Pd,Cu/TiO<sub>2</sub> and Pd,Sb/TiO<sub>2</sub> samples before and after thermal pretreatment in He as well as in 10 % H<sub>2</sub>/He are shown in Fig. 3.9.

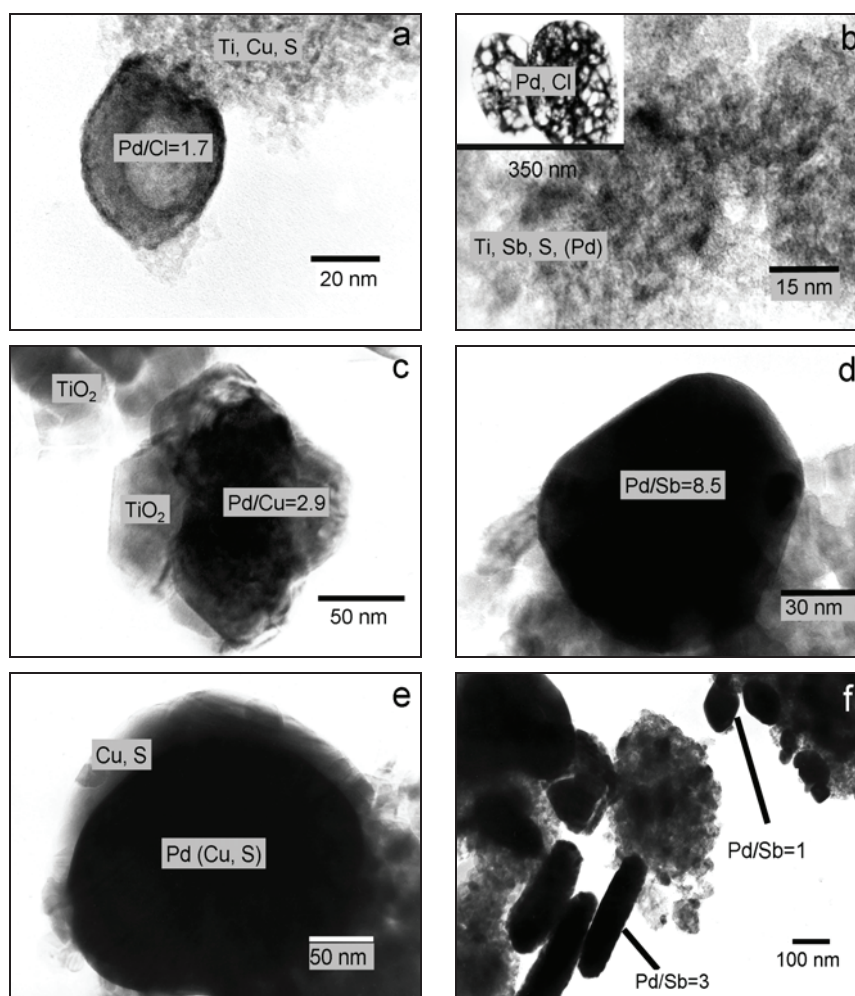


**Fig. 3.9** TEM micrographs of (a, c, e): Pd,Cu/TiO<sub>2</sub> and (b, d, f): Pd,Sb/TiO<sub>2</sub> samples in fresh, after the in-situ-XRD study in He and 10 % H<sub>2</sub>/He up to 650 °C. Transmission Electron Microscopy (TEM) investigations were carried out at 200 kV using a CM-20 microscope (Philips) equipped with an EDXS Noran Six (Thermo Scientific).



### 3.2.5.1 Non-pretreated samples

The non-pretreated Pd,Cu/TiO<sub>2</sub> sample (Fig. 3.9a) exhibits mainly TiO<sub>2</sub> support particles of around 5 nm. By EDX, a uniform distribution of copper was found on the support, while Pd was detected in the form of bubble-like PdCl<sub>2</sub> particles dispersed on the support. Since these bubbles were not stable under the electron beam, no precise information on their size can be derived. Besides, a homogeneous distribution of traces of sulfur has been detected as well. In the Pd,Sb/TiO<sub>2</sub> sample, as likewise observed for the Pd,Cu sample, the co-component Sb is homogeneously distributed over the TiO<sub>2</sub> particles, while Pd is found in form of bubble-like PdCl<sub>2</sub> particles, the size of which is markedly larger than in the Pd,Cu sample as shown in the insert (Fig. 3.9b).

### 3.2.5.2 Samples pretreated in helium

In the Pd,Cu/TiO<sub>2</sub> sample, Pd-particles of 50-200 nm were formed and TiO<sub>2</sub> particles increased from 5 nm to 50 nm. In the metal particles, Pd was always detected together with Cu, although the particular composition differs considerably from particle to particle. However, within one particle, the Pd to Cu ratio was found to be constant. As an example, a particle with Pd:Cu = 2.9 is shown in Fig. 3.9c. These results show clearly that particles with mixed Pd,Cu structures are formed, although no hint for alloy formation is found in the XRD patterns (Fig. 3.6). Probably, TEM micrographs reflect the mixed CuPd oxide structures detected also by XRD. The TEM picture of the Pd,Sb/TiO<sub>2</sub> sample confirms the existence of Pd-particles up to a size of about 150 nm (Fig. 3.9d). Frequently, traces of Sb were also detected on the periphery of those particles.

### 3.2.5.3 Samples pretreated in 10 % H<sub>2</sub>/He

After thermal pretreatment in reducing atmosphere, even larger metal particles of several hundred nanometers were detected in the Pd,Cu/TiO<sub>2</sub> catalysts, which clearly show a core-shell structure with a Pd core and a Cu shell (Fig. 3.9e). Considering the XRD results (*cf* Fig. 3.7), it is probable that the core of these particles consists rather of PdH, which cannot be distinguished from Pd by TEM. Besides, some traces of sulfur were also found, especially in the Cu shell. This agrees with the XRD results in which CuS and Pd<sub>13</sub>Cu<sub>3</sub>S<sub>7</sub> phases were detected in the same sample. It should be noted that core-shell structures of palladium and copper were also observed after use of such solids as catalysts in acetoxylation of toluene [11]. In the Pd,Sb/TiO<sub>2</sub> sample, a bimodal distribution of particles arises, consisting of spherical ones with a diameter of 50-120 nm and needle-like ones with a width of 90-130 nm and a length of 330-500 nm. EDX revealed an

approximate ratio of Pd/Sb = 1 which is in good agreement with the Pd<sub>1</sub>Sb<sub>1</sub> alloy phase found by XRD (*cf* Fig. 3.7). In the spherical particles, a lower Sb content (Pd/Sb = 3) was observed.

### 3.2.6 Surface and elemental compositional analysis by X-ray photo electron spectroscopy (XPS)

To obtain deeper insights in the valence state of each element and the composition in the near-surface-region, XPS measurements were performed. The Pd3d peaks of non-pretreated precursors and samples pretreated in helium as well as in 10 % H<sub>2</sub>/He are plotted in Fig. 3.10. Both the non-pretreated samples show only a single Pd3d<sub>5/2</sub> peak at a binding energy of E<sub>B</sub> = 338 eV which is characteristic for oxidic Pd [121].

No significant shift is observed for the Pd-peaks in presence of Cu. In contrast, those peaks are shifted to E<sub>B</sub> = 335.1 eV, being characteristic of zerovalent Pd [123] in the case of Pd,Sb/TiO<sub>2</sub>. This agrees properly with the XRD results in which a metallic Pd-phase was observed in Pd,Sb/TiO<sub>2</sub> but not in Pd,Cu/TiO<sub>2</sub> (*cf* Fig. 3.6).

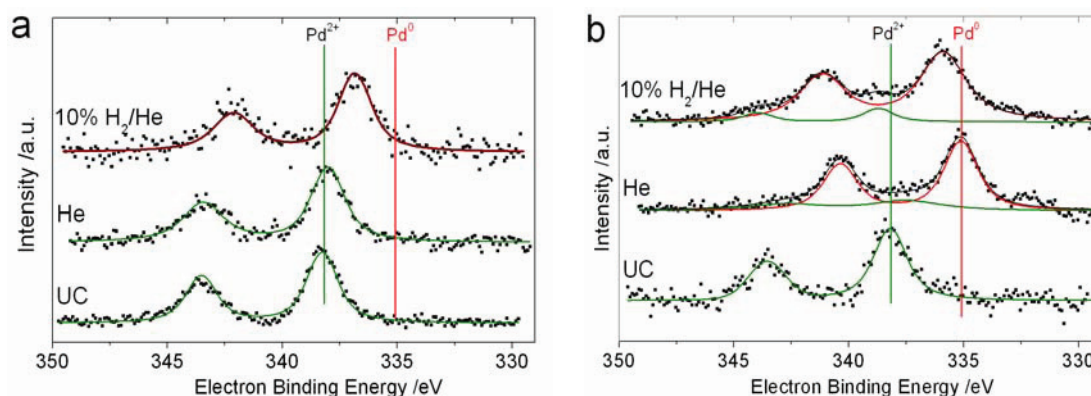


**Fig. 3.10** XP spectra of the Pd3d state of a) Pd,Cu/TiO<sub>2</sub>, b) Pd,Sb/TiO<sub>2</sub> samples in non pre-treated form (UC) and after the in-situ-XRD study in He (*compare* Fig. 3.6) and 10 % H<sub>2</sub>/He (*compare* Fig. 3.7).

After thermal pretreatment in the more reducing 10 % H<sub>2</sub>/He flow, the Pd3d peaks of the Pd,Cu/TiO<sub>2</sub> sample are shifted to lower binding energies; however, the E<sub>B</sub> value is still higher than expected for pure zerovalent Pd. This might be due to the formation of the sulfide-containing Pd-phase as already detected by XRD (*cf* Fig. 3.7), in which Pd should be at least partially positively charged. The existence of sulfide could be confirmed by XPS. Pd with a partial positive charge is also detected in the Pd,Sb/TiO<sub>2</sub> sample, while this sample shows essentially zerovalent Pd<sup>0</sup> after thermal pretreatment in pure He (Fig. 3.11). This can be explained by the formation of the Pd<sub>1</sub>Sb<sub>1</sub> alloy in the presence of H<sub>2</sub>, which leads to a partial shift of electron density from Pd to Sb. This is most probably due

to a  $\sigma$  donor- $\pi$  acceptor interaction between Sb and Pd. On the other hand, copper and antimony are found in the form of  $\text{Cu}^{2+}$  and  $\text{Sb}^{3+}$  in the near-surface region in all the samples.

XPS results suggest that Cu seems to stabilize oxidized rather than metallic Pd, whereas Sb facilitates the reduction of  $\text{Pd}^{2+}$  to  $\text{Pd}^0$  state. A reason may be the much lower redox potential of  $\text{Sb}^{3+}/\text{Sb}^0 = 0.15$  eV [124] in comparison to  $\text{Cu}^{2+}/\text{Cu}^0 = 0.3$  [125], and  $\text{Pd}^{2+}/\text{Pd}^0 = 0.95$  [124], which favors electron transfer from Sb to Pd rather than from Cu to Pd. In addition the affinity of  $\text{Cu}^{2+}$  species towards PdO (evidenced by XRD, TEM) and the ability of Sb to form alloys with Pd might be another reasons for stabilizing the palladium in oxidized and metallic states, respectively.

Interestingly, the surface Cu to Ti ratio increases from 0.06 to 0.29 after thermal pretreatment in helium, and even to 0.42 after thermal pretreatment in 10 %  $\text{H}_2/\text{He}$  (Fig. 3.11) This point to the migration of copper from the bulk to the surface, which is in nice agreement with the TEM results showing the presence of Pd core - Cu shell particles. A similar effect was observed previously in Pd,Cu/ $\text{TiO}_2$  supported catalysts used in toluene acetoxylation, in which core-shell particles with a Pd core and a Cu-containing shell were formed as well [11], but during the acetoxylation reaction. In contrast, no appreciable surface enrichment has been found for Sb (Fig. 3.11a), agreeing well the formation of a homogeneous  $\text{Pd}_1\text{Sb}_1$  alloy phase.

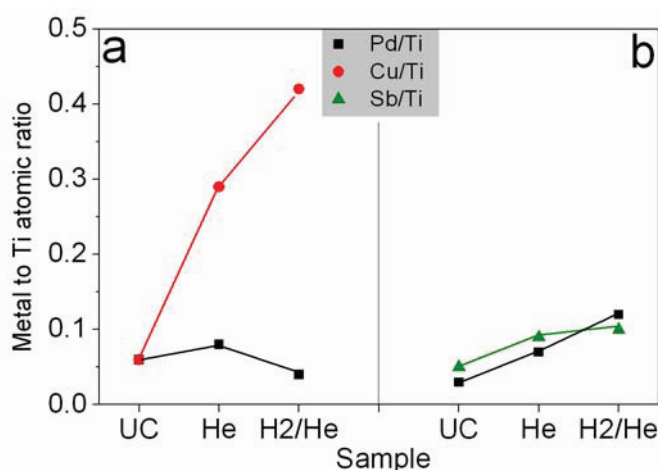


**Fig. 3.11** Metal (Cu, Sb, Pd) to Ti surface atomic ratios in a) Pd,Cu/ $\text{TiO}_2$ , b) Pd,Sb/ $\text{TiO}_2$  samples in non pre-treated form (UC) and after the in-situ-XRD study in He (compare Fig. 3.6) and 10 %  $\text{H}_2/\text{He}$  (compare Fig. 3.7). Surface atomic ratios were calculated from the areas of the XPS  $\text{Cu}2p$ ,  $\text{Pd}3d$ ,  $\text{Sb}3d_{3/2}$  and  $\text{Ti}2p$  peaks.

### 3.3 Influence of pretreatment on catalytic performance

Besides analyzing the influence of different metal precursors, additives and calcination procedures on the structure of the catalysts, it was one aim of this work to create Pd-particles



with a size as close as possible to that observed in equilibrated active catalysts (80-100 nm), since we are hoping that this helps to shorten the long conditioning times of such catalysts. To proof this assumption, a catalytic test has been performed with the Pd,Sb/TiO<sub>2</sub> catalyst. This catalyst was tested in fresh form with a 2 h thermal pretreatment in air at 300 °C within the reactor as well as after thermal pretreatment for 4 h at 600 °C in helium, which led to Pd-particles up to 150 nm in size. From Fig. 3.12(a) it is evident that the yield of benzyl acetate increases continuously from zero up to 20 % within 15 h time on stream. In contrast, the catalyst pretreated at 600 °C with the large Pd-particles reaches steady state already after 4 hours (Fig. 3.12(b)). This shows clearly that it is possible to shorten the equilibration time by creating large Pd-particles by suitable pretreatment procedures. However, it must be admitted, that the total benzyl acetate yield obtained with this Pd,Sb/TiO<sub>2</sub> catalyst is lower than in previous studies [9]. A possible reason could be that the Pd,Sb/TiO<sub>2</sub> catalysts in this work was not calcined in air but thermally pretreated in helium to avoid PdO formation. This, however, may be the reason for the formation of sulfides (not observed in previous preparations) which obviously poison the catalyst and lower the benzyl acetate yield. This issue will be further studied in the coming investigations (*see also* Chapter. 2).

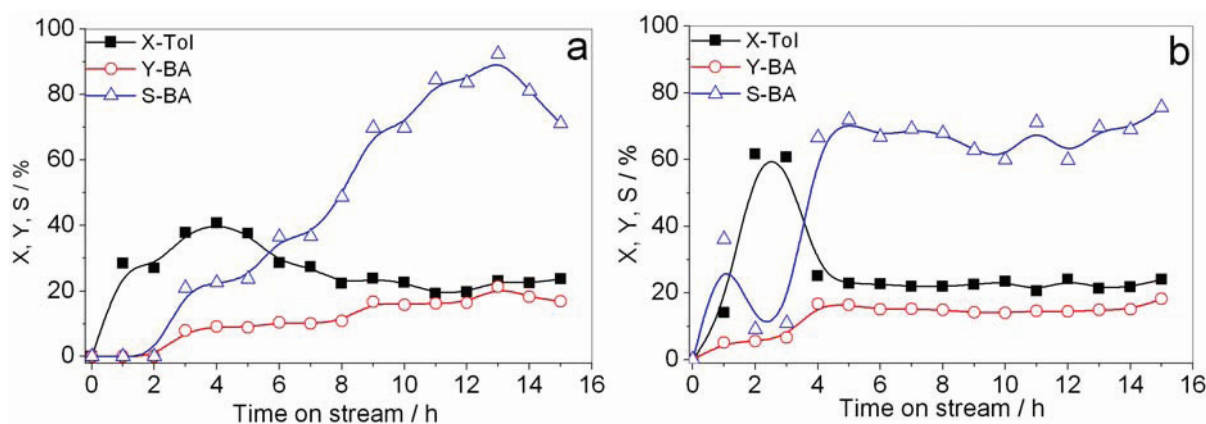


**Fig. 3.12** Catalytic performance of Pd,Sb/TiO<sub>2</sub> a) after calcination in air at 300 °C for 2 h with in the catalytic reactor and b) after external thermal pretreatment in helium at 600 °C for 4 h. X-Tol: Toluene conversion, S-BA: selectivity and Y-BA: yield of benzyl acetate

### 3.4 Conclusions

In this Chapter, we have investigated, how the composition and size of the metal particles in TiO<sub>2</sub>-supported mixed metal-Pd material is influenced by the metal co-component (Cu or Sb), the nature of the metal precursors (chlorides, nitrates or acetates) and chloride-removing additives (ammonium sulfate, nitrate, carbonate or urea) as well as the thermal pretreatment temperature and atmosphere (inert He or reducing H<sub>2</sub>/He). This was done with the aim to identify optimum conditions for the preferential synthesis of metallic nanostructured Pd-

particles with properties as close as possible to those of supported Pd-catalysts, which were recently found to catalyze the gas-phase acetoxylation of toluene very effectively, though with long conditioning times [10].

Among the metal precursors, chlorides revealed to be most beneficial for producing metallic Pd, while with nitrates the formation of PdO tentatively considered as undesired was observed and with acetates a complete loss of the Cu co-component as volatile  $\text{Cu}(\text{OAc})_2 \cdot \text{H}_2\text{O}$  occurred. Moreover, decomposition of the metal salts, being the crucial step to form metallic particles, started at lower temperature with chlorides.

The efficiency of the additives for removing chloride during thermal pretreatment increased in the order  $\text{NH}_4\text{NO}_3 < (\text{NH}_4)_2\text{CO}_3 < \text{Urea} < (\text{NH}_4)_2\text{SO}_4$ .  $(\text{NH}_4)_2\text{SO}_4$  revealed to be the additive which is able to remove Cl completely from both the Pd,Sb/TiO<sub>2</sub> and Pd,Cu/TiO<sub>2</sub> solids. Drawbacks of the other additives are incomplete Cl removal and poor crystallinity of the Pd-particles particularly with urea and  $\text{NH}_4\text{NO}_3$ . Interestingly, it was found that the decomposition of PdCl<sub>2</sub> to metallic Pd-crystallites proceeds via the intermediate formation of Pd-chloroamine complexes that start decomposing to metallic Pd already at around 200 °C. Probably, this facilitates the crystallization of Pd at low temperature.

Thermal pretreatment in helium flow produced Pd-crystallites for both the Pd,Sb and Pd,Cu systems of about 40 nm which aggregate to much larger Pd-particles of about 150 nm. In the Pd,Cu/TiO<sub>2</sub> sample, some oxidation to PdO and PdCuO<sub>2</sub> is observed above 350 °C, however only in the in situ-XRD runs. This is probably due to the accumulation of oxygen impurities.

Thermal pretreatment in reducing H<sub>2</sub>/He atmosphere promotes the formation of even larger metal particles. In the Pd,Cu/TiO<sub>2</sub> catalyst, these particles show a core-shell structure with a Pd and/or PdH core and a Cu shell [11]. These core-shell structures have already been observed previously, under catalytic acetoxylation conditions and prevail in the catalysts in their maximum active state [11]. Here, it is shown for the first time that they can be preformed by thermal pretreatment in H<sub>2</sub>/He atmosphere as well. Interestingly, no alloying occurs between Pd and Cu, which may be hindered by the formation of Cu chloroamine complexes that keep both the metals separated. When Pd,Sb/TiO<sub>2</sub> is pretreated in H<sub>2</sub>/He atmosphere, alloy particles are formed and the Sb to Pd ratio increases with the temperature of thermal pretreatment.

The important findings related to the effect of different metal precursors, co-components and thermal pretreatments on the nature of Pd-particles in Pd,Sb/TiO<sub>2</sub> and Pd,Cu/TiO<sub>2</sub> catalysts, are presented in Fig. 3. 13.

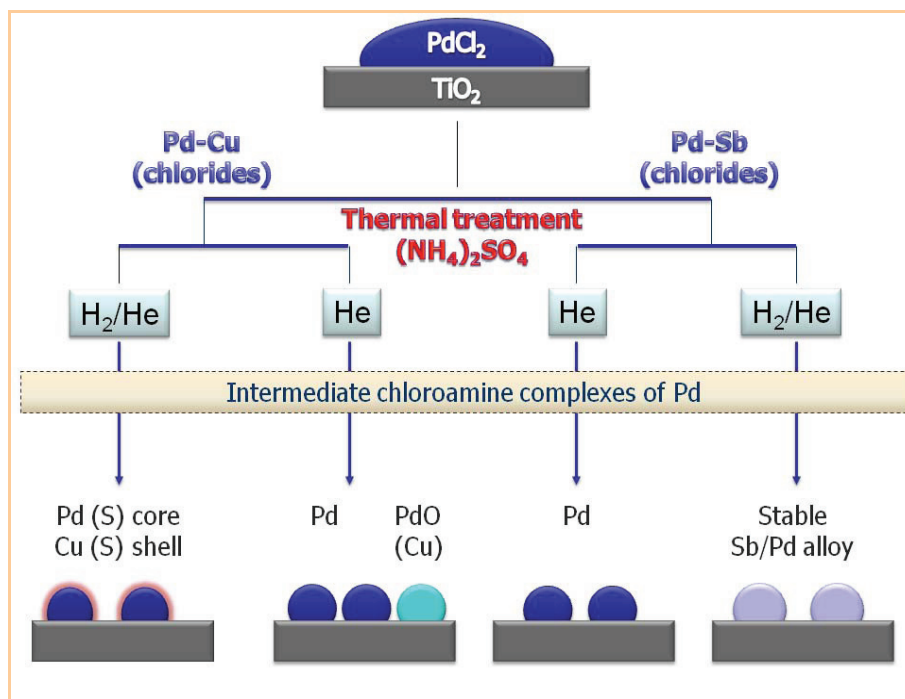


**Fig. 3.13** Summary of the important observations and findings related to the effect of different metal precursors, co-components and thermal pretreatments on the nature of Pd-particles in Pd,Sb/TiO<sub>2</sub> and Pd,Cu/TiO<sub>2</sub> catalysts.

In summary, we have found that it is possible to promote the metal particle growth to a size approaching that observed in active catalysts by suitable thermal pretreatment. Catalytic tests have shown that a thus pretreated catalyst reaches steady state much faster than a fresh one. The assessment of the influence of other properties besides particle size, such as residual sulfur species, metal particle composition and structure on the catalytic performance in toluene acetoxylation will be discussed in the next chapters.



## Chapter 4

### **Tailoring synthesis and thermal pretreatment of a 10Pd,16Sb/TiO<sub>2</sub> catalyst towards maximum performance and stability**

---

It has been shown in Chapter 3 that the conditioning time of a 10Pd,8Sb/TiO<sub>2</sub> (anatase) catalyst can indeed be markedly shortened when the Pd-particle size is purposefully increased prior to the catalytic test by a dedicated thermal pretreatment in helium atmosphere at 600 °C for 4 h, in comparison to a catalyst which was just heated in the reactor for 2 h in air at 300 °C before starting the acetoxylation reaction. However, the total benzyl acetate yield of the Pd,Sb/TiO<sub>2</sub> catalyst tested in this work is lower than in previous studies [10]. We believe that this is due to the formation of surface sulfides during thermal pretreatment in helium, which derives most probably from the reduction of ammonium sulfate added to remove chloride (resulting from the SbCl<sub>3</sub> starting compound) during thermal treatment.

To circumvent the addition of ammonium sulfate, we have developed a new synthesis procedure using Sb<sub>2</sub>O<sub>3</sub> instead of SbCl<sub>3</sub> as starting material and explored the influence of different thermal pre-treatment conditions on this catalyst. Moreover, the Sb content is doubled, in comparison to previous studies [10] and the catalysts described in chapter 3 of this thesis, to compensate for the loss volatile Sb during thermal treatment.

The new 10Pd,16Sb/TiO<sub>2</sub> catalyst described in this chapter has been prepared using the two-step procedure listed in chapter 2 with Sb<sub>2</sub>O<sub>3</sub> as precursor for the Sb co-component (Table 2.2 of Chapter 2). The as-received catalyst was thermally pre-treated for 2 h in air at 300 °C (in analogy to ref.[10]) and for 4 h in air or helium or 10 % H<sub>2</sub>/He at 600 °C. The results of catalytic tests of the new 10Pd,16Sb/TiO<sub>2</sub> catalyst after different thermal pre-treatment are discussed together with the structural properties after thermal pretreatment as well as after removing it from the catalytic reactor in its state of maximum activity. Changes experienced during subsequent deactivation are shortly mentioned as well. A detailed analysis of deactivated catalysts along with a discussion of key parameters for this deactivation is given in ref.[100].

---

## 4.1 Catalytic tests

In Fig. 4.1 the catalytic performance of the 10Pd,16Sb/TiO<sub>2</sub> catalyst obtained after the three different thermal pretreatment procedures (a: 300 °C-air; b: 600 °C-air; c: 600 °C-He) is compared. The catalytic performance after thermal pretreatment at 300 °C in air is similar to that of the conventionally prepared Pd,Sb/TiO<sub>2</sub> catalyst from ref.[10], which was pretreated after the same procedure but prepared using SbCl<sub>3</sub> and (NH<sub>4</sub>)<sub>2</sub>SO<sub>4</sub>. The maximum BA yields are continuously increasing and reach a maximum after about 10 h, followed by rapid deactivation. This confirms clearly that the new preparation method used in this work leads to equally effective catalysts as the conventional procedure used in ref.[10]. The structural properties (valance, morphology and composition) which influence apparently the performance of this sample have been derived through characterization with XRD, XPS and TEM, and the results are discussed in detail in Chapter 6.

A significant difference can be seen when precalcination in air is done at 600 °C (Fig. 4.1b). In this case, the conditioning period shortens to about 5-6 h during which the BA yield steeply increases and then reaches a plateau. On the other hand, the maximum BA selectivity is higher than after calcination at 300 °C (Fig. 4.1a). The main reason for the higher selectivity is most probably the less pronounced carbonization

of toluene over the catalysts pretreated at 600 °C leading to a significantly lower amount of carbon deposits in the used samples (Table 4.1). Equilibration time and maximum catalytic performance do not change when the atmosphere of the thermal pretreatment at 600 °C

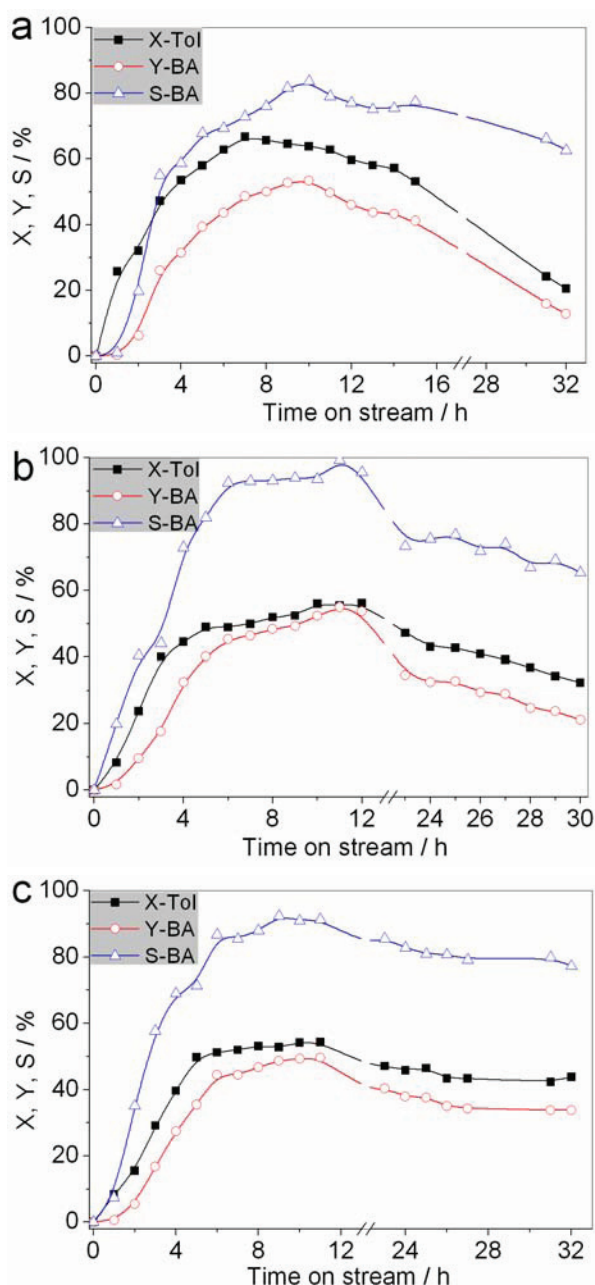


**Fig. 4.1** Toluene conversion (X-Tol), selectivity (S-BA) and yield (Y-BA) of benzyl acetate during time on stream over the 10Pd,16Sb/TiO<sub>2</sub> catalyst pretreated (a) at 300 °C in air for 2 h, (b) at 600 °C in air for 4 h and (c) at 600 °C in helium for 4 h.

changes from air to helium (Fig. 4.1c). However, a significant improvement of the catalyst stability is observed in the latter case, reflected by only a 10 % drop of the BA yield within 24 h on stream. The most surprising effect was seen with a catalyst after thermal pretreatment in 10 % H<sub>2</sub>/He at 600 °C. This sample revealed to be totally inactive with a toluene conversion of less than 1 %. Therefore, these results are not plotted in Fig. 4.1.

From these results it is clearly evident that the thermal pretreatment has a significant impact on the catalytic performance. While the pretreatment temperature is crucial for the duration of catalyst equilibration, the surrounding atmosphere is more important for the BA selectivity as long as it has no reducing properties which lead to complete activity loss. To get deeper insights into this unexpected behavior, detailed characterization of catalysts was performed after thermal pretreatment at 600 °C, after reaching maximum catalytic performance at 9 h and 6 h on stream for samples pretreated in air and He, respectively. For this purpose, the reaction feed was stopped and the system was cooled slowly to room temperature in inert atmosphere (a detailed study of the samples after 30 h of use is given in ref.[100]). In addition, analogous characterization was also done for 10Pd,16Sb/TiO<sub>2</sub> samples after thermal treatment in 10 % H<sub>2</sub>/He as well as after 8 h on stream to find reasons for its inactivity.

## 4.2 Catalyst characterization

### 4.2.1 Elemental analysis and N<sub>2</sub>-adsorption

**Table 4.1** Elemental composition, BET surface area and pore volume of pretreated 10Pd,16Sb/TiO<sub>2</sub> catalysts in air and He at 600 °C, and respective spent (9 and 6 h) samples. The Sulfur content in pure TiO<sub>2</sub> is also shown.

(Sample)-time on stream	Pd (wt.-%)	Sb (wt.-%)	S (wt.-%)	Na (wt.-%)	C (wt.-%)
(Pure TiO <sub>2</sub> )	-	-	2.3	-	-
(600 °C-air)	8.5	12.2	1.4	5.1	-
(600 °C-air)-9 h	8.6	12.2	1.3	5.0	0.5
(600 °C-He)	9.3	9.3	1.5	4.4	-
(600 °C-He)-6 h	8.2	10.2	1.6	5.9	0.65

Inspection of Table 4.1 shows that the Pd content of pretreated and used catalysts is almost equal to the nominal value. In contrast, the corresponding Sb value after thermal treatment is slightly lower, pointing to some loss of Sb as volatile species, especially for the He treated samples. No further change in the Pd and Sb contents is observed during use in the reaction. A minimum percentage of sulfur (1.5 wt.-%) is still detected in all the samples, which is however much smaller than the 6 - 7 wt.-% detected in the catalysts of Chapter 3



[12], in which (NH<sub>4</sub>)<sub>2</sub>SO<sub>4</sub> was used as an additive. This small amount of residual sulfur is part of the TiO<sub>2</sub> support, yet it might not have a detrimental impact on the catalytic performance, since sulfur-free anatase, which has also been tested as support, does not lead to improved catalysts.

An interesting trend is observed for the BET surface areas. A marked decrease in the surface area and pore volume of the pure support was observed upon loading with the metal components. This may be partly due to pore blocking of the support with the metal components. In addition, the intermediate calcination between step 1 and 2 in the preparation may also have affected the BET surface area. The decrease of the surface area and pore volume is partly reversible after calcination in air but not in helium at 600 °C (Table 4.2). On the other hand, these values decrease again when the air-calcined sample is used in the acetoxylation reaction while only a slight effect is observed for the helium-pretreated catalyst. This suggests that high-temperature treatment in oxidizing atmosphere may have an impact on the support structure, most probably on the TiO<sub>2</sub> crystallite size which is smaller for the samples after air pretreatment (Table 4.2). This may be the main reason for the difference in the BET surface areas.

**Table 4.2** BET surface area and pore volume of the pretreated 10Pd,16Sb/TiO<sub>2</sub> catalysts in air and He at 600 °C, and respective spent (9 and 6 h) samples. Crystallite Size of TiO<sub>2</sub> is also shown. Crystallite size was calculated with Scherer equation from the XRD patterns of Fig. 4.2.

(Sample)-time on stream	S <sub>BET</sub> (m <sup>2</sup> g <sup>-1</sup> )	Pore volume (cm <sup>3</sup> g <sup>-1</sup> )	Crystallite size of TiO <sub>2</sub> (nm)
(Pure TiO <sub>2</sub> )	315	0.27	8.36
(600 °C-air)	115.3	0.38	10.8
(600 °C-air)-9 h	71.6	0.15	10.9
(600 °C-He)	28.6	0.10	15.3
(600 °C-He)-6 h	40.6	0.13	16.8

As conclusion, the surface area of the TiO<sub>2</sub> support seems to be less important for the catalytic behavior. It decreases to a very different extent during thermal pretreatment at 600 °C in air and He, namely to 115.3 m<sup>2</sup>/g and 28.6 m<sup>2</sup>/g, respectively. Although this may be one reason why the metal particles after treatment in helium are larger in comparison to calcination in air (*compare* Fig. 4.3a1, a2 and 4.4a1, a2), this does obviously not influence the catalytic behavior during conditioning which is very similar in both cases (*see* Fig. 4.1b, c). This suggests that the performance of the catalysts is governed by the nature of the Pd-particles but not so much by its surface area.

### 4.2.2 X-ray diffraction (XRD)

XRD measurements were done for the samples after thermal treatment in air, helium and 10 % H<sub>2</sub>/He at 600 °C as well as for the respective spent (9, 6 and 8 h) samples. Diffractograms are shown in Fig. 4.2. Si has been added to all the samples as internal standard for the exact determination of peak positions and intensity.

In Fig. 4.2, the XRD patterns of all samples show of course the reflections of the TiO<sub>2</sub> anatase (★) support (PDF No. 21-1272) besides those of Si which was used as an internal standard (Fig. 4.2a). In addition, NaCl (□) (PDF No. 5-628) and Na<sub>2</sub>SO<sub>4</sub> (+) (PDF No. 75-914) are seen in certain samples, which might have formed from Na<sub>2</sub>CO<sub>3</sub> and PdCl<sub>2</sub> or sulfate contained in the TiO<sub>2</sub> support, respectively. All XRD patterns of the spent samples (except H<sub>2</sub>) and also of the fresh catalysts pretreated in He at 600 °C show clearly the presence of a metallic Pd (#) phase (PDF No. 88-2335), while Pd in the fresh catalyst calcined in air at 600 °C is present as PdO (o) (PDF No. 41-1107). In contrast, when thermal pretreatment is performed in 10 % H<sub>2</sub>/He at 600 °C, no Pd but a Pd<sub>8</sub>Sb<sub>3</sub> (☆) alloy phase (PDF No. 89-2059) is formed and is stable even with the time on stream. It reveals that this pretreatment converts the whole Pd amount into a well defined crystalline Pd<sub>8</sub>Sb<sub>3</sub> alloy, which is obviously inactive since there is no other Pd phase besides the Pd<sub>8</sub>Sb<sub>3</sub> phase.

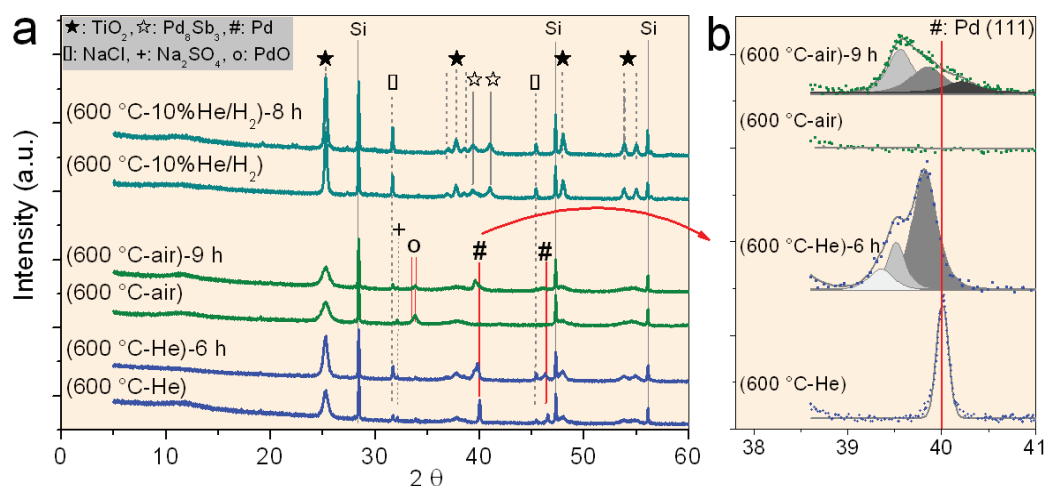


**Fig. 4.2:** a) XRD patterns of the pretreated 10Pd,16Sb/TiO<sub>2</sub> catalysts in air, He and 10 %H<sub>2</sub>/He at 600 °C, and respective spent (9, 6 and 8 h) samples; b) deconvolution of the metallic Pd(111) peak into sub peaks.

The Full Width at Half Maximum (FWHM) of the anatase peaks is broader for the samples calcined in air, suggesting lower crystallites size. This is evident from Table 4.2, in which the TiO<sub>2</sub> crystallite size, calculated by the Scherrer equation, for samples after thermal pretreatment in air and helium is compared. This could be one reason for the higher BET surface area observed in the air-calcined sample (Table 4.2). In addition to TiO<sub>2</sub> crystallites,

the changes of the BET surface described above can be explained also by the different Pd crystallite size. Very sharp Pd reflections indicating large crystallites were found for the sample after helium pretreatment with the lowest BET surface.

Significant differences are evident in the shape of the Pd(111) reflections, which have been deconvoluted into several subsignals (Fig. 4.2b). The position, intensity and FWHM of these signals are listed in Table 4.3. A single symmetric peak appears in the fresh sample after thermal pretreatment in He at 40.01°, which is consistent with the presence of a crystalline metallic Pd phase with cubic structure and a Fm-3m (225) space group [126]. After use in the catalytic reaction, this peak splits into three subsignals, which are all shifted to lower values of 2  $\theta$  in comparison to the peak of pure metallic Pd. This behavior points to a change of the Pd lattice during time on stream, which is most probably caused by the incorporation of other components such as Sb, C and/or H. Thus, the dissolution of C [51, 127] and H [128] into the Pd lattice led to slight downshifts of the 2  $\theta$  values, as likewise observed in Fig. 4.2b, while this was not observed for oxygen. In the latter case, only surface or bulk Pd oxides were formed, the XRD reflections of which do not appear in the metallic Pd region [129-132]. TEM measurements shown below confirm the incorporation of Sb into the Pd lattice of the helium-pretreated sample. According to the phase diagram, incorporation of Sb into the Pd lattice is possible for Pd/Sb ratios higher than 5, while for Pd/Sb ratios between 3 and 0.5 stable alloy phases such as Pd<sub>1</sub>Sb<sub>2</sub>, Pd<sub>1</sub>Sb<sub>1</sub>, Pd<sub>8</sub>Sb<sub>3</sub> and Pd<sub>20</sub>Sb<sub>7</sub> are formed [133]. In our case, this happened when the sample was pretreated in reducing atmosphere, namely 10 % H<sub>2</sub>/He. In Fig. 4.2a, the reflections of a Pd<sub>8</sub>Sb<sub>3</sub> alloy phase are clearly seen after this treatment.

**Table 4.3** Peak position, peak area and FWHM derived from XRD patterns of the pretreated 10Pd,16Sb/TiO<sub>2</sub> catalysts in air and He at 600 °C, and respective spent (9 and 6 h) samples.

Sample	Sub peak position 2 $\theta$ / °	Peak area	FWHM
He-Fresh	40.01	111.6	0.16
(600 °C-He)-6 h	39.3	40.2	0.32
	39.5	63.5	0.23
	39.8	221.2	0.31
(600 °C-air)-9 h	39.5	92.67	0.34
	39.9	69.68	0.45
	40.2	24.94	0.40

Inspection of the positions of the Pd reflections of the helium-pretreated catalyst after 6 h on stream (Fig. 4.2b, Table 4.3) clearly shows that all the subsignals are present in the lower 2  $\theta$  range (i.e. 39.3, 39.5, 39.8°) compared to metallic Pd at 40°, suggesting that the

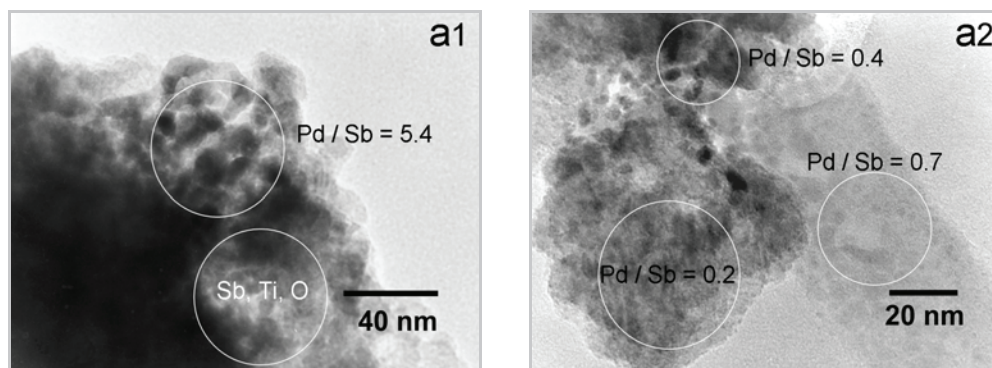
incorporation of Sb (and possibly also C) into Pd is more likely possible in this sample. When the catalysts had been pretreated in air instead of helium, the downshift of the Pd reflections with increasing time on stream is less pronounced, suggesting that a major part of the metal phase might persist as pure Pd.

Further information about composition, morphology and size of the metal particles has been derived by TEM described below.

### 4.2.3 Transmission electron microscopy (TEM)

#### 4.2.3.1 Air-pretreated samples

TEM, STEM-HAADF and EDX results of the catalysts after calcination in air at 600 °C and after 9 h use in the acetoxylation reaction are depicted in Fig. 4.3. After calcination in air, Pd-containing particles with a size of 5 - 10 nm are well dispersed over the whole support surface (Fig. 4.3a1, a2). With regard to the XRD pattern (*cf* Fig. 4.2a), it is most probable that these particles consist of PdO. From EDX alone this conclusion cannot be derived since, due to their small size, the electron beam spot cannot be exclusively focused on a Pd-containing particle alone but hits always a certain area of the support as well. Therefore, radiation emitted from oxygen in PdO and TiO<sub>2</sub> cannot be distinguished. Besides areas with a rather high Pd/Sb ratio, probably arising from the joint detection of small PdO particles and the underlying Sb-containing TiO<sub>2</sub> support (Pd/Sb = 5.4, Fig. 4.3a1), there are Sb-containing support areas without any Pd (Fig. 4.3a1) or with only traces of Pd (Fig. 4.3a2). This suggests that in contrast to Pd which forms a crystalline PdO phase, Sb is highly dispersed on the support. This agrees well with the fact that no crystalline Sb<sub>2</sub>O<sub>3</sub> has been observed by XRD.



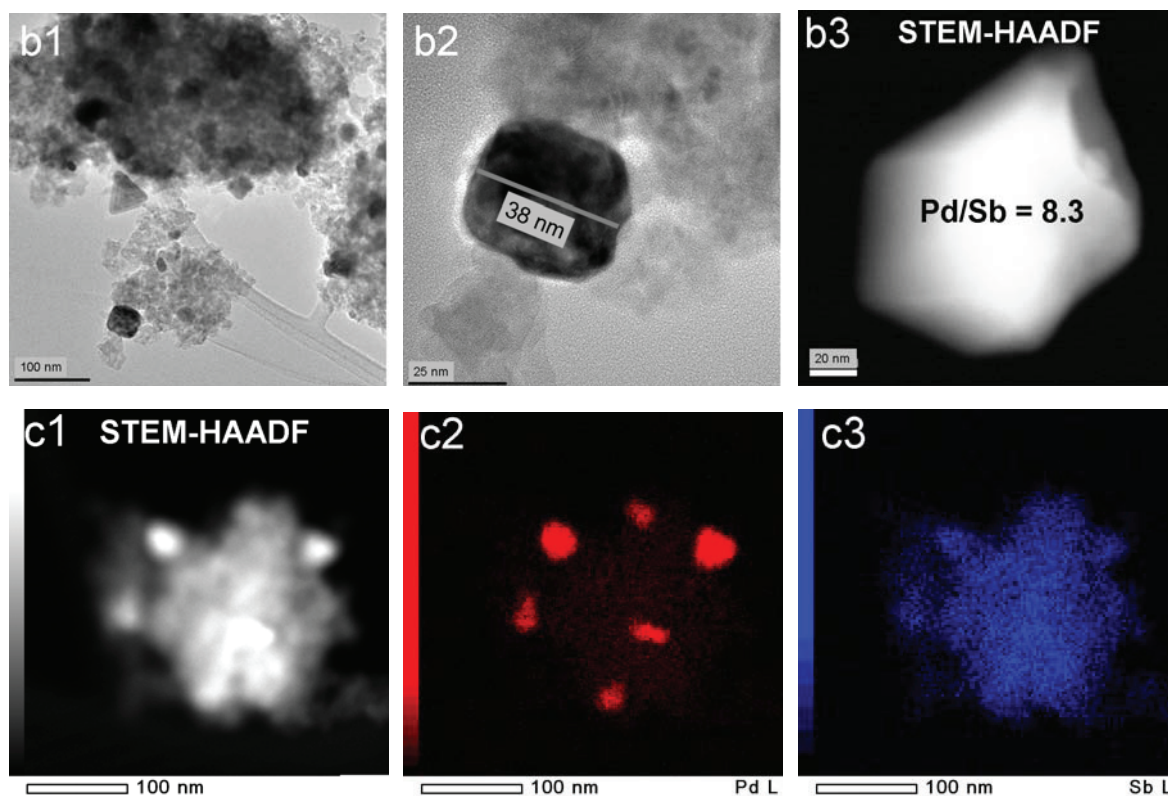


**Fig. 4.3** Electron microscopic images of fresh (a1, a2) and spent (b1, b2, b3, c1, c2, c3) 10Pd,16Sb/TiO<sub>2</sub> air-pretreated samples. TEM: a1, a2, b1, b2; STEM-HAADF: b3, c1; EDX map: c2 (Pd L) and c3 (Sb L).

After 9 h use in the catalytic reaction, Pd-particles of about 30 - 50 nm with different shapes (triangular, cubic as well as spherical) are formed, which are very well crystallized showing a faceted structure (Fig. 4.3b1, b2). These particles do contain only some traces of Sb. The atomic ratio between the Pd and Sb present in these particles, calculated from EDX, was found to be higher than 8. One such particle is shown in Fig. 4.3b3, which has a Pd/Sb atomic ratio of nearly 8.3. On the other hand, nearly Pd-free Sb particles were also observed. This shows clearly that the Pd and Sb components remain widely separated in the catalyst.

HAADF-STEM analysis was done to get an overview on the distribution of Pd and Sb. Since the high angle annular dark field depends strongly on the atomic number of the elements present in the specimen, we can see a good contrast between heavy and lighter elements. Brighter parts represent the heavier elements (Pd), whereas dark areas denote the lighter elements (Sb). A slight contrast between the bright and dark spots is visible in Fig. 4.3c1. EDX elemental maps for Pd L and Sb L reveal a high dispersion of Sb on the support as well as the intermixing of Sb with the Pd-particles, whereas most of the Pd is separated from the support and exists as bigger particles.

#### 4.2.3.2 Helium-pretreated samples

Very different results have been obtained for the catalyst pretreated in helium at 600 °C.



Large Pd-particles of up to 1-2  $\mu\text{m}$  diameter have been formed during pretreatment in helium, leaving a considerable part of the support free of Pd (Fig. 4.4a1, a2) but containing Sb as for the air calcined samples. After 6 h on stream in the catalytic reaction, surprisingly, a marked decrease of the particle size down to 30-50 nm was observed, which is equal to the size of the Pd-particles formed during time on stream from the air-pretreated catalyst (*compare* Fig. 4.3b1, b2 and 4.4b1, b2). However, in contrast to air-pretreated sample in which the Pd-particles are of different shapes, in helium-pretreated sample the formation of nearly spherical shaped particles is observed (Fig. 4.4b1, b2).

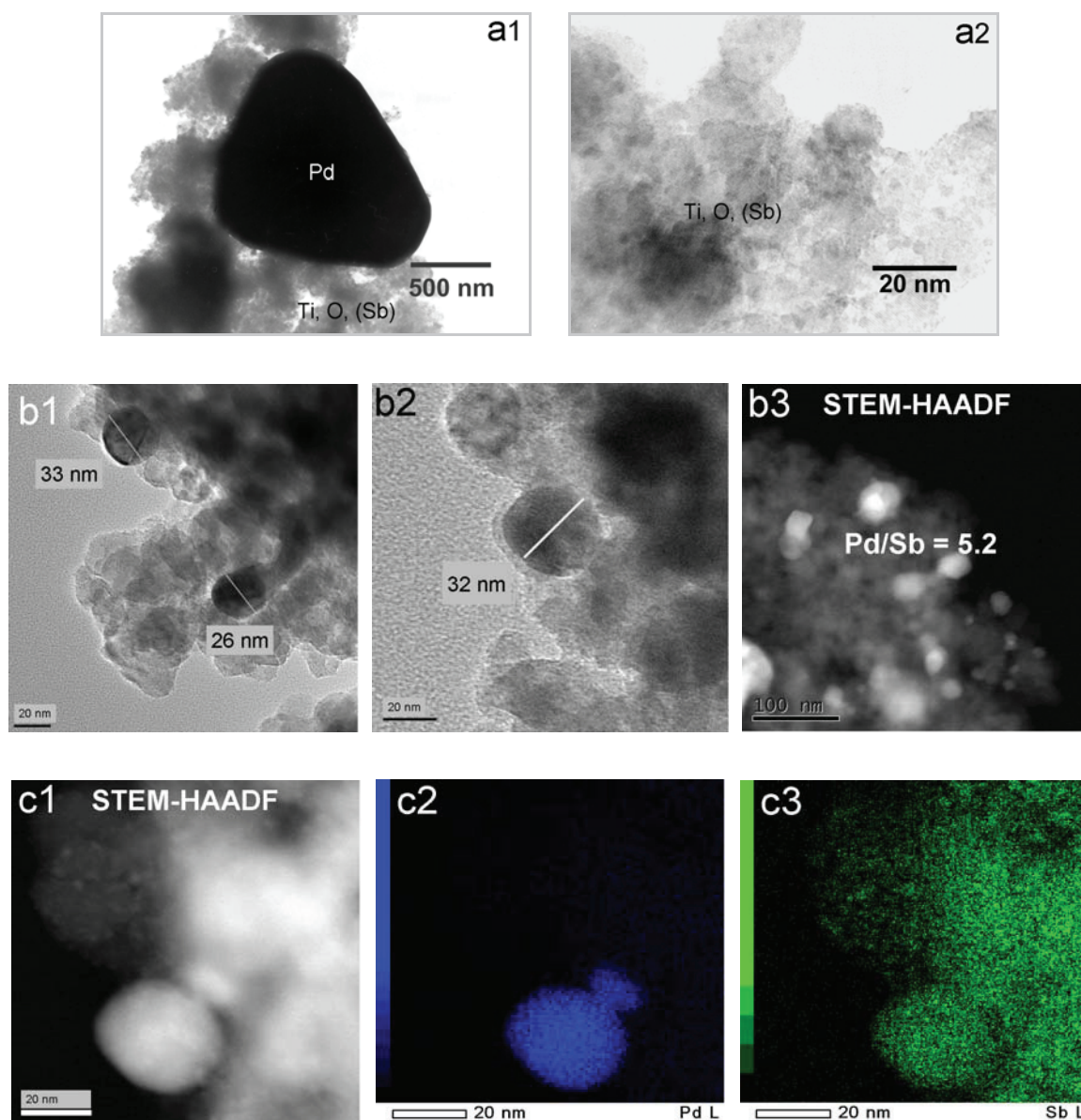


**Fig. 4.4** Electron microscopic images of fresh (a1, a2) and spent (b1, b2, b3, c1, c3, c3) 10Pd,16Sb/TiO<sub>2</sub> helium-pretreated samples. TEM: a1, a2, b1, b2; STEM-HAADF: b3, c1; EDX map: c2 (Pd L) and c3 (Sb L).

As in the air calcined samples after time on stream, helium-pretreated sample also

contain the metallic Pd-particles with some Sb. However, in contrast to the former catalyst, in which the formed Pd-particles contain only traces of Sb (*cf* Fig. 4.3b3), those in the helium-pretreated catalyst are richer in Sb, showing uniform Pd/Sb ratios around 5 (Fig. 4.4b3), while the rest of the Sb is spread over the TiO<sub>2</sub> support without forming a separate phase. However, the Sb content detected by EDX on the support is smaller than observed for the air-calcined catalyst, which might be a consequence of the higher Sb enrichment in the Pd-particles. Furthermore, on certain Pd-particles which are well separated from the support, traces of oxygen have been detected, suggesting a partial oxidation of their surface during time on stream. This has been further explored by XPS in the coming section.

As shown in Chapter 3, there is no doubt that the conditioning time can be shortened by pre-forming Pd-particles of suitable size using a tailored thermal pretreatment. However, inspection of catalytic activity profiles (Fig. 4.1) and TEM analysis (Fig. 4.3 and Fig. 4.4) of air and helium samples suggests that a rather small size of the starting particles might be sufficient for this effect. Despite the large difference in the starting particle size after air and helium pretreatment, the latter approach each other by restructuring during conditioning, which leads to Pd-particles of about 30 - 50 nm independent of the pretreatment atmosphere. More importantly, Pd-particles in both the samples at their maximum activity contain certain amount of Sb. Obviously this is caused by migration of Sb species from the support surface into the Pd-phase during conditioning.

Taking the catalytic test result into account, it appears that the intermixing of Pd and Sb within the metal particles is essential for ensuring high catalytic performance and long-term stability, as long as the incorporated Sb content remains low enough to prevent alloy formation, which is well known for Pd/Sb ratios of 3:1, 2:1, 1:1 and 1:2 [133]. However, the concentration of Sb inside the Pd-particles should not be too low to retain high stability. Obviously, very Pd-rich particles as formed in the spent air-pretreated catalyst (Fig. 4.3b3) lead to more pronounced deactivation. This deactivation aspect is described in detail as a doctoral thesis in ref.[100].

#### 4.2.4 X-ray photoelectron spectroscopy (XPS)

In Fig. 4.5 XP spectra of the Pd3d and Sb3d<sub>3/2</sub> regions are shown for samples after thermal pretreatment at 600 °C in helium or air and after stopping the catalytic test in the state of maximum activity (6 or 9 h on stream). The Pd3d<sub>5/2</sub> peak of the catalyst after calcination in air falls at 335.8 eV. These values are in the range of oxidic Pd. This agrees properly



with the XRD results in which a crystalline PdO phase has been detected for this catalyst (*cf* Fig. 4.2a). However, this value is considerably lower than the binding energy of 336.5 eV measured for pure PdO (Fig. 4.5) [134]. A strong interaction between TiO<sub>2</sub> and the tiny PdO particles can be assumed as reason for the lower binding energy compared to unsupported PdO. Remarkably, the spectrum of the catalyst after pretreatment in helium is almost identical to the one after air-calcination (Fig. 4.5), although metallic Pd was detected by XRD in this case. This might be due to the formation of surface oxide species on the large Pd-particles obtained after the pretreatment in helium. It is not likely that these species have been formed by contact with ambient atmosphere at room temperature since similar effects are not observed in other samples discussed below.

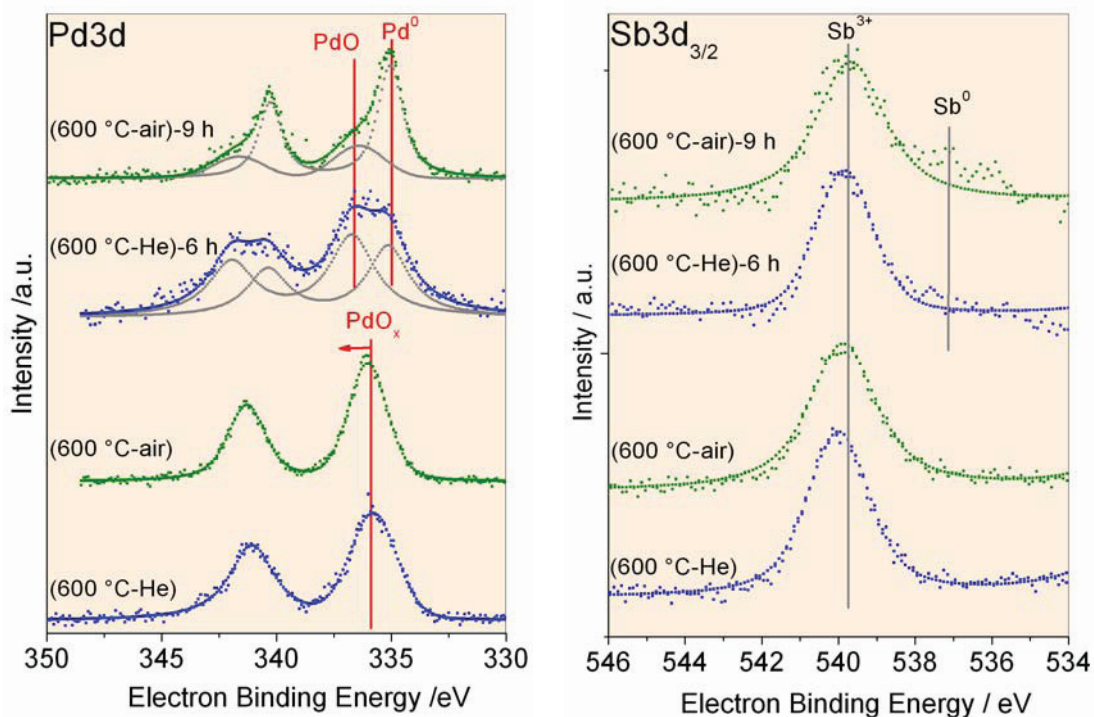


**Fig. 4.5** XP spectra of Pd3d and Sb3d<sub>3/2</sub> peaks of the pretreated 10Pd,16Sb/TiO<sub>2</sub> catalysts in air and helium at 600 °C, and respective spent (9 and 6 h) samples

In the catalysts removed from the reactor after reaching maximum activity (6 and 9 h), two Pd3d<sub>5/2</sub> peaks are observed with binding energies of 335.1 eV arising from pure metallic Pd [135] and 336.5 eV being characteristic for PdO [134]. In the helium-pretreated sample, the metallic Pd peak is broader, indicating a higher heterogeneity of the Pd environment and the PdO peak is more pronounced than in the air-calcined sample, in which the majority of Pd on the surface is purely metallic with only a minor contribution of PdO. This could be due to the prominent incorporation of Sb into the Pd-phase of the helium-pretreated catalyst (as evidenced by TEM and XRD), which might increase the heterogeneity of the Pd environment

and obviously stabilizes PdO surface species. Both effects are much less prominent in the XP spectrum of the air-calcined sample (9 h), in which TEM and XRD suggest that Pd and Sb are spatially widely separated.

In all samples, Sb is present mostly in oxidized form, evidenced by a Sb3d<sub>3/2</sub> peak with a binding energy of 540 eV, being characteristic for Sb<sub>2</sub>O<sub>3</sub> [136]. However, especially in spent samples, there is some noise in the metallic Sb region which may point to a small peak. Suspects the formation of metallic Sb during the reaction and in due course a certain quantity of Sb might be incorporated in the Pd-bulk lattice, while rest remains on the catalyst surface. These findings by XPS support the results obtained by XRD and TEM related to Sb incorporation.

The XP spectra of the samples pretreated in 10 % H<sub>2</sub>/He flow show the Pd3d<sub>5/2</sub> peak at a binding energy of 335.6 eV after both the pretreatment and after 8 h on stream, which can be explained by the formation of Pd<sub>8</sub>Sb<sub>3</sub> alloy. No evidence for PdO was found at these samples.

As conclusion, the co-existence of both Pd and PdO species is beneficial for high catalytic performance. This has also been proposed for supported Pd-catalysts in other oxidation reactions, example, the total oxidation of methane [137-139]. It was suggested that the hydrocarbons are adsorbed on the metallic Pd surface sites, while PdO is responsible for their oxidation. Probably, a similar mechanism is valid for the acetoxylation of toluene. Considering the composition of the metal particles, it may be assumed that dissolution of Sb within the Pd-particle surface stabilizes oxidized Pd in its vicinity.

### 4.3 Conclusions

The conditioning time of 10Pd,16Sb/TiO<sub>2</sub> catalysts can be markedly shortened by a thermal pretreatment which is severe enough (600 °C, 4 h) to initiate the pre-formation of Pd-containing particles from the PdCl<sub>2</sub> precursor on the TiO<sub>2</sub> support. However, the performance and particularly the stability of the catalysts depend on the atmosphere of the thermal pretreatment.

The most important observations of the present investigations are shown in Fig. 4.6. Reducing atmosphere (10 % H<sub>2</sub>/He) leads to the formation of completely inactive Pd-Sb alloy particles. Calcination in air creates PdO particles of 5 - 10 nm, which are reduced to almost pure Pd<sup>0</sup> with only traces of incorporated Sb during time on stream and which grow to 30 - 50 nm. In contrast, a helium pretreatment atmosphere forms very large initial Pd<sup>0</sup> particles (up to

1-2  $\mu\text{m}$ ) with a partially oxidized surface, that are restructured to smaller ones of 30 - 50 nm by incorporation of Sb up to a ratio of Pd/Sb  $\approx$  5, yet without formation of stable alloy phases. The surface of these particles contains both, metallic Pd<sup>0</sup> and PdO species while the surface of the Pd-particles of the air-pretreated catalyst, containing some oxidized Pd in the state of highest activity, becomes essentially free of PdO after extended time on stream (ref.[100]).

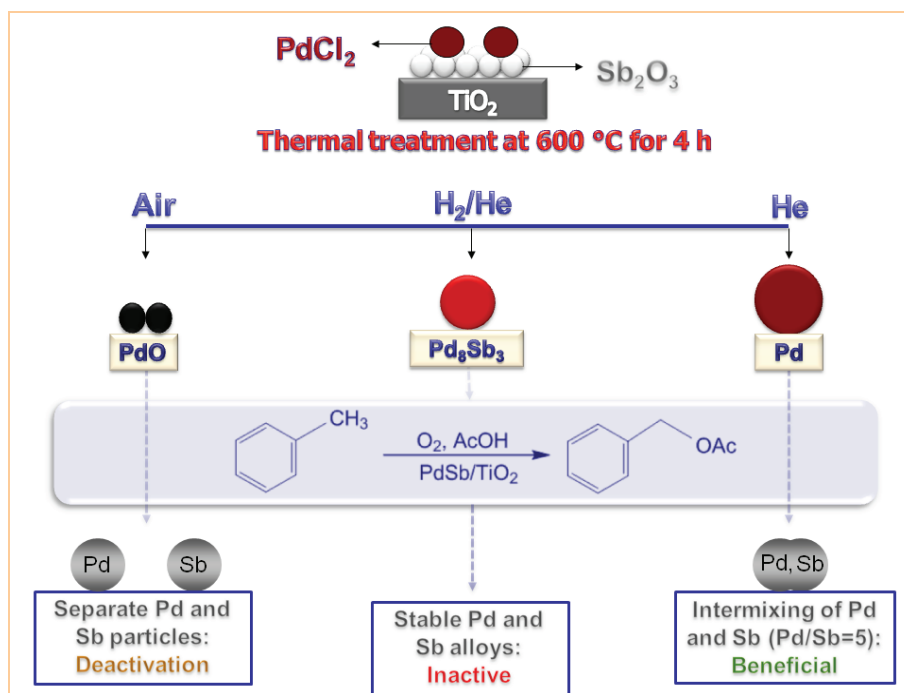


**Fig. 4.6** Impact of thermal treatment on the nature of Pd or Sb-particles and their influence on the acetoxylation activity of 10Pd,16Sb/TiO<sub>2</sub> catalysts.

Finally, among air and helium-pretreated catalysts, the one pretreated in helium shows a more stable toluene conversion and BA selectivity. This is most probably due to the co-existence of Pd<sup>0</sup> and PdO in the latter. This might be favored by the intermixing of Sb into the Pd-particles, which is assumed to stabilize oxidized Pd in its vicinity. In summary, it can be stated that the bulk properties of the metal particles formed during pretreatment play an important role for long-time stability by governing the formation of distinct Pd-species on the surface during time on stream.



## Chapter 5

### **Influence of co-components (M) on the state of Pd and on the performance of 10Pd,8M/TiO<sub>2</sub> (anatase) catalysts**

---

In the earlier investigations, the effect of co-components (Sb, Cu, Sn, Bi) on the catalytic performance of 10Pd,8M/TiO<sub>2</sub> catalysts in the gas phase acetoxylation of toluene [6] has been studied. However, the role of co-components on the state of palladium has not been adequately explored except for Sb or Cu [10, 11]. In addition, by choosing randomly the co-components, it is also difficult to get a clear consensus about their actual function. Therefore, for the present study, the co-components (Mn, Co, Au and Sb) with a wide range of standard reduction potentials ( $E^0$ :  $Mn^{2+}/Mn = -1.18$  eV,  $Co^{2+}/Co = -0.28$  eV,  $Sb^{3+}/Sb = +0.2$  eV and  $Au^{3+}/Au = +1.52$  eV) are chosen and their effect (geometric or electronic) on the state of Pd as well as on the catalytic performance of 10 wt.-% Pd, 8 wt.-% M/TiO<sub>2</sub> (M=Mn, Co, Sb, Au) catalysts in the gas phase acetoxylation of toluene to benzyl acetate is studied.

---

## 5.1 Catalytic tests

The catalytic performance of the supported Pd/TiO<sub>2</sub> catalysts promoted with Mn, Co, Sb and Au is shown in Fig. 5.1 (see Section 2.1.3 of Chapter 2, for details about the catalysts preparation). Catalysts are calcined at 300 °C in air for 2 h in the reactor, prior to the reaction. All catalysts show low toluene conversion (X-Tol) and benzyl acetate selectivity (S-BA) at the beginning which, however, increased considerably with time on stream. Such substantial enhancement of the catalytic performance was also observed previously and has been explained by the growth of Pd-particles during the course of the reaction [10]. Yet from Fig. 5.1 it is obvious that the performance of the catalyst in the acetoxylation reaction also depends on the nature of the co-component added.

With Mn as co-component, the conversion of toluene reached 55 % within 5 h on stream and then stays constant until the end of the measurements. The selectivity of BA shows the same trend with a maximum value of 60 % after 5 h. Catalysts promoted with Co, Sb and Au reached their highest catalytic performance after 10 h on stream with markedly higher BA selectivities in comparison to Mn, however, the initial conditioning period took longer time. The highest selectivity of 90 % was obtained with the Pd,Au/TiO<sub>2</sub> catalyst. Interestingly, the maximum conversion on this catalyst was already reached after the first 2-3 h, but decreased with further time on stream.

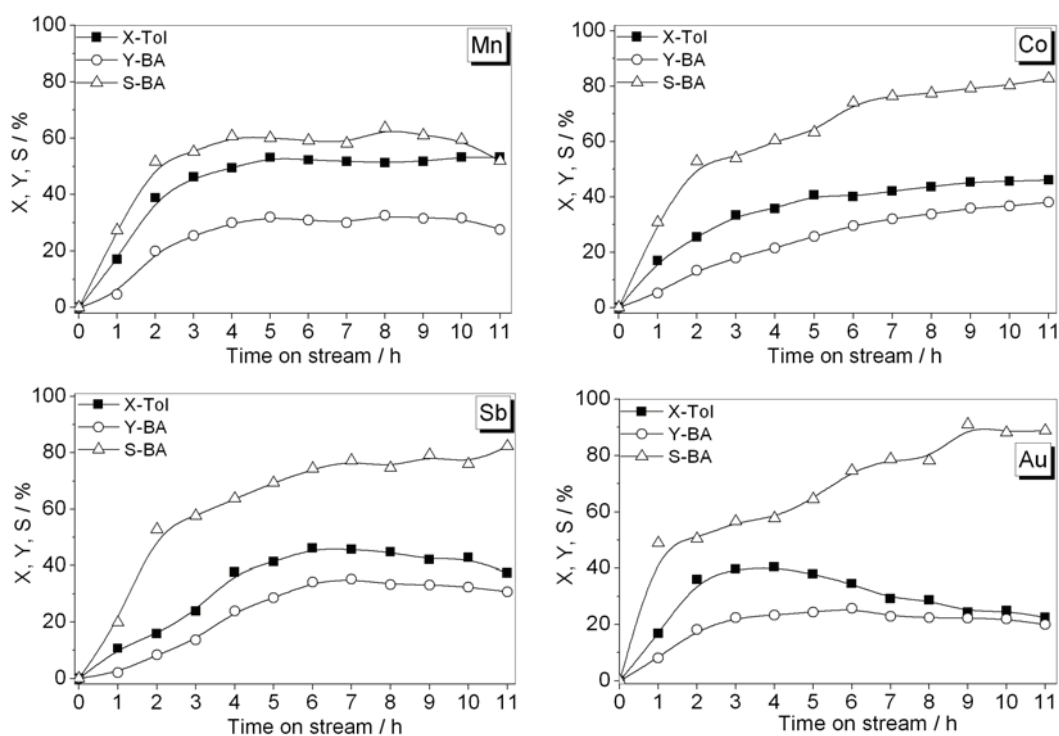


**Fig. 5.1** Toluene conversion (X-Tol), selectivity (S-BA) and yield (Y-BA) of benzyl acetate during time on stream over Pd,M/TiO<sub>2</sub> catalysts (M=Mn, Co, Sb, Au). See Table 5.1 for the weight content of elements.

In Fig. 5.2, catalytic parameters are plotted against the standard reduction potentials of the co-components. It can clearly be seen that the BA selectivity rises with increasing  $E^0$  of the co-component, while the opposite trend was observed for toluene conversion. Mn with a low  $E^0$  leads to a high X-Tol and low S-BA, while Au with a high  $E^0$  is beneficial for S-BA but not for X-Tol. The other two co-components with  $E^0$  around zero showed the best compromise between selectivity and activity.

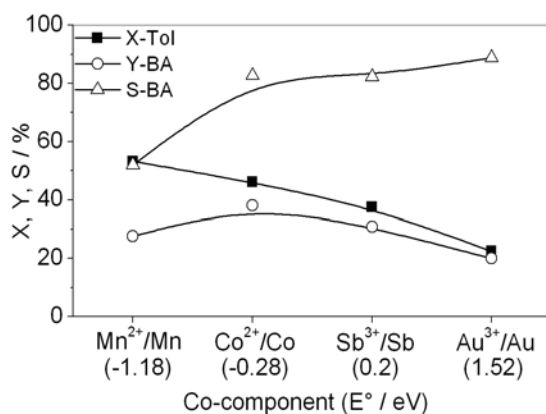


**Fig. 5.2** Comparison of standard reduction potentials ( $E^0$ ) of the co-components with the acetoxylation performance of Pd,M/TiO<sub>2</sub> (M=Mn, Co, Sb, Au) catalysts at 11<sup>th</sup> h. X-Tol: toluene conversion, S-BA: selectivity and Y-BA: yield of benzyl acetate.

Later, thermal pretreatment in helium at 600 °C is also done for the above four catalysts and tested for the acetoxylation of toluene. However, except for Sb, satisfactory results are not obtained literally due to sheer interactions of co-components with Pd or with the support.

Therefore, to elucidate the structural and electronic influence of the co-components on the state of Pd as well on the performance, the catalysts after mild calcination (300 °C-air) treatment and after 11 h on stream were characterized by several analytical techniques and the results are described below.

## 5.2 Catalyst characterization

### 5.2.1 Elemental analysis and surface Area

The chemical composition, surface area and pore properties of the catalysts after calcination at 300 °C in air and after 11 h use in the catalytic tests are presented in Table 5.1. The composition agrees with the elemental ratios expected according to the preparation procedure and amounts to ca. 9 wt.-% Pd and 5 to 6.5 wt.-% for the co-components. Only for Mn a significantly lower amount of ca. 4 wt.-% was detected, yet this amount is obviously sufficient for the catalyst to show high activity (Fig. 5.1). The weight content of Na (arising from Na<sub>2</sub>CO<sub>3</sub> introduced to maintain pH = 4 during the catalysts preparation step 2) is nearly



about 5 wt.-% in all the samples. Moreover, 1.5 wt.-% S was also detected, which is due to residual sulfate contained in the TiO<sub>2</sub> (anatase) support due to its production from a sulfate precursor. Leaching during time on stream does not occur since the elemental ratios of calcined and used catalysts do not differ much.

**Table 5.1** Elemental composition (Pd, M, Na, S, C) in wt.-%, BET surface area and pore volume of 10Pd8M/TiO<sub>2</sub> (M=Mn, Co, Sb, Au) calcined (300 °C-air) and spent (11 h) catalysts.

Sample	Pd <sup>I</sup>	M <sup>I</sup>	Na	S	C	BET surface area / m <sup>2</sup> g <sup>-1</sup>	Average pore volume / cm <sup>3</sup> g <sup>-1</sup>
Pd,Mn/TiO <sub>2</sub>							
Calcined (300 °C-air)	8.7	3.9	4.9	1.4	-	45.0	0.12
Spent-11 h	8.4	4.1	5.1	1.6	8.1	50.0	0.15
PdCo/TiO <sub>2</sub>							
Calcined (300 °C-air)	8.2	5.7	4.5	1.3	-	38.5	0.12
Spent-11 h	9.2	6.6	5.4	1.5	6.7	41.3	0.15
PdSb/TiO <sub>2</sub>							
Calcined (300 °C-air)	8.5	6.3	4.5	1.5	-	47.0	0.12
Spent-11 h	9.1	5.4	4.8	1.5	4.7	56.3	0.15
PdAu/TiO <sub>2</sub>							
Calcined (300 °C-air)	9.1	5.4	4.8	1.5	-	37.4	0.12
Spent-11 h	10.0	5.9	4.8	1.2	4.0	66.4	0.19

It is well known that coke deposition on active metal particles can lead to catalyst deactivation [10, 140]. Therefore, the amount of carbon was analyzed by CHNS in the samples before and after the reaction. As expected, for the calcined samples no carbon was found (Table 5.1). However, 8.1 wt.-% carbon was found in the used Mn containing catalyst, while only half of this amount is present on the used Au containing sample. It is obvious that the amount of deposited carbon is related to the trend in activity and reduction potential of the co-components since it drops with decreasing activity and rising E<sup>0</sup> (Fig. 5.2).

While the pore volumes of all calcined and spent catalysts are almost identical, the BET surface area of the spent Sb and Au containing catalysts are slightly higher in comparison to their fresh analogues and the respective Mn and Co containing samples. This may be a consequence of the different kind of carbon deposits formed on Au and Sb containing samples in comparison to those modified with Mn and Co. This is also confirmed by TG-DTA and XRD results discussed below.

### 5.2.2 TG-DTA analysis for spent samples

To obtain some information about the carbon deposited during reaction, TG-DTA analysis was done in air flow until 600 °C with a heating rate of 10 °C/min (Fig. 5.3). The weight loss was consistent with the total amount of carbon detected by chemical analysis (Fig. 5.3a, Table

5.1). However, DTA reveals distinct exothermic peaks between 200 and 400 °C (Fig. 5.3b). The most prominent peak is observed in the presence of Mn, yet the peak shape and position in the Co containing catalyst is very similar, which hints to a similar kind of carbon species.

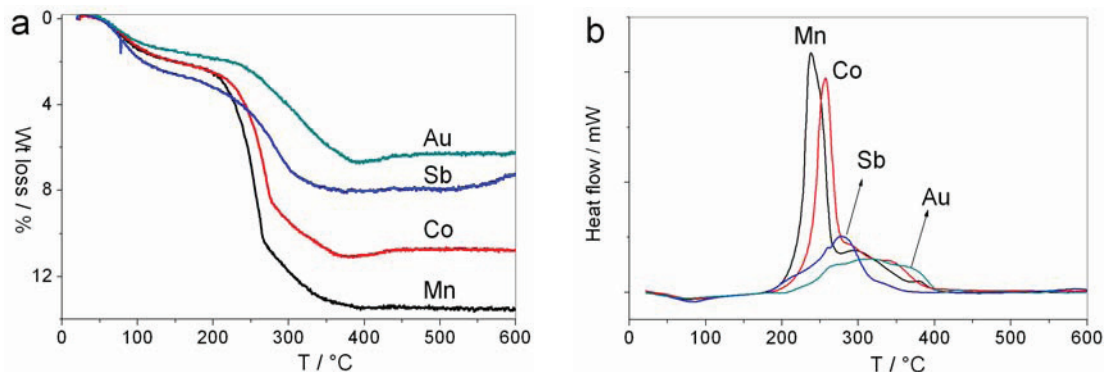


**Fig. 5.3:** a) TG and b) DTA analysis for spent Pd,M/TiO<sub>2</sub> (M=Mn, Co, Sb, Au) catalysts in air until 600 °C.

It is well known that carbon incorporated in the Pd-lattice can be removed effectively by calcination below 250 °C, while the removal of carbon deposited on the surface requires higher temperatures even of 380 °C [141]. Therefore, the peaks around 250 °C may be correlated with the removal of carbon incorporated in the Pd, which is dominant for Mn and Co containing catalysts. In contrast, the carbon species in the Sb and Au containing catalysts are removed at higher temperatures, which may rather point to carbon deposited on the catalyst surface. Moreover, the Au sample shows a very broad peak from 200 to 400 °C and also that of the Sb sample is not as narrow as the peaks observed for Mn and Co. This suggests that different type of surface carbon species might coexist in the latter two samples, particularly on the Au containing catalyst. It should also be mentioned that, besides carbon oxidation, the oxidation of metallic Pd to PdO [142] or the formation of PdAu alloys [143, 144] can contribute to the exothermic peaks in Fig. 5.3b as well.

## 5.2.3 X-ray diffraction (XRD)

### 5.2.3.1 XRD of calcined and spent samples

Fig. 5.4 shows the XRD patterns of Pd,M/TiO<sub>2</sub> (M=Mn, Co, Sb, Au) catalysts after calcination at 300 °C in air (a) and after 11 h on stream (b). All diffractograms contain the reflections of the anatase support (★) (PDF No. 21-1272) and NaCl (□) (PDF No. 70-2509), which might have been formed from Na<sub>2</sub>CO<sub>3</sub> and chloride (PdCl<sub>2</sub> + HCl) introduced during preparation. No crystalline phases containing the co-components Mn, Co and Sb have been detected in the calcined catalysts. Only for the Au containing sample, reflections of metallic

gold (▼) (PDF No. 65-8601) and a PdAu alloy (▼) (shoulder on the Au peak) were found [145, 146], suggesting that Au promotes the reduction of divalent Pd [66].

Pd is still present as a crystalline Na<sub>2</sub>PdCl<sub>4</sub> precursor (⊕) (PDF No 84.1946) after calcination in the presence of Mn, Co and Au. On the other hand, no such crystalline Na<sub>2</sub>PdCl<sub>4</sub> phase could be seen in the Sb containing catalyst, yet it cannot be excluded that it may exist in amorphous form in this sample. Apart from these differences in the phase composition, Sb, Mn and Co catalysts showed similar low initial activity. Obviously, time is needed for converting the Na<sub>2</sub>PdCl<sub>4</sub> precursor into an active Pd containing phases [10]. In contrast, the Au containing catalyst reached its highest X-Tol value within 2-3 h on stream, probably due to the presence of metallic Pd even in alloy form. It seems that PdAu alloys are not detrimental to catalyst activity.

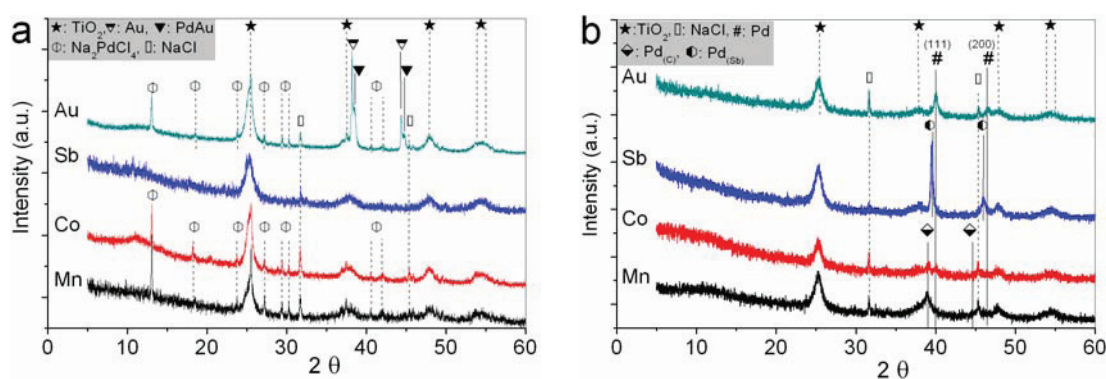


Fig. 5.4 XRD patterns of a) calcined and b) spent Pd,M/TiO<sub>2</sub> (M=Mn, Co, Sb, Au) catalysts.

In Fig. 5.4b, the XRD patterns of the spent samples are shown. All of them contain metallic Pd, which confirms that during time on stream the precursor Na<sub>2</sub>PdCl<sub>4</sub> is decomposed and transformed to a crystalline metallic Pd phase. Interestingly, the position of the metallic Pd reflections in the spent samples differs slightly, depending on the co-components used. In the presence of Au, the reflections are consistent with a pure metallic Pd phase (#) (PDF No. 88-2335). In the other three spent samples, the Pd reflections are shifted by 0.5° (for Sb) and 1° (for Co or Mn) to lower 2θ values indicating an expansion of the Pd lattice. This lattice expansion is certainly due to the incorporation of other elements, which may be the co-components (Sb) or carbon [127].

TG-DTA analysis discussed above suggests that the incorporation of carbon into the Pd lattice is most pronounced for the Mn sample. Based on this finding, it is possible to distinguish between the different Pd modifications with incorporated C or Sb. The corresponding Pd reflections are indicated as Pd<sub>(C)</sub> (◊) and Pd<sub>(Sb)</sub> (●) in Fig. 5.4b, respectively.

### 5.3.3.2 XRD of the spent samples after carbon removal

As can be clearly seen from Fig. 5.3a, carbon removal is possible for spent Mn, Co, Sb [14] and Au containing catalysts. After treatment for 2 h at 300 °C in air, CHNS analysis reveals almost complete removal of carbon from Mn and Co samples, while small amounts of C are still present in Sb (1.16 wt.-%) and Au (1.09 wt.-%) catalysts. Obviously, the temperature of 300 °C was too low to remove all of the deposited carbon in these cases. The XRD patterns of the spent samples after carbon removal are shown in Fig. 5.5. It is evident that the reflections related to the carbon incorporated Pd-phase (Pd<sub>(C)</sub>) at 2  $\theta$  of 38° and 45.5° are completely eliminated in Mn and Co samples by calcination at 300 °C, and metallic Pd and PdO phases are formed. In contrast, in the presence of Sb, no differences are visible between the spent and reoxidized sample (i.e. after carbon removal).

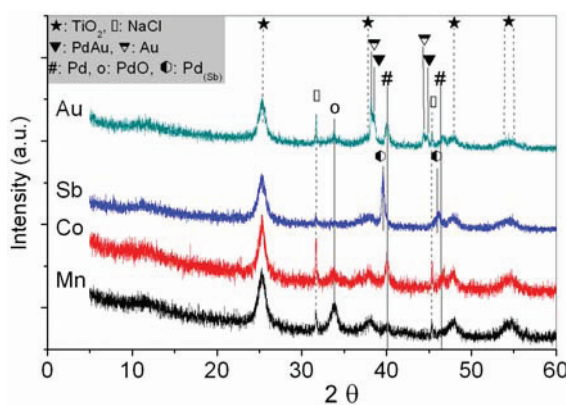


**Fig. 5.5** XRD patterns of spent Pd,M/TiO<sub>2</sub> (M=Mn, Co, Sb, Au) catalyst after treatment in air at 300 °C for 2 h.

This result suggests that the expansion of the Pd-lattice mentioned above is indeed caused by the incorporation of Sb and not of C. This conclusion has been verified by the preparation of a sample under slightly reductive conditions without the presence of any carbon containing compounds, for which a XRD pattern similar to the spent and reoxidized samples was obtained. For that, a Pd,Sb/TiO<sub>2</sub> catalyst has been prepared by the same procedure as described in the experimental section. However, instead of Na<sub>2</sub>CO<sub>3</sub>, NH<sub>4</sub>OH was used in the second step of preparation. Although there was no carbon present in the system, a shift of the metallic Pd-peak by 0.5 ° to lower 2  $\theta$  values was detected, indicating a lattice expansion, which is most probably due to the incorporation of Sb. Besides metallic Pd (Fig. 5.5), crystalline PdO (PDF 41-1107) is also observed in all the reoxidized samples. Interestingly, the intensity of the PdO peak (2 $\theta$  = 33.8°) is highest in the Mn sample and very low for Au and Sb, while the reverse trend was observed for the metallic Pd-phase. This indicates clearly that Mn with a low standard reduction potential

$E^0$  facilitates the oxidation of Pd in the active sample, while noble metals like Au with high  $E^0$  retain Pd mostly in the metallic state.

### 5.3.4 X-ray absorption near edge structure (XANES) studies

To obtain insights into the valence state of Pd, the XAS signal was measured at the Pd K-edge (transitions from 1s level). Fig. 5.6a shows the normalized XANES spectra of the calcined (300 °C-air) samples and Fig. 5.6b is related to spent (11 h) ones. XANES spectra of reference materials like metallic Pd foil and PdO are also inserted. The spectra of the calcined samples do not differ much. The positions of their absorption edges are very close to that of the PdO reference, only the slopes of the edge are slightly different. This suggests that Pd in the calcined samples is mostly oxidized but does not exist as pure PdO. This observation is further supported by XRD, in which Pd exists mostly in the form of a Na<sub>2</sub>PdCl<sub>4</sub> phase.

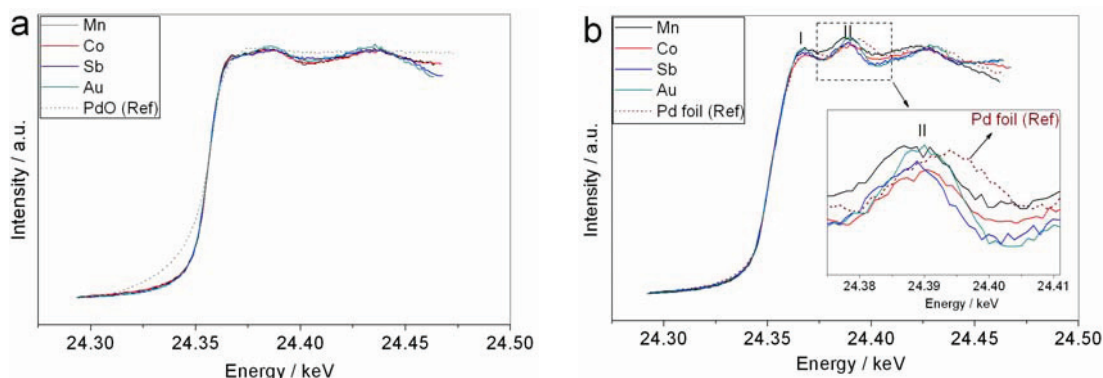


**Fig. 5.6** Normalized XANES spectra of a) calcined and b) spent Pd,M/TiO<sub>2</sub> (M=Mn, Co, Sb, Au) catalysts. Spectra of references (Pd foil and PdO) are also inserted.

In contrast to the calcined catalysts, the spectra of the spent samples show two distinct maxima (labeled I and II in Fig. 5.6b, due to the 1s → 5p,pd and 1s → 4f transitions) which are typical for metallic Pd. It is obvious that palladium was reduced to its metallic state with time on stream. However, in comparison to the Pd foil reference, the 1s → 5p,pd and 1s → 4f transition maxima are shifted to lower energies for all spent catalysts (inset in Fig. 5.6b). This effect can be explained by an expansion of the Pd-lattice [127] due to incorporation of C and/or the co-components. This agrees with the XRD results showing a Pd-lattice expansion for the catalysts containing Mn, Co and Sb. Only for the spent Au containing sample no indication for an expansion was found by XRD (*cf* Fig. 5.4b). A reason may be that such mixed PdAu phases, though existent in the spent sample, are X-ray amorphous and crystallize only upon subsequent treatment in air (*cf* Fig. 5.5).



### 5.3.5 X-ray photo electron spectroscopy (XPS)

XPS analysis was done to gain information on electronic properties, surface concentration and atomic ratio of the elements present on the surface of the catalysts. Fig. 5.7a shows the Pd3d spectra of the calcined samples. Deconvolution of the broad Pd3d peaks points to the presence of at least three different states which may be correlated with Pd<sup>0</sup> [135], slightly oxidized Pd (but not bulk PdO) and divalent Pd<sup>2+</sup> bound to Cl [147] according to binding energy of 335.1, 336.1 and 337.8 eV. The peak at 337.8 eV arises probably from the Na<sub>2</sub>PdCl<sub>4</sub> phase detected by XRD (*cf* Fig. 5.4a) for all samples except for the one containing Sb. Hence, this might be the most probable reason for the low intensity of this peak in Sb sample. Finally, these results reveal that a minor part of the Pd is reduced to metallic Pd, while the major part exists as oxidized Pd after calcination.

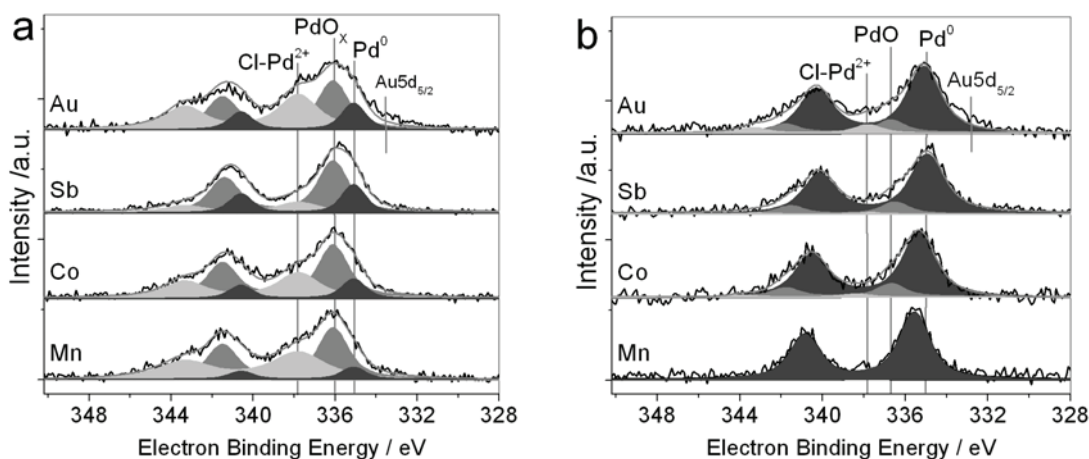


**Fig. 5.7** XP spectra of the Pd3d peak of a) calcined and b) spent Pd,M/TiO<sub>2</sub> (M=Mn, Co, Sb, Au) catalysts. The superimposed Au5d<sub>5/2</sub> peak in the Au sample is related to metallic Au.

Pd3d spectra of the spent samples after 11 h on stream are shown in Fig. 5.7b. Mainly two states of palladium were detected: PdO at 336.7 eV and a second state with binding energies between 334.9 eV and 335.6 eV depending on the co-component used. The peak related to the Pd-Cl compound disappeared, in agreement with the XRD results. Only for the Au containing catalyst, traces of this compound still remain in the XP spectrum. The major part of the Pd was reduced during time on stream. However, the degree of the reduction depends mainly on the co-component used. In the presence of Au or Sb, the major peak is around 335.0 eV which is typical for metallic Pd, while a slightly higher binding energy of 335.3 eV was observed for the Co containing sample and an even more pronounced shift to 335.6 eV is observed with Mn. This suggests the formation of a Pd surface oxide [148]. Next to this state, PdO reflected by a small peak at 336.6 eV was found in the presence of Co, Sb and Au. On the other hand, all the co-components except Au were found to be present in oxidized form in calcined and

spent samples. Only Au is present in metallic state, which is probably due to its high reduction potential value.

The Pd/Ti surface atomic ratio (Fig. 5.8a) decreases for all spent samples indicating particle growth and/or covering of Pd by carbon during time on stream. In contrast, the M/Ti surface atomic ratios (M = Mn, Sb, Au, Co) show a different behavior, which again depends on the nature of co-component used (Fig. 5.8b). The M/Ti ratio increases for Mn and Co solids, remains more or less constant for Au and decreases slightly for Sb. In the case of Sb, a possible reason may be the incorporation of Sb into the Pd-particles during the time-on-stream, which is confirmed by the XRD results. In contrast, the surface enrichment of Co can be explained by the strong interaction between Co and TiO<sub>2</sub>, which may lead to spreading of Co on the TiO<sub>2</sub> surface [149].

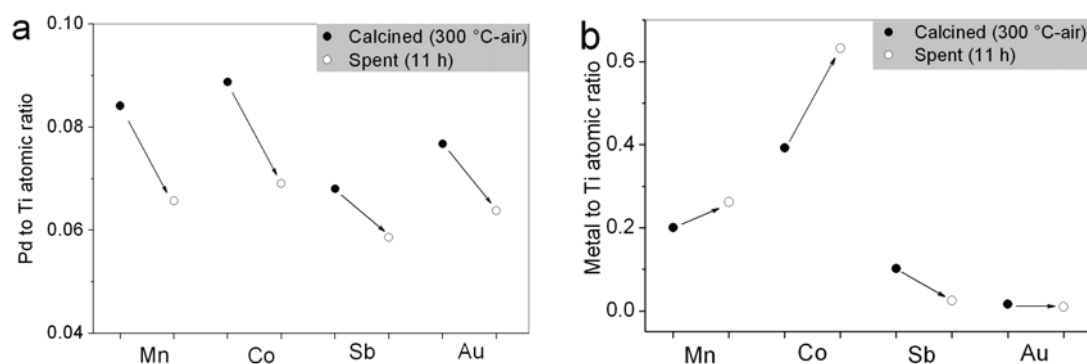


**Fig. 5.8:** a) Pd to Ti and b) M to Ti surface atomic ratios in calcined and spent Pd,M/TiO<sub>2</sub> (M=Mn, Co, Sb, Au) catalysts. Surface atomic ratios were calculated from the areas of the XPS Pd3d, Mn2p, Co2p, Sb3d<sub>3/2</sub>, Au4f and Ti2p peaks.

In summary, XPS results show clearly that the more noble co-components especially Au, favor the formation of metallic Pd during time on stream, whereas in the presence of Co and Mn slightly oxidized Pd is formed. Furthermore, Sb and Au are incorporated into the Pd-lattice, while the less noble co-components Mn and, more pronounced Co are enriched at the surface probably due to a strong interaction between these co-components and the oxide support [150].

### 5.3.6 FT-IR analysis of CO adsorption

The FTIR spectra of adsorbed CO of the calcined (300 °C-air) samples are shown in Fig. 5.9a. The spectra are very similar to those of CO adsorbed on Al<sub>2</sub>O<sub>3</sub>-supported sub-stoichiometric PdO<sub>X<1</sub> [151]. With respect to this study, the prominent band around 2160 cm<sup>-1</sup> can be assigned to  $\nu\text{Pd}^{\delta+}\text{-CO}$  with Pd<sup>δ+</sup> being partially oxidized Pd. It must be noted that comparative investigations show that CO does not adsorb on bulk PdO at room temperature,



which is consistent with the literature [151]. The observation of partially oxidized Pd agrees properly with the XPS results in which the binding energy of 336.1 eV observed for Pd<sub>5/2</sub> electrons in the calcined samples is between the values of metallic Pd (335.1 eV) and divalent Pd (337.0 eV) [147]. The bands observed around 2000 cm<sup>-1</sup> and 2100 cm<sup>-1</sup> result from linearly bound CO on Pd<sup>0</sup> and/or Pd<sup>+</sup>, respectively. An intense band in the range 1923 - 1948 cm<sup>-1</sup> is observed in all samples, which is related to νPd<sup>0</sup>-CO of bridged coordinated CO [152]. Rather broad and intense bands were observed for the Sb- and Au- containing catalysts. In the Au sample, an additional shoulder at 1974 cm<sup>-1</sup> occurs, which obviously results from CO adsorption on a PdAu alloy that is formed after activation (*cf.* Fig. 5.4a). This result indicates the presence of alloy species in the outermost layer of the catalyst after calcination.

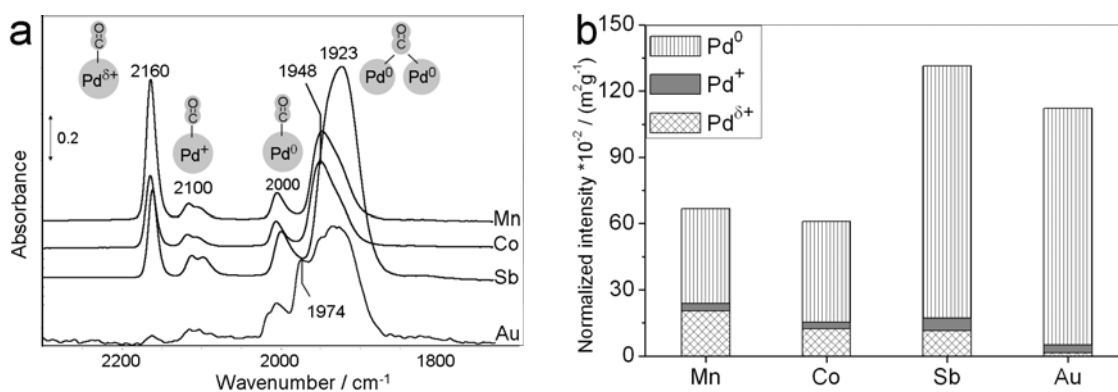


**Fig. 5.9:** a) The FTIR spectra of adsorbed CO for pretreated Pd,M/TiO<sub>2</sub> (M=Mn, Sb, Au, Co) catalysts, b) normalized intensity of bands related to BET surface area. Pretreatment was at 300 °C for 2 h in air prior to adsorption experiments for all samples.

The carbonyl band intensities of various Pd-species were normalized on the BET surface area to get semi-quantitative information about the metal species on the catalyst surface (Fig. 5.9b). From the results presented in this figure, it is obvious that the catalyst with Mn, which has a low  $E^0$ , has a relatively high amount of Pd<sup>δ+</sup> on the outermost surface, while for Au only a small portion of Pd<sup>δ+</sup> is detected. The opposite trend is observed for metallic Pd. These results suggest that Pd<sup>δ+</sup> is stabilized in presence of the less noble metals, while the more noble metals lead to a high amount of metallic Pd. XPS indicates the existence of oxidized Pd in high amounts for the pretreated samples, but the CO adsorption experiments point to an enrichment of metallic Pd in the outermost surface. It cannot be excluded that a part of the metallic Pd is formed by reduction of partially oxidized Pd with CO, which was observed at substoichiometric PdO under similar conditions [151]. Nevertheless, both techniques reflect the impact of the co-components on the reducibility of the Pd in a comparable way.

CO adsorption experiments were also performed for the spent catalysts, but only very weak CO bands could be observed. The deposition of carbon obviously hinders the adsorption

of CO on the Pd. Very broad bands between 1400 cm<sup>-1</sup> and 1600 cm<sup>-1</sup> confirm the deposition of coke and carboxylic compounds on the surface of all catalysts (not shown).

### 5.3 Conclusions

The nature of the co-component influences crucially the valence state of the Pd and, in turn, the performance in the acetoxylation of toluene to BA. The Pd,M/TiO<sub>2</sub> catalyst containing the least noble metal Mn ( $E^0$  [Mn<sup>2+</sup>/Mn = -1.18 eV) as co-component is highly active but poorly selective to BA, while the noble metal Au ( $E^0$  [Au<sup>3+</sup>/Au = 1.52 eV) leads to the opposite trend with a high selectivity, but only a low activity. The catalysts with Co and Sb show intermediate activity and selectivity. Especially, surface-sensitive methods like XPS and CO adsorption experiments showed that the reducibility of oxidic Pd at the surface depends on the co-component: Metals with low  $E^0$  stabilize oxidic Pd, while nearly all Pd is metallic in the presence of Au due to its high  $E^0$  (Fig. 5.10).

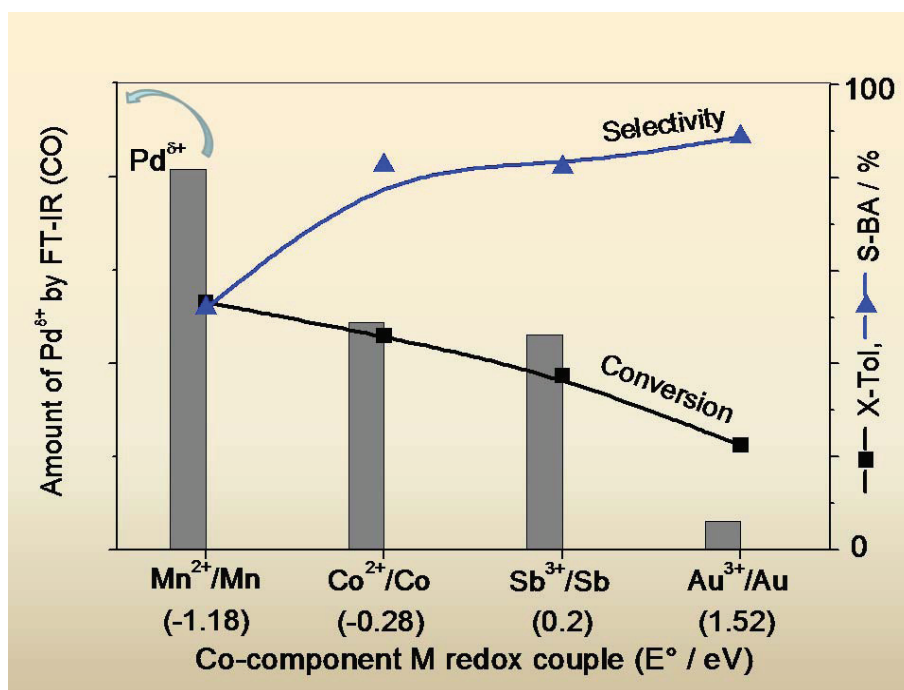


**Fig. 5.10** Influence of standard reduction potential ( $E^0$ ) of the co-component on the surface state of Pd (from FTIR spectra of adsorbed CO) and on the activity of Pd,M/TiO<sub>2</sub> (M=Mn, Sb, Au, Co) catalysts in the gas phase acetoxylation of toluene.

In contrast, XANES results revealed no significant differences in the valence states of the various catalysts for the bulk Pd-atoms. Incorporation of other elements into the Pd-particles could be observed by the XANES and XRD investigations. It could be shown that carbon migrates into the Pd-lattice for the samples, which contain less noble co-components (Mn or Co), whereas the co-components like Sb or Au are incorporated themselves into the Pd-lattice.

It seems that Mn and Co are spread on the titania surface. These differences allow a higher carbon acceptance for the catalysts with Mn and Co until deactivation is observed. From all these observations, it can be concluded that both, geometrical effects like the incorporation of different components into the Pd-lattice and electronic effects (i.e. the stabilization of oxidic Pd depending on the co-component) are critical for the better catalytic performance. An important result of our investigations is that a rather high amount of partially oxidized Pd favors the activity of the catalysts, whereas metallic Pd is beneficial for a high selectivity.

These insights allow the possibility to tune the catalytic performance by choosing appropriate co-components. Combining two or more co-components with different standard reduction potentials seems to be a promising way to optimize performance of the catalysts.



## Chapter 6

### **Role of supports (anatase, rutile) on the improved performance of 10 wt.-% Pd, 16 wt.-% Sb catalyst**

---

Previously, 10Pd,8Sb catalysts on different supports such as TiO<sub>2</sub>, SiO<sub>2</sub>, ZrO<sub>2</sub>,  $\gamma$ -Al<sub>2</sub>O<sub>3</sub> were tested for gas phase acetoxylation of toluene [9]. It was observed that the 10Pd,8Sb catalyst supported especially on TiO<sub>2</sub> (anatase) showed better performance in terms of toluene conversion and yield of benzyl acetate. The trend in the yield of benzyl acetate as well as Pd-particle size is as follows TiO<sub>2</sub> > SiO<sub>2</sub> > ZrO<sub>2</sub> >  $\gamma$ -Al<sub>2</sub>O<sub>3</sub>. It was claimed that the Pd-particles of size 80-100 nm are active for this reaction, and TiO<sub>2</sub> (anatase) was supporting the formation of such bigger Pd-particles during the time on stream.

By taking the above observations into account the current investigation is focused to study the role of TiO<sub>2</sub> support phases (anatase and rutile) on the Pd-particle growth as well as on the performance of 10 wt.-% Pd, 16 wt.-% Sb catalyst in the gas phase acetoxylation of toluene. Catalysts have been characterized with several analytical techniques like XRD, TEM, HAADF-STEM, XPS and FT-IR of adsorbed CO, to derive relation between structure, activity and selectivity.

---

## 6.1 Catalytic tests

Fig. 6.1 shows the acetoxylation performance of 10 wt.-% Pd, 16 wt.-% Sb on anatase and rutile (see Section 2.1.2 of Chapter 2, for catalysts preparation). It is evident from the Fig. 6.1 that the anatase sample displays a rapid increase in the toluene conversion ( $\sim 67\%$ ) and shows maximum activity at the 7<sup>th</sup> hour. Note that the conditioning time is reduced by nearly 5 h compare to conventional 10Pd,8Sb/TiO<sub>2</sub> catalyst [9]. This is might be due to the fact the amount of Sb used in the present sample is almost twice to the conventional sample. However, similar to the conventional sample, the present sample also showed deactivation further on stream. On the other hand, BA selectivity is also following the same trend as toluene conversion but with considerably lower values.

Surprisingly, the rutile sample showed very high selectivity  $> 95\%$  yet with comparable BA yields as that of anatase. More importantly, it exhibited long term stability ( $> 30$  h) while maintaining more or less similar yields of BA. The remarkable observation from this rutile sample is that it displayed high selectivity even from the beginning of the reaction ( $\approx 4$  h). From these results, it can be concluded that, 10Pd,16Sb supported on rutile is an efficient catalyst among all samples studied for gas phase acetoxylation of toluene in the present investigations.

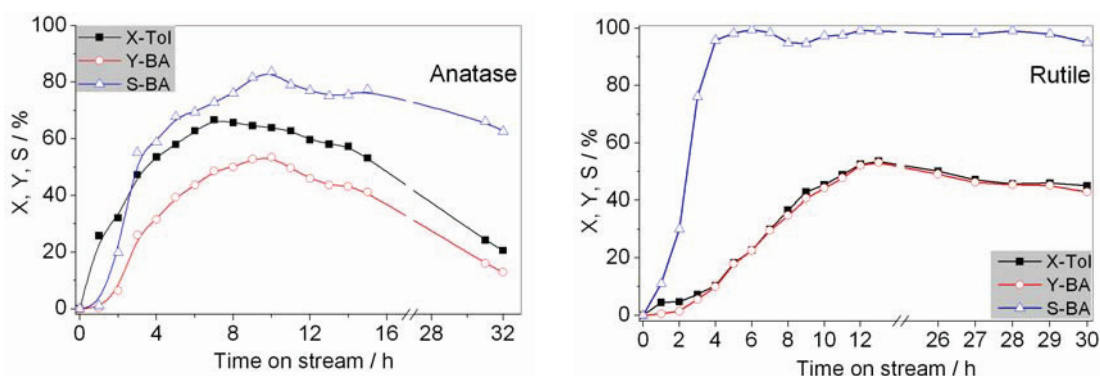


**Fig. 6.1** Toluene conversion (X-Tol), selectivity (S-BA) and yield (Y-BA) of benzyl acetate during time on stream over the Pd,Sb catalysts supported on anatase and rutile. Samples were calcined in air at 300 °C for 2 h prior to the time on stream.

These results suggest that anatase as a support promotes mainly the activity of the catalyst, while rutile assists in the formation of particular species which are necessary for high selectivity. To find out the nature of these species which are responsible for this interesting behavior, comprehensive characterization was done for fresh (i. e after calcination at 300 °C for 2 h) and spent ( $> 30$  h) Pd,Sb catalysts supported on anatase and rutile.

On the other hand, a detailed study about the Pd,Sb/anatase sample at five different stages of the reaction including the samples after 30 h on stream is given in ref.[100].

## 6.2 Catalyst characterization

### 6.2.1 Elemental analysis

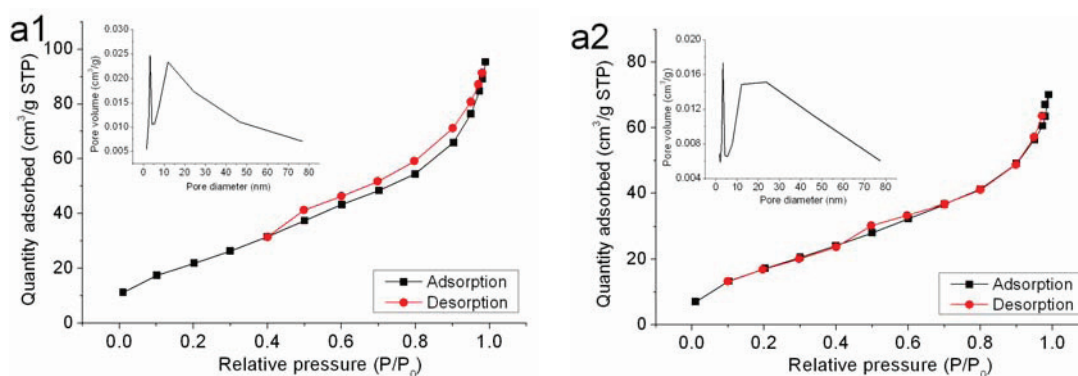
ICP analysis confirms nearly 10 wt.-% of Pd and 10-12 wt.-% of Sb (Table 6.1). In addition, nearly 5 wt.-% of Na is present in all the samples. There seems to be no marked difference in the composition of Pd or Sb in anatase and rutile samples. However, variations are apparent in the amount of deposited carbon in spent samples (> 30 h). Nearly twice the amount of carbon was deposited on the anatase (4.25 wt.-%) catalyst compare to the rutile catalyst (2.49 wt.-%) during the reaction. TG-DTA analysis also confirms the high amount of carbon. Moreover, it hints to different types of carbon in anatase and rutile samples. This is described in below Section 6.2.3.

**Table 6.1** Elemental composition from ICP-OES and CHNS analysis of Pd,Sb catalysts supported on anatase and rutile, and respective spent (> 30 h) samples.

Sample	Pd (wt.-%)	Sb (wt.-%)	C (wt.-%)	BET (m <sup>2</sup> /g)
Anatase (300 °C-air)	7.7	10.5	-	81.5
Spent - 32 h	8.1	9.7	4.25	64.6
Rutile (300 °C-air)	9.0	11.8	-	33.3
Spent - 30 h	9.2	12.2	2.49	43.5

### 6.2.2 N<sub>2</sub>-physisorption

N<sub>2</sub>-physisorption experiments were done to determine the BET surface area ( $S_{BET}$ ) and pore properties of the solid samples.  $S_{BET}$  values are shown in Table. 6.1, whereas Fig. 6.2 contains the N<sub>2</sub>-adsorption and desorption isotherms of Pd,Sb catalysts supported on anatase (a1, a2) and rutile (b1, b2). In addition, pore size distribution patterns are inserted in each figure.





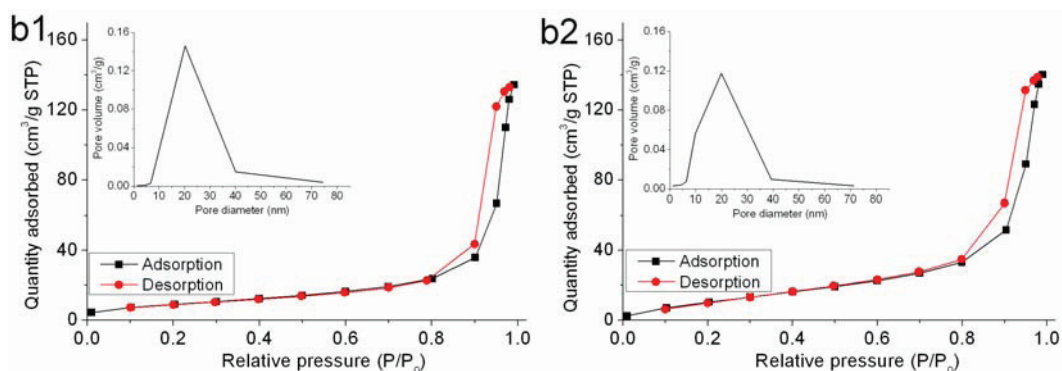


**Fig. 6.2** N<sub>2</sub> adsorption and desorption isotherms and pore size distribution (inserted graphs) of Pd,Sb catalysts supported on anatase (a1 (calcined), a2 (spent)) and rutile (b1 (calcined), b2 (spent)).

All the isotherms in Fig. 6.2 can be assigned to type IV with H<sub>3</sub> and H<sub>1</sub> hysteresis loops for anatase and rutile samples, respectively, according to IUPAC classification [106]. The N<sub>2</sub> pore size distribution (inserted figure) for anatase samples shows bi or trimodal distribution, whereas rutile samples showed unimodal distribution with a maximum nearly at 20 nm. An obvious relation between the pore size distribution and the catalyst performance cannot be derived; however it can be assumed that high surface area of anatase might lead to high dispersion of active components, which in turn reinforces the activity of the catalyst and leads to high toluene conversion. This kind of phenomena was also noticed in several reactions for example, cobalt oxide supported on barium hexaaluminate showed high surface area and the highest activity for methane combustion [153].

### 6.2.3 Thermogravimetry-differential thermal analysis (TG-DTA)

TG-DTA analysis was done in air flow until 600 °C with a heating rate of 10 °C/min for the spent (> 30 h) anatase and rutile samples, with an aim to identify different kinds of carbon species present in the samples. The corresponding spectra are shown in Fig. 6.3.

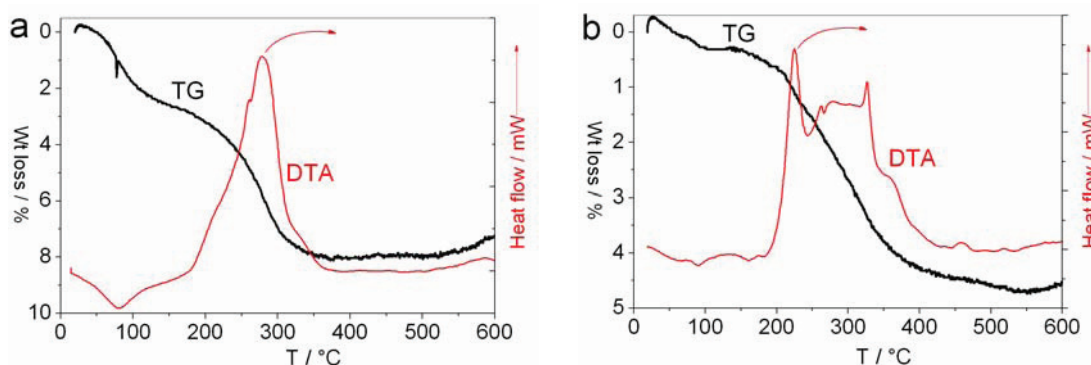


**Fig. 6.3** TG-DTA analysis of spent (> 30 h) Pd,Sb catalysts supported on anatase (a) and rutile (b).

TG analysis showed a weight loss of nearly 8 wt.-% in the anatase sample, whereas it

was only 5 wt.-% in the rutile sample. CHNS bulk analysis showed 4.25 wt.-% and 2.49 wt.-% C in anatase and rutile, respectively. Therefore, the additional weight loss might be due to the physisorbed water ( $< 100\text{ }^{\circ}\text{C}$ ). On the other hand, DTA spectra of anatase and rutile samples are clearly different from each other. The anatase sample showed a broad exothermic peak from 200 to 350  $^{\circ}\text{C}$ , under which three components at 200, 280 and 320  $^{\circ}\text{C}$  seem to be present, whereas the DTA peaks in the rutile sample are entirely different from anatase. Assignment of a particular carbon state to all these peaks is rather difficult. However, we can explain these differences between the anatase and rutile samples based on the TEM analysis, in which an amorphous carbon layer was found on Pd-particles in anatase (*cf* Fig. 6.5, Fig. 6.6), whereas it was found on the support in the rutile sample.

#### 6.2.4 X-ray diffraction (XRD)

XRD patterns of the fresh and spent anatase and rutile samples are displayed in Fig. 6.4. XRD patterns show the reflections related to the respective supports (anatase (★) (PDF. No 21-1272) or rutile (●) (PDF. No 21-1276) and NaCl (□) (PDF. No 5-628) in all the samples. In addition, in case of anatase after calcination, reflections related palladium represent two types of Pd. One is a  $\text{Pd}_{20}\text{Sb}_7$  alloy (◇) (PDF. No 31-102) and the other might be a Pd-species with incorporated Sb, as evidence from the shift of  $0.5^{\circ}$  in the metallic Pd peak to lower 2-theta values. As discussed in Chapter 4 and 5, such shift is directly related to a Pd-lattice expansion [13]. This is not the case with the rutile sample. In contrast to anatase, the  $\text{Na}_2\text{PdCl}_4$  phase still exists even after calcination (300  $^{\circ}\text{C}$  / air / 2 h).

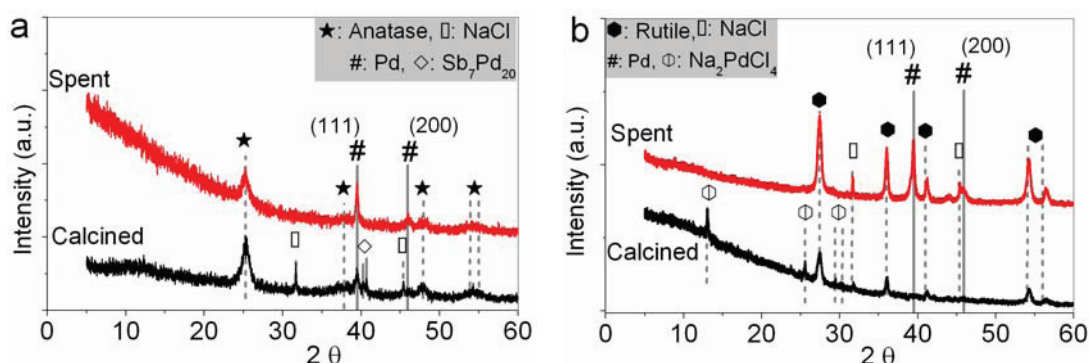


Fig. 6.4 XRD diffractograms of calcined and spent Pd,Sb catalysts supported on a) anatase and b) rutile.

However, with time on stream ( $> 30\text{ h}$ ),  $\text{Na}_2\text{PdCl}_4$  phase is completely disappeared and the Sb containing Pd-phase is observed in the rutile as well as in the anatase samples. In our recent studies we proposed that such Sb-incorporation is beneficial if the atomic ratio

of Pd to Sb is nearly 5. In this case, a mixed Pd<sup>0</sup>/PdO surface was formed during time on stream [13]. However, from XRD it is not possible to derive the exact composition of the Pd/Sb particles. Therefore, electron microscope analysis and XPS was done to find out the composition, morphology and surface state of Pd-particles.

## 6.2.5 Transmission electron microscopy (TEM)

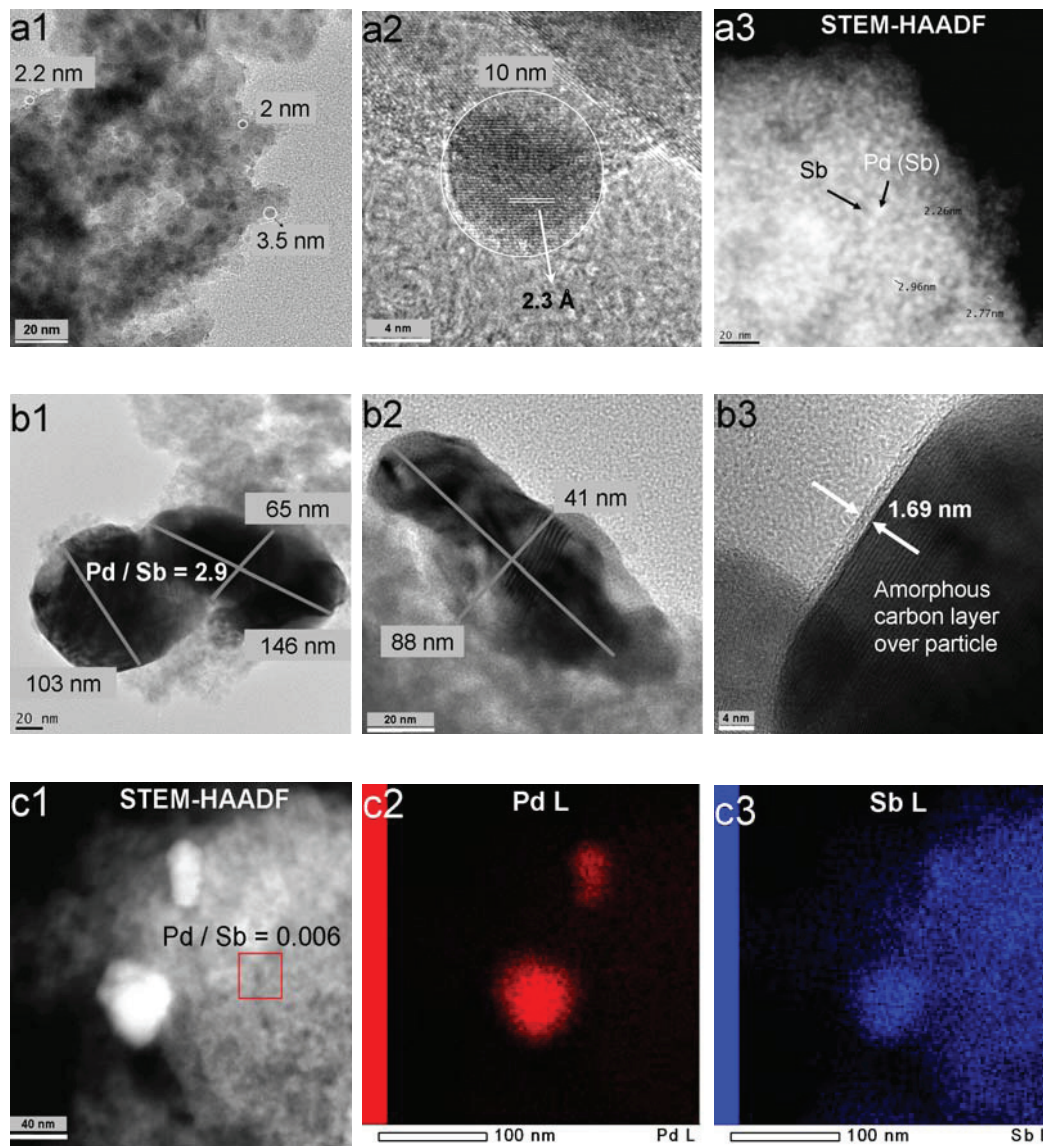
### 6.2.5.1 Anatase samples

Fig. 6.5 shows the micrographs of calcined (a1, a2, a3) and spent (b1, b2, b3 and c1, c2, c3) anatase samples. It seems that the majority of the particles have a size between 2 to 5 nm, before the reaction. STEM-HAADF studies showed (Fig. 6.5a3) a uniform distribution of bright and dark spots representing the heavier and lighter elements, respectively. EDX analysis revealed that, the bright particles are comprised of Pd with some amounts of Sb, whereas dark areas are due to Sb only. The accuracy of the calculated Sb amount in small Pd-particles is rather limited due to overlapping of contributions from Sb present on the support as well. Apart from these small particles, some particles of 10 nm were also observed and contain lattice fringes of 2.3 Å (see Fig. 6.5a2). This value is slightly higher than that of Pd(111) fringes, indicating the expansion of the lattice. Such kind of modification was also observed by TEM for Si(111) crystal planes with incorporated carbon [154]. Likewise, such expansion was also noticed in the ZnO lattice with Al doping [155]. Such modification may also be possible in the anatase sample and lead to expansion of the Pd-lattice (*also evidenced from XRD*) with the Sb incorporation.

On the other hand, Pd-particles were irrefutably grown with time on stream (> 30 h), however in an irregular fashion (see Fig. 3b1, b2). Surprisingly, the atomic ratio of Pd to Sb is found to be < 3 in the spent sample and this Pd/Sb ratio is close to the value for the stable Pd<sub>20</sub>Sb<sub>7</sub> alloy. Previous investigations (see Chapter 4) clearly demonstrated that Pd-Sb alloy phases with an atomic ratio of Pd/Sb < 3 are detrimental for catalyst activity, but beneficial if the ratio is nearly 5 and this ratio certainly stabilized the mixed Pd<sup>0</sup>/PdO surface species [13]. Therefore, the deactivation of the present anatase sample might be due to the lack of such beneficial ratio.

By HRTEM analysis, a carbon layer (1.69 nm) is detected on the Pd-particles (Fig. 6.5b3). It is well known that, carbon deposition might block the active surface sites and lead to activity loss in many oxidation reactions [156, 157]. This situation is also very likely possible in the present case, in which it slows down the adsorption of reactants and

dwindles the activity. STEM-HAADF (Fig. 6.5c1) and EDX (Pd L and Sb L mapping in Fig. 6.5c2, c3) revealed that the Sb is well distributed over support as well as intermixed with Pd in an atomic ratio of Pd:Sb close to the alloy range (0.5 - 3).



**Fig. 6.5** Electron microscopic images of calcined (a1, a2, a3) and spent (b1, b2, b3, c1, c3, c3) Pd,Sb/anatase catalysts. TEM: a1, a2, b1, b2, b3; STEM-HAADF: a3, c1; EDX map: c2 (Pd L) and c3 (Sb L).

### 6.2.5.2 Rutile samples

In contrast to the anatase sample, particles were found to be of different sizes ranging from 3 to 60 nm (Fig. 6.6a1, a2, a3) on rutile before the reaction. Interestingly, with time on stream the particles were restructured to almost a uniform size (Fig. 6.6b1, b2) and EDX coupled with STEM-HAADF (Fig. 6.6c1, c2, c3) studies showed an atomic ratio of Pd to Sb between 5 and 6. Some particles with 10 nm were also found and contain the Pd/Sb ratio nearly 5.7. It seems that this particular ratio is somehow well stabilized



especially in the rutile sample. Another interesting observation is that an amorphous carbon layer (1.32 nm) is formed on rutile crystals (Fig. 6.6b3), whereas it was on the Pd-particles in the anatase sample. These processes altogether might protect the desired properties like valance and composition of the Pd-particles on rutile which are necessary for better performance.

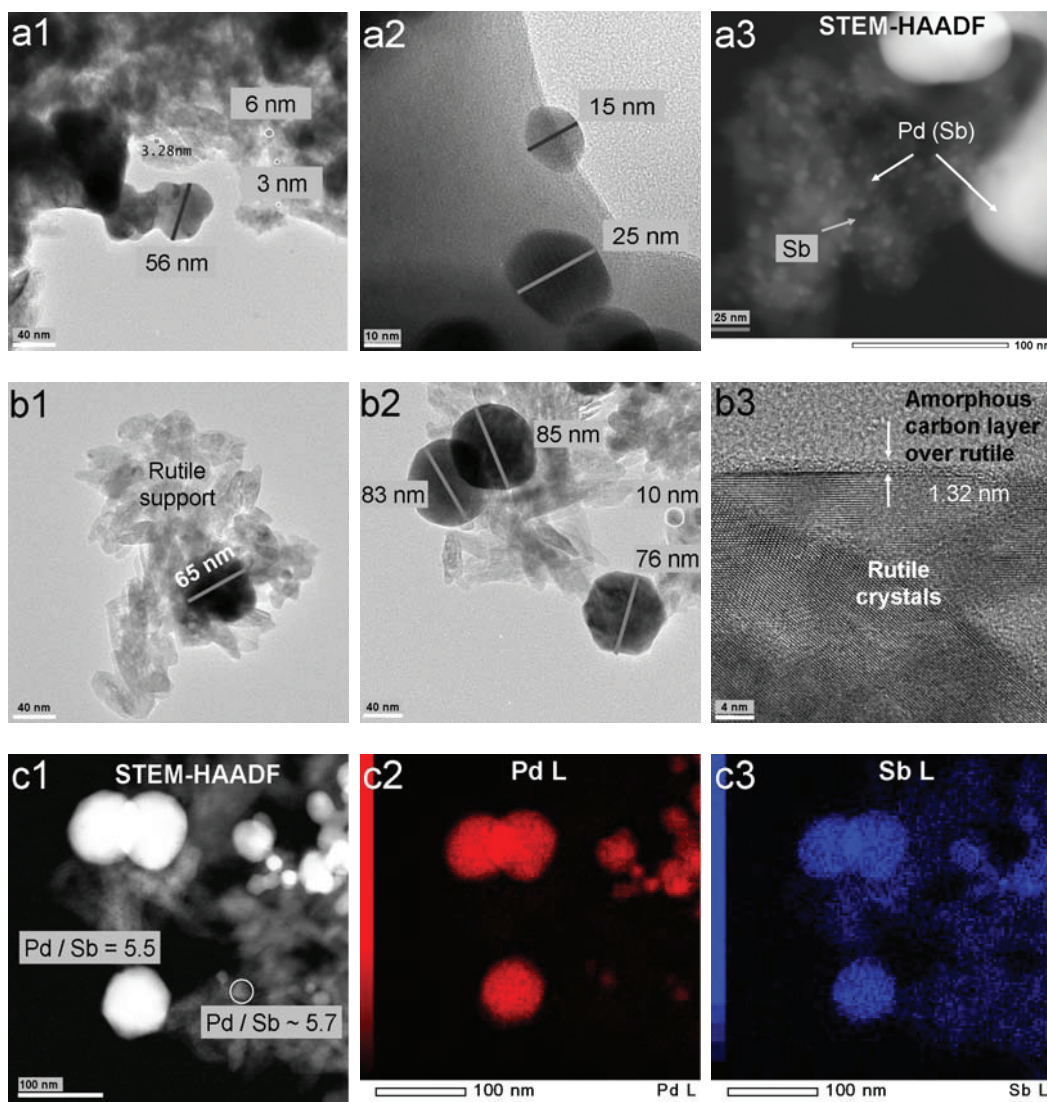


**Fig. 6.6** Electron microscopic images of calcined (a1, a2, a3) and spent (b1, b2, b3, c1, c3, c3) Pd,Sb/rutile. TEM: a1, a2, b1, b2, b3; STEM-HAADF: a3, c1; EDX map: c2 (Pd L) and c3 (Sb L).

### 6.2.6 X-ray photoelectron spectroscopy (XPS)

Fig. 6.7 shows the scan over the Pd3d region of anatase (a) and rutile (b) samples before and after the reaction. The calcined anatase sample has a broad peak (FWHM > 3, hinting to heterogeneity) with a maximum at 336.1 eV related to slightly oxidized states (PdO<sub>x</sub>), whereas a sharp and rather narrow peak is observed in rutile. In addition, a small peak related to metallic Pd peak (335.1 eV) [147] is also observed in the rutile sample after calcination.

With time on stream, metallic Pd and a slightly reduced state ( $\text{Pd}^{\delta-}$ ) appear in the anatase sample. The presence of the latter state is evidenced by a peak with a 1.1 eV lower BE than  $\text{Pd}^0$ , which was observed in ref.[10]. This reduced state is due to the interaction of  $\text{Pd}^0$  with deposited coke [10]. Coke formation was also seen by TEM Fig. 6.5b3. However, this is not the case with the rutile sample, in which the desired states for palladium like  $\text{Pd}^0$  and  $\text{PdO}$  were clearly observed. Thus, this might be the adequate reason for the rutile sample to show high BA selectivity ( $> 95\%$ ) and to maintain long term stability with considerable conversions.

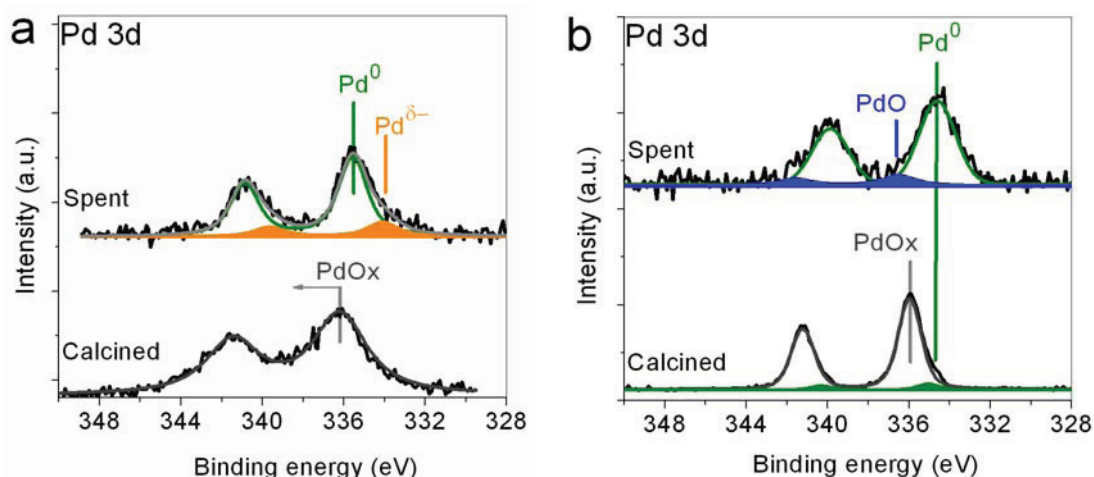


Fig. 6.7 Pd3d scan (XPS) for calcined and spent Pd,Sb catalysts supported on a) anatase and b) rutile.

Another interesting observation in the rutile sample is the valance state of Sb. The XPS  $\text{Sb}3d_{3/2}$  regions of anatase and rutile samples before and after the reaction are shown in Fig. 6.8. Due to the overlap of the  $\text{Sb}3d_{5/2}$  region with  $\text{O}1s$ , only the  $\text{Sb}3d_{3/2}$  region is shown. Fig. 6.8a reveals clearly only trivalent  $\text{Sb}^{3+}$  before and after the reaction on anatase.

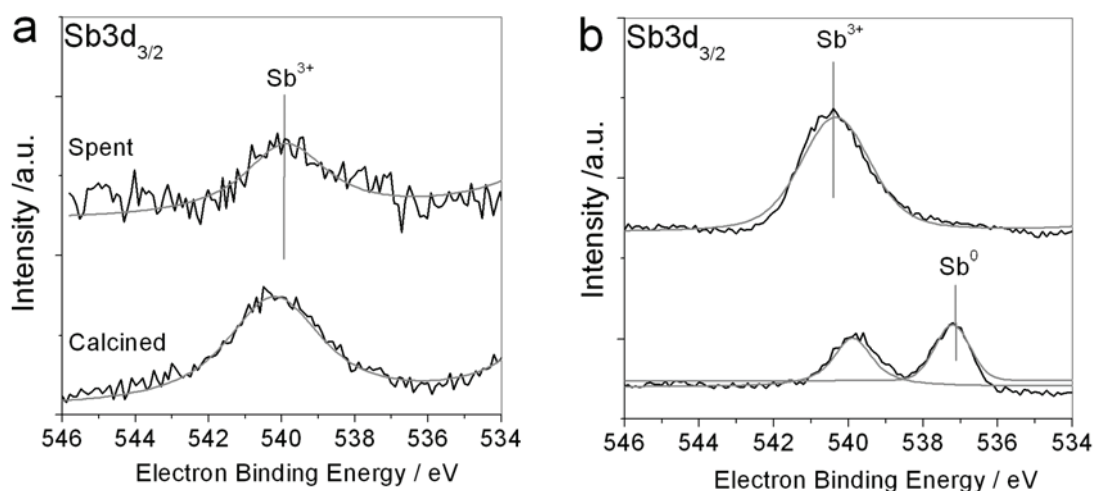
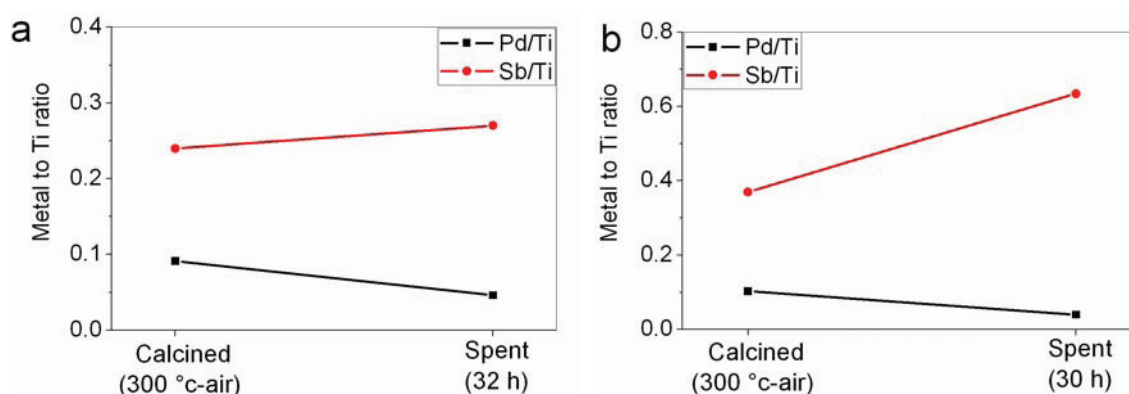


Fig. 6.8 XPS  $\text{Sb}3d_{3/2}$  region of calcined and spent Pd,Sb catalysts supported on a) anatase and b) rutile.

The situation is different in rutile samples. After calcination, a clear peak for metallic Sb was observed along with  $\text{Sb}^{3+}$ . In the previous investigations, small peak in the metallic Sb region (*see* Fig. 4.5 of Chapter. 4) was noticed in anatase samples pretreated in air or helium at their maximum activity. However, in the rutile sample very significant peak is noticed. This result is in fact remarkable and giving indirect evidence for the Sb-incorporation into Pd-lattice in the form of metallic Sb. More importantly, the eventual enrichment of Sb at the surface in the form of  $\text{Sb}^{3+}$  is observed in the spent sample which might decrease the possibility of alloy formation with the Pd bulk.

To find out the concentration of the species on the surface, atomic ratios of Pd or Sb to Ti are calculated from the Pd3d, Sb3d<sub>3/2</sub> and Ti2p peaks. Fig. 6.9a is related to the change in the Pd or Sb to Ti surface atomic ratios with time on stream of anatase samples, whereas Fig. 6.9b is related to rutile. It is clear from the Fig. 6.9a that the Pd/Ti atomic ratio is decreased with time on stream in both the samples. This decrease might be due to the particle growth (evidence by TEM) or coke formation (CHNS and TG analysis).



**Fig. 6.9** Pd/Ti and Sb/Ti surface atomic ratios of calcined and spent Pd,Sb catalysts supported on a) anatase and b) rutile. Calculations were done from the areas of the XPS Pd3d, Sb3d<sub>3/2</sub> and Ti2p peaks.

Surprisingly, ratio of the Sb/Ti is increased predominantly in rutile samples with time on stream. This enrichment of Sb on the surface might decrease the possibility of further alloying with Pd. Thus, stabilizing the metal particles with minimum amount of Sb (Pd/Sb  $\approx$  5) is obviously useful for improved performance. From this it can be concluded that, if migration of Sb into the Pd-bulk predominates, then the formation of a Pd-Sb alloy with ratio of Pd/Sb  $<$  3 is more likely. Thereby problems like particle agglomeration, less adsorption of reactants and eventual deactivation will definitely arise. From these observations, it can be concluded that incorporation of metallic Sb into Pd-lattice (TEM), evidenced by a Pd-lattice expansion (XRD), is certainly possible and useful if the amount of Sb remains low enough to prevent the formation of any crystalline alloys with Pd.



### 6.2.7 FT-IR of adsorbed CO

Fig. 6.10a shows the FT-IR spectra of CO adsorption for calcined Pd,Sb catalysts supported on anatase and rutile. The intensity of the bands normalized to the BET surface area assigned to various Pd-species on the catalyst surface is shown in Fig. 6.10b. Prior to the analysis, samples were calcined at 300 °C in air for 2 h. Fig. 6.10a shows an intense band at 1925 cm<sup>-1</sup> in the anatase samples and two bands near 1917 and 1935 cm<sup>-1</sup> in the rutile sample, which are related to adsorption of bridged CO on Pd<sup>0</sup>. It was described as 2-fold CO on Pd(111) surface [152]. Both the samples also contain linearly adsorbed CO on Pd<sup>0</sup> at 2000 cm<sup>-1</sup>. In addition, they contain Pd<sup>+</sup> and Pd<sup>δ+</sup> states as well evidenced by bands at 2100 and 2160 cm<sup>-1</sup>, respectively [151].

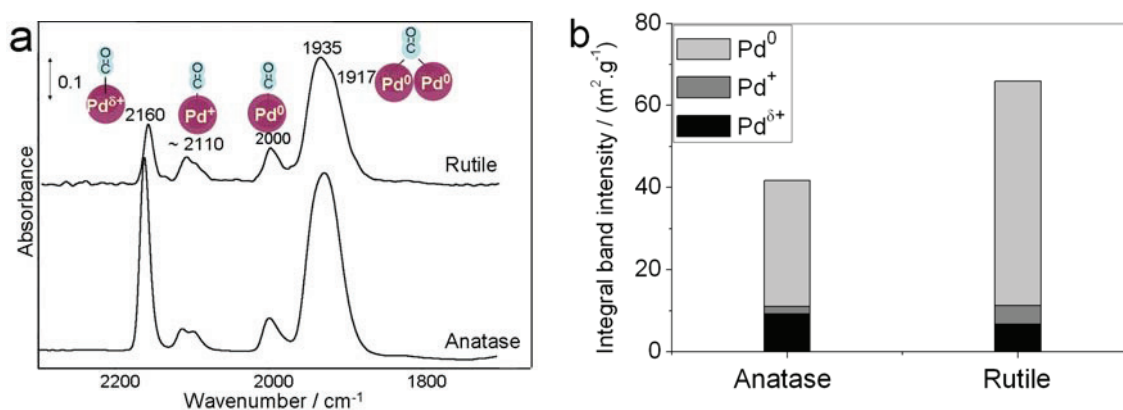


**Fig. 6.10** FT-IR spectra of CO adsorption of calcined Pd,Sb catalysts supported on anatase and rutile and b) normalized intensity of bands related to BET surface area

Apart from their similar peak position, they differ well in terms of peak intensity. Even though the absolute intensity of the peaks in anatase is higher, the normalized intensity is lower since  $S_{\text{BET}}$  is higher for anatase samples (*see* Table 6.1). Yet, even after normalization, the intensity of Pd<sup>δ+</sup> is higher in anatase compared to rutile. On the other hand, the rutile sample contains a high amount of metallic Pd in the outermost layer. FT-IR (CO) adsorption studies indicates that the rutile support favors the enrichment of metallic Pd, which might be the probable reason for high selectivity, whereas oxidized species being more abundant on anatase are probably responsible for the activity which is higher for the anatase sample.

### 6.3 Conclusions

High selectivity ( $\approx 100\%$ ) for benzyl acetate and long-term stability of a 10 wt.-% Pd, 16 wt.-% Sb/TiO<sub>2</sub> catalyst is achieved by changing the support from anatase to rutile. The performance of the catalysts is merely governed by the particle composition and surface

properties. Sb incorporation into the Pd-lattice was observed in both the samples with time on stream and the amount of Sb in the particles is directing the reaction. The deactivated anatase sample contain a Pd/Sb atomic ratio in the stable alloy range ( $< 3$ ), whereas in the rutile sample, particles with a Pd/Sb atomic ratio  $\approx 5$  are formed that contain surface Pd<sup>0</sup>/PdO species, yet without formation of stable alloy phases. Stabilization of Pd<sup>0</sup>/PdO moieties on the surface is essential for high performance. These are obviously promoted by Sb incorporated in the Pd-bulk with the atomic ratio of Pd to Sb nearly 5. An overview about the important observation in the present in investigation is shown in Fig. 6.11.

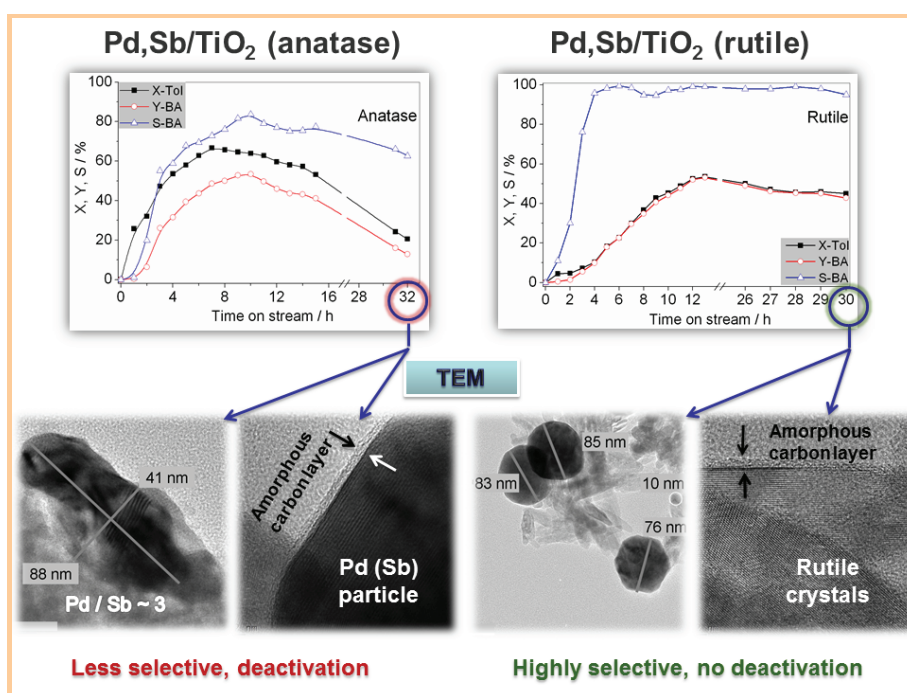


**Fig. 6.11** Role of TiO<sub>2</sub> support phases (anatase and rutile) on the acetoxylation activity of Pd,Sb supported catalysts and on the Pd-particle size and the composition.

Finally, FT-IR (CO) adsorption studies showed higher specific concentration of metallic Pd in the rutile samples, which lead to high selectivity, whereas a rather high concentration of oxidized Pd-species were observed in anatase sample, which lead to high activity.

Possibly, the catalyst performance may be improved by using a combined anatase and rutile support in a specific ratio, for future investigations.

## Summary

Different metal precursors (chlorides, nitrates and acetates) and chloride-removing additives (ammonium sulfate, nitrate, carbonate or urea) as well as the thermal pretreatment temperature (600 °C) and atmosphere (inert He or reducing H<sub>2</sub>/He) influenced significantly the size and nature of Pd-metal particles in 10 wt.-% Pd, 8 wt.-% Cu or Sb/TiO<sub>2</sub> (anatase) catalyst. Chlorides are the most beneficial precursors for producing the metallic Pd, while PdO is formed with nitrate precursors, whereas acetate precursors showed instability during thermal treatments. Metallic Pd-particle formation is observed even at low temperature from chloride precursors due to the formation of intermediate Pd-chloroamine complexes. Ammonia molecules originate obviously from the added additives like NH<sub>4</sub>NO<sub>3</sub>, (NH<sub>4</sub>)<sub>2</sub>CO<sub>3</sub>, urea, and (NH<sub>4</sub>)<sub>2</sub>SO<sub>4</sub> which is found to be the most effective agent to remove Cl from both the Pd-Cu and Pd-Sb catalyst systems. After treatment in H<sub>2</sub>/He, a Cu-shell and a Pd-core containing S are observed while Pd<sub>1</sub>Sb<sub>1</sub> and Pd<sub>20</sub>Sb<sub>7</sub> alloy phases are formed in Pd,Sb/TiO<sub>2</sub> sample. The best effective thermal pretreatment to form the desired large Pd-particles was at 600 °C in He, but, unfortunately, due to the formation of sulfur residues from (NH<sub>4</sub>)<sub>2</sub>SO<sub>4</sub> the drop off in the total yield of benzyl acetate was noticed

To circumvent these undesired sulfur residues a slurry method is developed by using Sb<sub>2</sub>O<sub>3</sub> as precursor for antimony and avoided the addition of (NH<sub>4</sub>)<sub>2</sub>SO<sub>4</sub>. Then, by using Sb<sub>2</sub>O<sub>3</sub>, PdCl<sub>2</sub> and without any additives 10 wt.-% Pd, 16 wt.-% Sb/TiO<sub>2</sub> catalysts have been prepared and tested for gas phase acetoxylation of toluene. Prior to the testing, catalysts were thermally treated in the reactor at 300 °C / 2 h or externally treated at 600 °C / 4 h in air, helium and 10 % H<sub>2</sub>/He. The conditioning time of 10 wt.-% Pd, 16 wt.-% Sb/TiO<sub>2</sub> catalysts is markedly shortened by a thermal pretreatment at 600 °C in presence of air or helium. However, the performance of the catalysts and nature of Pd-particles clearly depend on the atmosphere of the thermal pretreatment. The catalyst after thermal treatment in H<sub>2</sub>/He showed inactivity. On the other hand, air samples suffered with deactivation, whereas the sample after treatment in helium displayed long term stability. Inactive Pd<sub>8</sub>Sb<sub>3</sub> alloy particles were formed after H<sub>2</sub>/He treatment, whereas small (1-5 nm) PdO particles were noticed after air treatment which are reduced to Pd<sup>0</sup> and grown to 30 - 50 nm by incorporation of trace amounts of Sb with time on steam. Very large Pd<sup>0</sup> particles (up to 1-2 μm) were formed after helium pretreatment, however, particle of similar size as observed in air samples are observed with time on stream. Surprisingly, rather high amount of Sb is incorporated into Pd-particles. The atomic ratio of Pd/Sb was found be ≈ 5, yet without formation of stable alloy phases. In addition, the co-existence of Pd<sup>0</sup> and PdO on the surface is noticed by XPS. Incorporation of Sb into the Pd-particles in a specific ratio of Pd/Sb ≈ 5 favored the stabilization of oxidized Pd in its vicinity.

Influence of the co-components (Mn, Co, Sb, Au) on the valence state of the Pd and on the performance in the acetoxylation of toluene to BA is clearly noticed. High activity ( $\approx 55$  % toluene conversion) shown by Pd/TiO<sub>2</sub> catalyst containing Mn ( $E^0$  [Mn<sup>2+</sup>/Mn] = -1.18 eV), whereas high selectivity is reached by changing co-components from Mn to Au ( $E^0$  [Au<sup>3+</sup>/Au] = 1.52 eV) however displayed low activity. The catalysts with Co and Sb exhibited intermediate activity and selectivity. Performance of the catalyst is influenced by electronic and geometrical effects in presence of different co-components. Geometrical effects like incorporation of either carbon in presence of Mn and Co, or Sb and Au into the Pd lattice affect the catalyst activity. XPS showed the surface enrichment of Mn and Co. These differences allow a higher carbon acceptance for the catalysts with Mn and Co leads to high conversion. XPS and CO adsorption experiments showed that the co-components with low  $E^0$  stabilize oxidic Pd, while nearly all Pd is metallic in the presence of Au due to its high  $E^0$ . By combining all the observation from XRD, XPS and CO adsorption, it can be conclude that a rather high amount of partially oxidized Pd favors the toluene conversion, whereas metallic Pd is beneficial for a high selectivity of benzyl acetate.

An apparent influence of composition of the metallic Pd-particles and surface state, on the 10 wt.-% Pd, 16 wt.-% Sb/TiO<sub>2</sub> catalyst performance was noticed by using anatase and rutile as supports. Surprisingly, the rutile supported sample showed an extremely high selectivity above 95 % and a good long-term stability, whereas the anatase supported sample displayed higher activity, but deactivated after a few hours on stream. Agglomerated particles with Pd/Sb atomic ratio nearly 3 is observed in the deactivated anatase sample. This ratio is close to the detrimental alloy species. Moreover, double amount of carbon was deposited during the reaction in anatase sample ( $\approx 4$  wt.-%). This deposited carbon was accumulated over the Pd-particles. The strong interaction between this deposited carbon and Pd leads to slightly reduced state for metallic Pd (Pd <sup>$\delta^-$</sup> ), which has been claimed as detrimental for this reaction. On the other hand, on the rutile supported sample Pd-particles with incorporated Sb in an atomic ratio  $\approx 5$  are some how well established with surface Pd<sup>0</sup>/PdO species. This observation explains the good long-term stability of this catalyst. The extremely high selectivity ( $> 95$  %) for benzyl acetate could be explained by the high Pd concentration in rutile, whereas relatively high concentration of oxidized species led to high activity in anatase sample. Moreover, high surface area of anatase might also induce high toluene conversion for anatase sample.

Tuning the long term stability, high activity and selectivity is possible by varying the different synthesis parameters such as co-components, metal precursors, thermal pretreatments and supports. Combination of two or more co-components or using a mixture of TiO<sub>2</sub> phases as supports might improve the performance of further catalysts.

## References

- [1] M.H. T. Okada, A. Hattori, H. Hamaji, T. Miyake, S. Tokumaru, N. Nagira, S. Ikumi, T. Hori, N. Norimasa, , EP. Pat., 0 778 257 B1, (1996).
- [2] A. Benhmid, K.V. Narayana, A. Martin, B. Lucke, Chem. Commun. (2004) 2118-2119.
- [3] A. Benhmid, K.V. Narayana, A. Martin, B. Lücke, S. Bischoff, M.M. Pohl, J. Radnik, M. Schneider, J. Catal. 230 (2005) 420-435.
- [4] A. Benhmid, K.V. Narayana, A. Martin, B. Lucke, M.M. Pohl, Chem. Commun. (2004) 2416-2417.
- [5] A. Benhmid, K.V. Narayana, A. Martin, B. Lücke, M.M. Pohl, Catal. Today. 112 (2006) 192-196.
- [6] A. Benhmid, K.V. Narayana, A. Martin, B. lücke, M.M. Pohl, Chem. Lett. 33 (2004) 1238-1239.
- [7] D.R. Bryant, J.E. McKeon, B.C. Ream, J. Org. Chem. 33 (1968) 4123-4127.
- [8] V.N. Kalevaru, A. Benhmid, J. Radnik, B. Lücke, A. Martin, J. Catal. 243 (2006) 25-35.
- [9] V.N. Kalevaru, A. Benhmid, J. Radnik, M.M. Pohl, U. Bentrup, A. Martin, J. Catal. 246 (2007) 399-412.
- [10] J. Radnik, A. Benhmid, V.N. Kalevaru, M.-M. Pohl, A. Martin, B. Lücke, U. Dingerdissen, Angew. Chem. Int. Ed. 44 (2005) 6771-6774
- [11] J. Radnik, M.M. Pohl, V.N. Kalevaru, A. Martin, J. Phys. Chem. C. 111 (2007) 10166-10169.
- [12] G. Suresh, J. Radnik, V.N. Kalevaru, M.-M. Pohl, M. Schneider, B. Lucke, A. Martin, N. Madaan, A. Bruckner, Phys. Chem. Chem. Phys. 12 (2010) 4833-4842.
- [13] S. Gatla, N. Madaan, J. Radnik, V.N. Kalevaru, M.M. Pohl, B. Lücke, A. Martin, A. Brückner, Appl. Catal. A. 398 (2011) 104-112.
- [14] N. Madaan, S. Gatla, V.N. Kalevaru, J. Radnik, B. Lücke, A. Brückner, A. Martin, J. Catal. 282 (2011) 103-111.
- [15] S. Gatla, N. Madaan, J. Radnik, V.N. Kalevaru, B. Lücke, A. Martin, U. Bentrup, A. Brückner, Impact of co-components on the state of Pd and the performance of supported Pd/TiO<sub>2</sub> catalysts in the gas phase acetoxylation of toluene (accepted in ChemCatChem, 2011).
- [16] T.C. Bissot, US patent, 4,048,096.
- [17] K. Ebitani, K.-M. Choi, T. Mizugaki, K. Kaneda, Langmuir. 18 (2002) 1849-1855.
- [18] T. Komatsu, K. Inaba, T. Uezono, A. Onda, T. Yashima, Appl. Catal. A. 251 (2003) 315-326.
- [19] S.K. Tanielyan, R.L. Augustine, J. Mol. Catal. 87 (1994) 311-328.
- [20] G. Ertl, H. Knözinger, F. SchÜth, J. Weitkamp, Handbook of heterogeneous catalysis, vol 4. Wiley-VCH Verlag GmbH & Co. KGaA, Weinheim (2008).
- [21] S.M. George, Chem. Rev. (Washington, DC, U. S.). 95 (1995) 475-476.
- [22] G. Brieger, T.J. Nestrick, Chem. Rev. (Washington, DC, U. S.). 74 (1974) 567-580.
- [23] R. Mélendrez, G. Del Angel, V. Bertin, M.A. Valenzuela, J. Barbier, J. Mol. Catal. A: Chem. 157 (2000) 143-149.
- [24] C.R. Lederhos, M.J. Maccarrone, J.M. Badano, G. Torres, F. Coloma-Pascual, J.C. Yori, M.E. Quiroga, Appl. Catal. A. 396 (2011) 170-176.
- [25] L. Gucci, Z. Schay, G. Stefler, L.F. Liotta, G. Deganello, A.M. Venezia, J. Catal. 182 (1999) 456-462.
- [26] E. Gbenedio, Z. Wu, I. Hatim, B.F.K. Kingsbury, K. Li, Catal. Today. 156 (2010) 93-99.
- [27] V.M. Gryaznov, M.M. Ermilova, N.V. Orekhova, Catal. Today. 67 (2001) 185-188.
- [28] R. Maatman, W. Ribbens, B. Vonk, J. Catal. 31 (1973) 384-388.
- [29] L. Rodríguez, D. Romero, D. Rodríguez, J. Sánchez, F. Domínguez, G. Arteaga, Appl. Catal. A. 373 (2010) 66-70.
- [30] J.A. Moulijn, P.W.N.M. van Leeuwen, R.A. van Santen, in: P.W.N.M.v.L. J.A. Moulijn, R.A.v. Santen (Eds.), Stud. Surf. Sci. Catal., Elsevier, 1993, pp. v-viii.
- [31] Y. Bi, H. Xu, W. Li, A. Goldbach, International Journal of Hydrogen Energy. 34 (2009) 2965-2971.
- [32] Y. Sato, K. Terada, S. Hasegawa, T. Miyao, S. Naito, Appl. Catal. A. 296 (2005) 80-89.
- [33] L.S.F. Feio, C.E. Hori, S. Damyanova, F.B. Noronha, W.H. Cassinelli, C.M.P. Marques, J.M.C. Bueno, Appl. Catal. A. 316 (2007) 107-116.
- [34] N. Iwasa, T. Mayanagi, W. Nomura, M. Arai, N. Takezawa, Appl. Catal. A. 248 (2003) 153-160.
- [35] A. Lycourghiotis, Synthesis of Solid Catalysts, Wiley-VCH Verlag GmbH & Co. KGaA, 2009, pp. 13-31.
- [36] J.A. Schwarz, C. Contescu, A. Contescu, Chem. Rev. (Washington, DC, U. S.). 95 (1995) 477-510.



- [37] S. Golunski, R. Rajaram, N. Hodge, G.J. Hutchings, C.J. Kiely, *Catal. Today*. 72 (2002) 107-113.
- [38] N.S. Babu, N. Lingaiah, N. Pasha, J.V. Kumar, P.S.S. Prasad, *Catal. Today*. 141 (2009) 120-124.
- [39] H. Huang, D.Y.C. Leung, *ACS Catalysis*. 1 (2011) 348-354.
- [40] E. Marceau, X. Carrier, M. Che, *Synthesis of Solid Catalysts*, Wiley-VCH Verlag GmbH & Co. KGaA, 2009, pp. 59-82.
- [41] G. Agostini, E. Groppo, A. Piovano, R. Pellegrini, G. Leofanti, C. Lamberti, *Langmuir*. 26 (2010) 11204-11211.
- [42] C. Sivaraj, C. Contescu, J.A. Schwarz, *J. Catal.* 132 (1991) 422-431.
- [43] W. Zou, R.D. Gonzalez, *Catal. Lett.* 12 (1992) 73-86.
- [44] G. Farkas, L. Hegedus, A. Tungler, T. Máthé, J.L. Figueiredo, M. Freitas, *J. Mol. Catal. A: Chem.* 153 (2000) 215-219.
- [45] M. Gurrath, T. Kuretzky, H.P. Boehm, L.B. Okhlopkova, A.S. Lisitsyn, V.A. Likholobov, *Carbon*. 38 (2000) 1241-1255.
- [46] K.-i. Fujimoto, F.H. Ribeiro, M. Avalos-Borja, E. Iglesia, *J. Catal.* 179 (1998) 431-442.
- [47] N.M. Kinnunen, J.T. Hirvi, T. Venäläinen, M. Suvanto, T.A. Pakkanen, *Appl. Catal. A*. 397 (2011) 54-61.
- [48] T.V. Choudhary, S. Banerjee, V.R. Choudhary, *Appl. Catal. A*. 234 (2002) 1-23.
- [49] X. Guo, G. Zhi, X. Yan, G. Jin, X. Guo, P. Brault, *Catal. Commun.* 12 (2011) 870-874.
- [50] G.D. Zakumbaeva, N.A. Zakarina, N.F. Toktabaeva, B.B. Dyusenbina, V.F. Vozdvizhenskii, O.M. Pakhorukova, *React. Kinet. Catal. Lett.* 37 (1988) 187-192.
- [51] N. Krishnankutty, J. Li, M. Albert Vannice, *Appl. Catal. A*. 173 (1998) 137-144.
- [52] N. Krishnankutty, M.A. Vannice, *J. Catal.* 155 (1995) 327-335.
- [53] T. Mallat, S. Szabó, M. Schürch, U.W. Göbel, A. Baiker, *Catal. Lett.* 47 (1997) 221-227.
- [54] C. Mondelli, J.-D. Grunwaldt, D. Ferri, A. Baiker, *Phys. Chem. Chem. Phys.* 12 (2010) 5307-5316.
- [55] J.L. Haan, K.M. Stafford, R.I. Masel, *J. Phys. Chem. C*. 114 (2010) 11665-11672.
- [56] M. Chen, D. Kumar, C.-W. Yi, D.W. Goodman, *Science*. 310 (2005) 291-293.
- [57] C. Keresszegi, J.-D. Grunwaldt, T. Mallat, A. Baiker, *J. Catal.* 222 (2004) 268-280.
- [58] D.I. Enache, J.K. Edwards, P. Landon, B. Solsona-Espriu, A.F. Carley, A.A. Herzing, M. Watanabe, C.J. Kiely, D.W. Knight, G.J. Hutchings, *Science*. 311 (2006) 362-365.
- [59] A.B. Hungria, M. Fernández-García, J.A. Anderson, A. Martínez-Arias, *J. Catal.* 235 (2005) 262-271.
- [60] S. Nakamura, T. Yasui, *J. Catal.* 17 (1970) 366-374.
- [61] Y.F. Han, D. Kumar, C. Sivadinarayana, D.W. Goodman, *J. Catal.* 224 (2004) 60-68.
- [62] E.A. Crathorne, D. Macgowan, S.R. Morris, A.P. Rawlinson, *J. Catal.* 149 (1994) 254-267.
- [63] D. Kumar, M.S. Chen, D.W. Goodman, *Catal. Today*. 123 (2007) 77-85.
- [64] M.-M. Pohl, J. Radnik, M. Schneider, U. Bentrup, D. Linke, A. Brückner, E. Ferguson, *J. Catal.* 262 (2009) 314-323.
- [65] C. Mondelli, D. Ferri, J.-D. Grunwaldt, F. Krumeich, S. Mangold, R. Psaro, A. Baiker, *J. Catal.* 252 (2007) 77-87.
- [66] K. Qian, W. Huang, *Catal. Today*. 164 (2011) 320-324.
- [67] J.R. Regalbuto, *Synthesis of Solid Catalysts*, Wiley-VCH Verlag GmbH & Co. KGaA, 2009, pp. 33-58.
- [68] Q.-c. Zhu, B.-x. Shen, H. Ling, R. Gu, *Catal. Lett.* 132 (2009) 464-471.
- [69] J. Lee, S. Hwang, J.G. Seo, U.G. Hong, J.C. Jung, I.K. Song, *J. Ind. Eng. Chem.* 17 (2011) 310-315.
- [70] B. Karimi, A. Zamani, S. Abedi, J.H. Clark, *Green Chem.* 11 (2009) 109-119.
- [71] L. Liu, F. Zhou, L. Wang, X. Qi, F. Shi, Y. Deng, *J. Catal.* 274 (2010) 1-10.
- [72] J. Barbier, L. Oliviero, B. Renard, D. Duprez, *Top. Catal.* 33 (2005) 77-86.
- [73] J.H. Kwak, J. Hu, D. Mei, C.-W. Yi, D.H. Kim, C.H.F. Peden, L.F. Allard, J. Szanyi, *Science*. 325 (2009) 1670-1673.
- [74] M.V. Ganduglia-Pirovano, A. Hofmann, J. Sauer, *Surf. Sci. Rep.* 62 (2007) 219-270.
- [75] R. Schaub, E. Wahlström, A. Rønnau, E. Lægsgaard, I. Stensgaard, F. Besenbacher, *Science*. 299 (2003) 377-379.
- [76] X.-Q. Gong, A. Selloni, O. Dulub, P. Jacobson, U. Diebold, *J. Am. Chem. Soc.* 130 (2007) 370-381.
- [77] N. Lopez, J.K. Nørskov, T.V.W. Janssens, A. Carlsson, A. Puig-Molina, B.S. Clausen, J.D. Grunwaldt, *J. Catal.* 225 (2004) 86-94.

- [78] U. Diebold, Surf. Sci. Rep. 48 (2003) 53-229.
- [79] Wahlstr, ouml, E. m, N. Lopez, R. Schaub, P. Thostrup, oslash, A. nnau, C. Africh, aelig, E. gsgaard, J.K. rskov, F. Besenbacher, Phys. Rev. Lett. 90 (2003) 026101.
- [80] M. Li, W. Hebenstreit, U. Diebold, A.M. Tyryshkin, M.K. Bowman, G.G. Dunham, M.A. Henderson, J. Phys. Chem B. 104 (2000) 4944-4950.
- [81] R. Schaub, P. Thostrup, N. Lopez, aelig, E. gsgaard, I. Stensgaard, oslash, J.K. rskov, F. Besenbacher, Phys. Rev. Lett. 87 (2001) 266104.
- [82] H. Cheng, A. Selloni, Phys. Rev. B. 79 (2009) 092101.
- [83] J. Panpranot, K. Kontapakdee, P. Praserthdam, Appl. Catal. A. 314 (2006) 128-133.
- [84] T. Pabisiak, A. Kiejna, Solid State Commun. 144 (2007) 324-328.
- [85] T. Okada, Y. Kamiya, Bull. Chem. Soc. Jpn. 52 (1979) 3321-3325.
- [86] D.R. Bryant, J.E. McKeon, B.C. Ream, Tetrahedron Lett. 9 (1968) 3371-3373.
- [87] K. Walter, F. Bruno, DE 1618364.
- [88] R.L. Augustine, S.K. Tanielyan, US Patent. 5206423
- [89] J.M. Davidson, C. Triggs, J. Chem. Soc. A: Inorganic, Physical, Theoretical (1968) 1331-1334.
- [90] K. Walter, F. Bruno, DE 1262992.
- [91] L.N. Rachkovskaya, K.I. Matveev, G.N. Il'inich, N.K. Eremenko, Kinet. Katal. 18 (1977) 1040-1042.
- [92] M.K. Starchevskii, M.N. Vargaftik, I.I. Moiseev, Kinet. Katal. 20 (1979) 1163-1169.
- [93] M.K. Starchevskii, M.N. Vargaftik, O.M. Nefedov, I.I. Moiseev, Kinet. Katal. 21 (1980) 1451-1457.
- [94] E. Benazzi, C.J. Cameron, H. Mimoun, J. Mol. Catal. 69 (1991) 299-321.
- [95] E. Benazzi, H. Mimoun, C.J. Cameron, J. Catal. 140 (1993) 311-327.
- [96] S.K. Tanielyan, R.L. Augustine, J. Mol. Catal. 87 (1994) 311-328.
- [97] L. Ebersson, L. Jönsson, Acta Chem. Scand. 28b (1974) 597-602.
- [98] Q. Shu, X. Wang, D. Cao, S. Ren, Cuihua Xuebao. 25 (2004) 511-512.
- [99] Q. Shu, X. Wang, S. Ren, W. Shi, Cuihua Xuebao. 26 (2005) 869-873.
- [100] N. Madaan, Gas Phase Acetoxylation of Methyl Aromatics to their Corresponding Esters over PdSb/TiO<sub>2</sub> Catalysts: Activation, Steady-State Operation, Deactivation and Regeneration, Department of heterogeneous catalytic process, Leibniz Institute für Katalyse an der Universität Rostock (2011).
- [101] S. Greenfield, I.L. Jones, C.T. Berry, Analyst. 89 (1964) 713-720.
- [102] J.M. Mermet, J. Anal. At. Spectrom. 20 (2005) 11-16.
- [103] R.H. Wendt, V.A. Fassel, Anal. Chem. 37 (1965) 920-922.
- [104] [http://www-odp.tamu.edu/publications/tnotes/tn30/tn30\\_10.htm](http://www-odp.tamu.edu/publications/tnotes/tn30/tn30_10.htm).
- [105] [http://www.rsc.org/images/brief%2029\\_tcm18-119169.pdf](http://www.rsc.org/images/brief%2029_tcm18-119169.pdf) (CHNS).
- [106] K.S.W. Sing, D.H. Everett, R.A.W. Haul, L. Moscou, R.A. Pierotti, J. Rouquerol, T. Siemieniowska, Pure Appl. Chem. 57 (1985) 603-619.
- [107] S. Brunauer, P.H. Emmett, E. Teller, J. Am. Chem. Soc. 60 (1938) 309-319.
- [108] A. Davydov, *Molecular Spectroscopy of Oxide Catalyst Surfaces*, Wiley, Chichester, **2003**, p. 95.
- [109] H.K.D.H. Bhadeshia, University of Cambridge, Material Science and Metallurgy. [www.msm.cam.ac.uk/phase-trans/2002/Thermal1.pdf](http://www.msm.cam.ac.uk/phase-trans/2002/Thermal1.pdf).
- [110] K. Siegbahn, Electron Spectroscopy for Atoms, Molecules and Condensed Matter, Nobel Lecture, December 8, 1981. [http://nobelprize.org/nobel\\_prizes/physics/laureates/1981/siegbahn-lecture.pdf](http://nobelprize.org/nobel_prizes/physics/laureates/1981/siegbahn-lecture.pdf).
- [111] H. Li, Y. Yang, Y. Wen, L. Liu, Compos. Sci. Technol. 67 (2007) 2675-2682.
- [112] Z. Ding, W. Martens, R.L. Frost, J. Mater. Sci. Lett. 21 (2002) 1415-1417.
- [113] A. Obaid, A. Alyoubi, A. Samarkandy, S. Al-Thabaiti, S. Al-Juaid, A. El-Bellihi, E.-H. Deifallah, J. Therm. Anal. Calorim. 61 (2000) 985-994.
- [114] P.K. Gallagher, M.E. Gross, J. Therm. Anal. Calorim. 31 (1986) 1231-1241.
- [115] X. Zhu, M. Elomaa, F. Sundholm, C.H. Lochmüller, Polym. Degrad. Stab. 62 (1998) 487-494.
- [116] H. Darabi, K. Aghapoor, F. Mohsenzadeh, F. Taala, N. Asadollahnejad, A. Badiiei, Catal. Lett. 133 (2009) 84-89.
- [117] L. Costa, G. Paganetto, G. Bertelli, G. Camino, J. Therm. Anal. Calorim. 36 (1990) 1141-1153.
- [118] R. Gunawan, D. Zhang, J. Hazard. Mater. 165 (2009) 751-758.
- [119] P.M. Schaber, J. Colson, S. Higgins, D. Thielen, B. Anspach, J. Brauer, Thermochem. Acta. 424 (2004) 131-142.



- [120] G.T. Kerr, A.W. Chester, W.J. Reagan, D.H. Olson, *Inorg. Chem.* 13 (1974) 2294-2296.
- [121] K.R. Priolkar, P. Bera, P.R. Sarode, M.S. Hegde, S. Emura, R. Kumashiro, N.P. Lalla, *Chem. Mater.* 14 (2002) 2120-2128.
- [122] Q. Smejkal, D. Linke, U. Bentrup, M.M. Pohl, H. Berndt, M. Baerns, A. Brückner, *Appl. Catal. A.* 268 (2004) 67-76.
- [123] S.S. Maluf, A.L. Gobbi, P.I. Paulin-Filho, P.A.P. Nascente, *Surf. Interface Anal.* 36 (2004) 931-934.
- [124] R. C. Weast, *CRC Handbook of Chemistry and Physics*, CRC Press Inc, Boca-Raton, 67th edn, 1986-1987, p. 151.
- [125] N.N. Greenwood, A. Earnshaw, *Chemistry of the Elements*, Butterworth-Heinemann, Oxford, UK, 2nd edn, 1997.
- [126] J. Häglund, A.F. Guillermet, G. Grimvall, M. Körling, *Phys. Rev. B.* 48 (1993) 11685.
- [127] N. Krishnankutty, M.A. Vannice, *J. Catal.* 155 (1995) 312-326.
- [128] M. Khanuja, B.R. Mehta, P. Agar, P.K. Kulriya, D.K. Avasthi, *J. Appl. Phys.* 106 (2009) 093515-093518.
- [129] E.H. Voogt, A.J.M. Mens, O.L.J. Gijzeman, J.W. Geus, *Surf. Sci.* 373 (1997) 210-220.
- [130] F.P. Leisenberger, G. Koller, M. Sock, S. Surnev, M.G. Ramsey, F.P. Netzer, B. Klötzer, K. Hayek, *Surf. Sci.* 445 (2000) 380-393.
- [131] V.A. Bondzie, P. Kleban, D.J. Dwyer, *Surf. Sci.* 347 (1996) 319-328.
- [132] B. Klötzer, K. Hayek, C. Konvicka, E. Lundgren, P. Varga, *Surf. Sci.* 482-485 (2001) 237-242.
- [133] H. Okamoto, *J. Phase Equilib.* 13 (1992) 578-579.
- [134] C.J. Powell, *Appl. Surf. Sci.* 89 (1995) 141-149.
- [135] H. Gabasch, W. Unterberger, K. Hayek, B. Klötzer, E. Kleimenov, D. Teschner, S. Zafeiratos, M. Hävecker, A. Knop-Gericke, R. Schlögl, J. Han, F.H. Ribeiro, B. Aszalos-Kiss, T. Curtin, D. Zemlyanov, *Surf. Sci.* 600 (2006) 2980-2989.
- [136] R. Delobel, H. Baussart, J.-M. Leroy, J. Grimblot, L. Gengembre, *J. Chem. Soc., Faraday Trans. 1.* 79 (1983) 879-891.
- [137] J.G. McCarty, *Catal. Today.* 26 (1995) 283-293.
- [138] S.H. Oh, P.J. Mitchell, R.M. Siewert, *J. Catal.* 132 (1991) 287-301.
- [139] P. Salomonsson, S. Johansson, B. Kasemo, *Catal. Lett.* 33 (1995) 1-13.
- [140] R. Mann, *Catal. Today.* 37 (1997) 331-349.
- [141] M. Maciejewski, A. Baiker, *Pure Appl. Chem.* 11 (1995) 1879-1884.
- [142] T. Paryjczak, J.M. Farbotko, W.J. K, *React. Kinet. Catal. Lett.* 20 (1982) 227-231.
- [143] B. Pawelec, A.M. Venezia, V. La Parola, E. Cano-Serrano, J.M. Campos-Martin, J.L.G. Fierro, *Appl. Surf. Sci.* 242 (2005) 380-391.
- [144] R.J. Davis, M. Boudart, *J. Phys. Chem.* 98 (1994) 5471-5477.
- [145] M. Tian, M. Malig, S. Chen, A. Chen, *Electrochem. Commun.* 13 (2011) 370-373.
- [146] G. Zhang, Y. Wang, X. Wang, Y. Chen, Y. Zhou, Y. Tang, L. Lu, J. Bao, T. Lu, *Appl. Catal. B.* 102 (2011) 614-619.
- [147] NIST, Standard Reference Database 20, version 3.5, <http://srdata.nist.gov/xps>.
- [148] G. Ketteler, D.F. Ogletree, H. Bluhm, H. Liu, E.L.D. Hebenstreit, M. Salmeron, *J. Am. Chem. Soc.* 127 (2005) 18269-18273.
- [149] W. Huang, Z. Zuo, P. Han, Z. Li, T. Zhao, *J. Electron Spectrosc. Relat. Phenom.* 173 (2009) 88-95.
- [150] T.E. Feltes, Y. Zhao, R.F. Klie, R.J. Meyer, J.R. Regalbuto, *ChemCatChem.* 2 (2010) 1065-1068.
- [151] K. Zorn, S. Giorgio, E. Halwax, C.R. Henry, H. Grönbeck, G.n. Rupprechter, *J. Phys. Chem. C.* 115 (2010) 1103-1111.
- [152] H. Tiznado, S. Fuentes, F. Zaera, *Langmuir.* 20 (2004) 10490-10497.
- [153] M. Machida, K. Eguchi, H. Arai, *J. Catal.* 103 (1987) 385-393.
- [154] K. Scheerschmidt, M. Werner, *physica status solidi (a).* 202 (2005) 2368-2375.
- [155] H. Yue, A. Wu, Y. Feng, X. Zhang, T. Li, *Thin Solid Films.* 519 (2011) 5577-5581.
- [156] J.H. Kolts, G.A. Delzer, *Science.* 232 (1986) 744-746.
- [157] A.M. Squires, M. Kwauk, A.A. Avidan, *Science.* 230 (1985) 1329-1337.

## List of scientific publications

Scientific publications, fully or partially related to the work reported in this thesis, are listed below and some part of this work which is unpublished yet is in preparation for relevant publications.

- 1) Gatla Suresh, Jörg Radnik, Venkata Narayana Kalevaru, Marga-Martina Pohl, Matthias Schneider, Bernhard Lücke, Andreas Martin, Neetika Madaan and Angelika Brückner, *Phys. Chem. Chem. Phys.* 12 (2010) 4833-4842.
- 2) S. Gatla, N. Madaan, J. Radnik, V.N. Kalevaru, M.M. Pohl, B. Lücke, A. Martin, A. Brückner, *Appl. Catal. A*. 398 (2011) 104-112.
- 3) N. Madaan, S. Gatla, V. N. Kalevaru, J. Radnik, B. Lücke, A. Brückner, A. Martin, *J. Catal.* (2011). doi:10.1016/j.jcat.2011.06.005.
- 4) N. Madaan, S. Gatla, V.N. Kalevaru, J. Radnik, B. Lücke, A. Brückner, A. Martin, *Top. Catal.* (2011) accepted
- 5) S. Gatla, N. Madaan, J. Radnik, V.N. Kalevaru, U. Bentrup, B. Lücke, A. Martin and A. Brückner “Role of co-components on the state of Pd and the catalytic performance in the gas phase acetoxylation of toluene”, *ChemCatChem*. (2011), accepted
- 6) N. Madaan, S. Gatla, V. N. Kalevaru, J. Radnik, B. Lücke, A. Brückner, A. Martin. “Effect of reaction pressure on the performance of 10Pd16Sb/TiO<sub>2</sub> catalyst in gas phase acetoxylation of toluene to benzyl acetate”, *Catal. Commun.* (2011) submitted.
- 7) Gatla Suresh, Neetika Madaan, Jörg Radnik, Venkata Narayana Kalevaru, Marga-Martina Pohl, Bernhard Lücke, Andreas Martin, Angelika Brückner. “Highly selective rutile supported Pd,Sb catalyst in the gas phase acetolxyation of toluene” (to be submitted)

## Additional scientific publications

- 1) A. Ratnamala, G. Suresh, V.D. Kumari, M. Subrahmanyam, *Mater. Chem. Phys.* 110 (2008) 176-179.
- 2) J. Krishna Reddy, G. Suresh, C.H. Hymavathi, V. Durga Kumari, M. Subrahmanyam, *Catal. Today*. 141 (2009) 89-93.

Rostock, 26<sup>th</sup> August 2011

Suresh Gatla

## List of contribution in conferences

- 1) 42 Jahrestreffen Deutscher Katalytiker in Weimar, Germany, from 11 to 13 March 2009 “Influence of synthesis and calcination conditions on composition and particle size of active Pd-containing methyl aromatic acetoxylation catalysts”; G. Suresh, J. Radnik, N. Madaan, V.N. Kalevaru, M.-M Pohl, M. Schneider, B. Lücke, A. Martin, A. Brückner. (Poster presentation)
- 2) The 10th International Symposium on the "Scientific Bases for the Preparation of Heterogeneous Catalysts" in Louvain-la-Neuve, Belgium, from 11-15 July 2010. “Tuning the active Pd-catalysts by thermal treatments: Effect of metal precursors, ammonium additives and calcination atmospheres”; G. Suresh, J. Radnik, N. Madaan, V.N. Kalevaru, M.-M Pohl, M. Schneider, B. Lücke, A. Martin, A. Brückner. (Poster presentation)
- 3) 14th Nordic Symposium on Catalysis, August 29-31, 2010 in Helsingør, Denmark. “Influence of thermal treatment on the catalytic performance of Pd-Sb/TiO<sub>2</sub> catalyst for acetoxylation of toluene”; N. Madaan, S. Gatla, V.N. Kalevaru, J. Radnik, B. Lücke, A. Brückner, A. Martin. (Poster presentation)
- 4) 9th Congress on Catalysis applied to Fine Chemicals (CAFC9), Zaragoza, Spain, from 13-16 September 2010. “Tailoring the synthesis of supported Pd acetoxylation catalysts towards high stability and selectivity”; S. Gatla, N. Madaan, J. Radnik, V.N. Kalevaru, B. Lücke, A. Martin, A. Brückner. (Oral presentation)
- 5) DECHEMA-Jahrestagung der Biotechnologen und ProcessNet-Jahrestagung 2010., Eurogress Aachen, Germany, from 21-23 September 2010. “Novel preparation routes for Pd,Sb/TiO<sub>2</sub> catalysts for the acetoxylation of toluene”; G. Suresh, N. Madaan, J. Radnik, V.N. Kalevaru, B. Lücke, A. Martin, A. Brückner. (Poster presentation)
- 6) 13th Norddeutsches Doktorandenkolloquium at Ernst-Moritz-Arndt Universität Greifswald, Germany, from 24-25 September 2010 “Improving the performance of promoted Pd/TiO<sub>2</sub> catalysts in the acetoxylation of toluene by tailored synthesis procedures”; S. Gatla, N. Madaan, J. Radnik, V.N. Kalevaru, B. Lücke, A. Martin, A. Brückner. (Oral presentation)
- 7) 44 Jahrestreffen Deutscher Katalytiker in Weimar, Germany, from 16-18 March “Effect of varying reaction parameters on activation, deactivation and regeneration of Pd,Sb/TiO<sub>2</sub> in gas phase acetoxylation of toluene”; N. Madaan, S. Gatla, V.N. Kalevaru, J. Radnik, B. Lücke, A. Brückner, A. Martin. (Oral presentation)
- 8) 44 Jahrestreffen Deutscher Katalytiker in Weimar, Germany, from 16-18 March 2011 “Effect of co-components on the performance of Pd based catalysts for the gas phase acetoxylation of toluene”; S. Gatla, N. Madaan, J. Radnik, V.N. Kalevaru, B. Lücke, A. Martin, U. Bentrup, A. Brückner. (Poster presentation)

- 9) 13th JCF Fruhjahrssymposium, Erlangen, Germany, March 23-26 2011  
“Investigations on the deactivation and regeneration of Pd,Sb/TiO<sub>2</sub> catalysts in gas phase acetoxylation of toluene”; N. Madaan, S. Gatla, V.N. Kalevaru, J. Radnik, B. Lücke, A. Brückner, A. Martin. (Poster presentation)
- 10) 2nd Indo-German Catalysis Conference: Catalysis for renewable energy, Rostock, Germany, from 19-22 June 2011. “Effect of total pressure on the catalytic performance of a 10Pd16Sb/TiO<sub>2</sub> catalyst in the gas phase acetoxylation of toluene”; N. Madaan, S. Gatla, V.N. Kalevaru, J. Radnik, B. Lücke, A. Brückner, A. Martin. (Poster presentation)
- 11) 2nd Indo-German Catalysis Conference: Catalysis for renewable energy, Rostock, Germany, from 19-22 June 2011. “Influence of metals M on the performance of Pd,M/TiO<sub>2</sub> catalysts in the gas phase acetoxylation of toluene to benzyl acetate”; S. Gatla, N. Madaan, J. Radnik, V.N. Kalevaru, B. Lücke, A. Martin, U. Bentrup, A. Brückner. (Poster presentation)
- 12) 2nd Indo-German Catalysis Conference, Catalysis for renewable energy, Rostock, Germany, from 19-22 June 2011. “Dependence of catalytic performance on the particle size of Pd in acetoxylation of toluene; V.N. Kalevaru, N. Madaan, S. Gatla, J. Radnik, B. Lücke, A. Brückner, A. Martin. (Keynote lecture)

# Lebenslauf

## Persönliche Daten

Name: Suresh Gatla

Geburtsdatum: 10.04.1983

Geburtsort: Velpur, Indien

Nationalität: Indisch

Geschlecht: Männlich

Familienstand: ledig

## Bildung

- |             |   |
|-------------|---|
| 2000 – 2003 | B.Sc. in Chemie; Andhra Loyola College, Vijayawada, Acharya<br>Universität, Indien.     |
| 2003 – 2005 | M.Sc. physikalische Chemie; Andhra Universität, Rajahmundry, Indien.                    |
| 2006 – 2008 | Doktorand in Indian Institute of Chemical Technology, Hyderabad,<br>Indien.             |
| 2008 – 2011 | Doktorand im Leibniz-Institut für Katalyse e. V. an der Universität<br>Rostock (LIKAT). |